2019

Formulation Development, Preclinical Testing, and Primary Packaging Optimization for Cannabinoids and Other Therapeutics

Pranjal Taskar
University of Mississippi

FORMULATION DEVELOPMENT, PRECLINICAL TESTING, AND PRIMARY PACKAGING OPTIMIZATION FOR CANNABINOIDS AND OTHER THERAPEUTICS

A Dissertation

presented in partial fulfillment of requirements

for the degree of Doctor of Philosophy

in Pharmaceutical Sciences with an emphasis in Pharmaceutics and Drug Delivery

The University of Mississippi

by

PRANJAL S. TASKAR

December 2018

ABSTRACT

Through the process of drug development, a molecule goes through discovery screening; lead selection and optimization, ADME testing, toxicity profiling, dosage form determination, preclinical testing in an *in vitro* and *in vivo* setup, followed by clinical research, FDA review and approval until eventually it is manufactured in the determined dosage form and reaches the patient. At every point through this process, scientists actively work towards a smoother transition and a quick and safe approval of the molecule towards the next step. The different chapters in this research would cover various phases of drug development; from discovery stage to fill-finish and primary container compatibility.

Cannabidiol (CBD), has therapeutic potential in the management of diabetic retinopathy induced pain and inflammation, however, being a lipophilic molecule, is challenged by delivery to the back of the eye through the topical route. This work aims at improving ocular penetration of CBD by means of drug design and analog derivatization. Another cannabinoid, Δ^9-Tetrahydrocannabinol-Valine-Hemisuccinate, a relatively hydrophilic prodrug of Δ^9-Tetrahydrocannabinol, synthesized with the aim of improving ocular bioavailability of the parent molecule. This work brings forth importance of combination of prodrug strategy with ophthalmic formulation development. Triamcinolone Acetonide (TA) is a corticosteroid administered intravitreally for the management of ocular inflammatory conditions such as diabetic retinopathy. Currently, there is a need for the development of a topical formulation of TA, designed to achieve drug levels at the back of the eye. Nanostructured lipid carriers (NLCs) are lipid-based nanoparticles made up of a combination of solid and liquid lipids. This project aims at the

development of TA-NLC formulations. Voriconazole (VRC) has emerged as a promising candidate for the treatment of fungal keratitis. Antifungal drugs such as VRC have been reported to have a synergistic effect with fluoroquinolones such as Ciprofloxacin (CIP). The goal of this project is use of statistical techniques for the development of a dual drug, VRC and CIP, loaded NLC carrier for the treatment of fungal keratitis. The final chapter focuses on development of a capping mechanism that would enable a vial-stopper combination to maintain integrity and product quality at storage temperatures of -55ºC and below.

DEDICATION

This work is dedicated to

My parents, for making me the person I am

My sister, my confidante

And all the positive influences in my life,

helping me get there

Ankur, I could not have done it without you

ABBREVIATIONS

ADME	Absorption Distribution Metabolism Elimination
RO5	Rule of 5
THC	Δ^9- Tetrahydrocannabinol
CBD	Cannabidiol
SLN	Solid lipid nanoparticles
NLC	Nanostructured lipid carriers
BAB	Blood-Aqueous Barrier
BRB	Blood-Retinal Barrier
QbD	Quality by Design
CQA	Critical quality attributes
CPP	Critical process parameters
DOE	Design of experiment
PAT	Process analytical technologies
PK-PD	Pharmacokinetic-Pharmacodynamic
IOP	Intra-ocular pressure
DR	Diabetic retinopathy
VEGF	Vascular endothelial growth factor
TNFα	Tumor necrosis factor alpha
CNS	Central nervous system

ROS	Reactive oxygen species
CBD-AA	CBD-amino acid ester
CBD-Mono-Val	CBD-monovalinate
CBD-Di-Val	CBD-divalinate
CBD-DCA	CBD-dicarboxylic acid
CBD-HS	CBD-hemisuccinate
CBD-AA-DCA	CBD-amino acid- dicarboxylic acid ester
CBD-Mono-VHS	CBD-monovalinate-monohemisuccinate
CBD-Di-VHS	CBD-divalinate-hemisuccinate
DMAP	4-dimethylaminopyridine
DCM	Dichloromethane
DCC	dicyclohexylcarbodiimide
TLC	Thin layer chromatography
THF	Tetrahydrofuran
AH	Aqueous humor
VH	Vitreous humor
IC	Iris-ciliary bodies
RC	Retina-choroid
IPBS	Isotonic phosphate buffer
ANOVA	Analysis of Variance

RGC	Retinal ganglion cell
IOP	Intra-ocular pressure
TM	Trabecular meshwork
THC	Δ^9-Tetrahydrocannabinol
THC-VHS	Δ^9-Tetrahydrocannabinol-Valine-Hemisuccinate
STEM	Scanning transmission electron microscopy
PDI	Polydispersity Index
DLS	Dynamic Light Scattering
PL	Plasma
THC-HG	Δ^9-Tetrahydrocannabinol-Hemiglutarate
TA	Triamcinolone Acetonide
CH	Chitosan
TMC	Tri-methyl chitosan
RMβCD	Randomly methylated β cyclodextrin
TPP	Sodium tripolyphosphate
DQ	Degree of quaternization
DM	Degree of di-methylation
MP	Melting point
NP	Nanoparticles
EE	Entrapment Efficiency

r^2	Regression coefficient
Cor	Cornea
SC	Sclera
ESI	Electrospray ionization
MRT	Mean residence time
CL	Clearance
VRC	Voriconazole
CIP	Ciprofloxacin
DL	Drug load
CCD	Central composite design
RSM	Response surface methodology
DP	Drug product
CCS	Container closure systems
T_g’	Glass transition temperature
CCI	Container closure integrity
RSF	Residual Seal Force

ACKNOWLEDGEMENT

Graduating from The University of Mississippi with a doctorate would not have been possible without the guidance of my mentor, Dr. Soumyajit Majumdar. Dr. Majumdar has played a vital role in my graduate career; from starting out as a novice bachelors graduate, moving my way through the past four years, polishing my technical skills and all-round growth. He has provided me with innumerable opportunities, supported my decisions to tackle challenges head-on and fueled my research ideas. Words fail to pen down my gratitude; I indeed lucked out with an amazing mentor for my graduate journey. I thank him for his support with all my heart.

I would like to express gratitude towards my committee members, Dr. Michael Repka, Dr. Seong Bong Jo and Dr. Samir Ross for their time, inputs and suggestions. Their timely interventions and comments contributed to speeding up the writing process. A brief thanks to the other professors in the department of Pharmaceutics and Drug Delivery; Dr. Bonnie Avery, Dr. Narasimha Murthy, Dr. Christy Wyandt and Dr. Chalet Tan for their contributions in helping me develop strong academic foundations through my course-work. A shout out to Ms. Deborah King and Abigail Sims for their administrative efforts in running the department and in turn my graduate journey, smoothly!

Moving on to the running force of the department, the graduate students, I would like to thank all my colleagues, lab-mates and friends for their technical, experimental and moral support. All of them have been a pleasure to work with, but I do have to pause and thank Akash Patil and Prit Lakhani, my lab-mates (and friends). Be it debates over study design or back-breaking animal work; their help, input and overall presence underlays every positive (and negative) experimental

report in this dissertation. Thank you, we did keep pushing each other till the goal-line! Goutham Adelli, thank you for stepping in and teaching me the ropes, you have been a great teacher and an amazing friend; I cherish the limited time I had to work with you. I would also like to thank Sai Prachetan and Akshaya Tatke, their presence was imperative in this journey.

The internship opportunity I had with BioMarin Pharmaceutical Inc. was a great chance for learning and professional development. I would like to thank my manager, Saeed Moshashaee for his continuous support and guidance all through my time at BioMarin. I would also like to thank Joyce Chou, Director of Formulation at BioMarin for allowing me to carry out this project at this esteemed organization. I sincerely thank the rest of my team, Pooja Sane and Stephanie Kishbaugh for their insightful suggestions and encouragement. I express my heartfelt gratitude to the rest of Formulation group; Eric, Pranav, Terrence, Natalie, Sunil, Kaveh, Kidisti and Marcus for their continued support and encouragement through my time at BioMarin.

Lastly, I would like to thank my friends and family scattered across the globe for their overflowing love and support. Ajinkya, Nicole (Akash and Prit), my friends, my family in Oxford, you guys have given me some of the best years of my life, thank you for helping me make a new home in a foreign world. My fiancé, Ankur, thank you for being my pillar of support through every challenge I have had to face in this journey, being the constant positive presence in my life, pushing me and believing in me. To my family back home; my sister and my parents, you are what puts my life into perspective, your vote of confidence in my decisions has given me the strength to move smoothly through my graduate life. Thank you!

Table of Contents

LIST OF TABLES

LIST OF FIGURES

CHAPTER 1

INTRODUCTION AND SPECIFIC AIMS

Introduction

The number of compounds which can be classified as "drug-like" are few, these compounds possess acceptable ADME properties and a toxicity profile, enabling them to survive through Phase 1 clinical trials. [1] Lipinski et al. proposed few guidelines for an orally absorbable molecule, the Lipinski's rule of 5 (RO5) which determines limitations for drug design for an oral targeted molecule to be successful through all the stages of drug development (molecular weight 500, log P 5, H-bond donors 5, H-bond acceptors 10). With a few modifications, we can utilize the Lipinski's RO5 in designing molecules for non-oral routes of delivery. [2-3] Investigational studies conducted have tried to determine the applicability of RO5 to non-oral routes of delivery, such as ophthalmic delivery. [2-3] Taking into consideration the ocular barriers, designing a molecule permeating across the cornea is more challenging than targeting intestinal permeation. However, as the dosage requirements of most of ophthalmic molecules for local treatment is low in comparison to oral molecules, the reduction in the overall bioavailability is balanced, allowing us to follow RO5 guidelines in drug design. [2-3]

Chemical derivatization strategies such as prodrug derivatization, have been employed to improve trans-membrane permeation. The prodrug approach provides a strategy to modulate the lipophilicity, solubility, ionization and stability of the drug candidate and, thus, improve ocular penetration.[4] Hussain et al. introduced the prodrug concept was introduced to the field of

ophthalmology in 1976[5] to enhance the absorption of a highly polar molecule, epinephrine, through lipid membranes.[6] Since then, various prodrugs have been designed to improve physicochemical properties of therapeutic agents. This strategy involves modification of the active moiety into various derivatives in a fashion that imparts some advantage, such as membrane permeability, site specificity, transporter targeting and improved aqueous solubility, over the parent compound. The application of prodrug strategies to ocular drug delivery provides an option of enhancing drug penetration into the ocular tissues, and overall ocular bioavailability, with minimum disruption of the ocular diffusion barriers. A prodrug/analog strategy has been, and is being, employed to overcome barriers in ocular delivery for some drug molecules, utilizing a chemical modification approach rather than a formulation-based approach. Although success of the prodrug strategy is contingent on various factors, such as the chemical structure of the parent molecule, aqueous solubility and solution stability, capacity of targeted transporters and bioreversion characteristics, this approach has been successfully utilized, commercially and therapeutically, in several cases. Ocular bioavailability cannabinoids such as Δ^9- Tetrahydrocannabinol (THC) and Cannabidiol (CBD) can be enhanced by employing this strategy.

The other strategy, that can be employed to improve bioavailability, is a formulation-based approach. Retention of the formulation on the ocular surface and penetration of the active ingredient into the ocular tissues are critical parameters governing the effectiveness of topical application. Conventional formulation strategies involve the use of viscosity enhancers such as hydroxyethyl cellulose and hydroxypropyl methyl cellulose, or penetration enhancers such as cyclodextrins, benzalkonium chloride or surfactants, in solution and suspension formulations.[7] The formulator may also opt for gels, ointments and other viscous formulations to improve residence time on the surface.[8-9]

Improving the viscosity improves the contact time of the active ingredient with the corneal surface and improves flux but does not improve the corneal membrane permeation characteristics of the molecules. Nanocarriers, such as liposomes, niosomes, lipid nanoparticles and nanoemulsions, are a few of the innovative strategies that can encapsulate a wide range of drugs. Vesicular carriers such as liposomes have an added advantage in that they can load both hydrophilic as well as lipophilic molecules and provide an option for surface modification. The use of a vesicular system is, however, associated with problems such as limited drug loading, short-term stability, unwanted side effects and difficulty with sterilization.[10-11] Lipid-based nanoparticulate systems have recently gained interest for ocular delivery. Solid lipid nanoparticles (SLN) and nanostructured lipid carriers (NLC) show promise because of better biocompatibility, enhanced corneal retention and permeation of the nanoparticles.[12-13] The formulation approaches, however, do not change the ability of the compounds themselves to diffuse across membranes.

Ocular drug delivery remains a major challenge for formulators because of the unique structural organization of the eye. To understand the fate of the drug in the ocular tissues and overcome the barriers to drug absorption, it is necessary to study the anatomy of the eye (Figure 1.), organized into an anterior segment and a posterior segment. Therapeutic agents may need to be targeted to one or both segments of the eye.

Anatomical and physiological considerations for drug delivery

Ocular drug delivery remains a major challenge for formulators because of the unique structural organization of the eye.[14-16] To understand the fate of the drug in the ocular tissues and overcome the barriers to drug absorption, it is necessary to study the anatomy of the eye (Figure 1.), which is organized into an anterior segment and a posterior segment.[17] Therapeutic agents may need to be targeted to one or both segments of the eye. The anterior segment is composed of the

crystalline lens suspended from the ciliary body, and the structures anterior to it; namely, the cornea, the iris and the two chambers containing aqueous humor: the anterior and the posterior chambers. The anterior chamber contains approximately 0.25 mL of aqueous humor and is bound anteriorly by the back of the cornea and posteriorly by the iris and a part of the ciliary body. The posterior chamber consists of approximately 0.06 mL of aqueous humor and is bound anteriorly by the iris and a part of the ciliary body and posteriorly by the crystalline lens.[18-19] The aqueous humor is a clear, colorless fluid, secreted by non-pigmented epithelial cells of the ciliary body, with a chemical composition similar to that of blood plasma, but with a low protein content.[20] The sclera, retina-choroid, vitreous humor and optic nerve make up the posterior segment, of which the vitreous humor, a hydrophilic gel matrix, makes up 80% of the volume of the eye.[14, 18, 21-24]

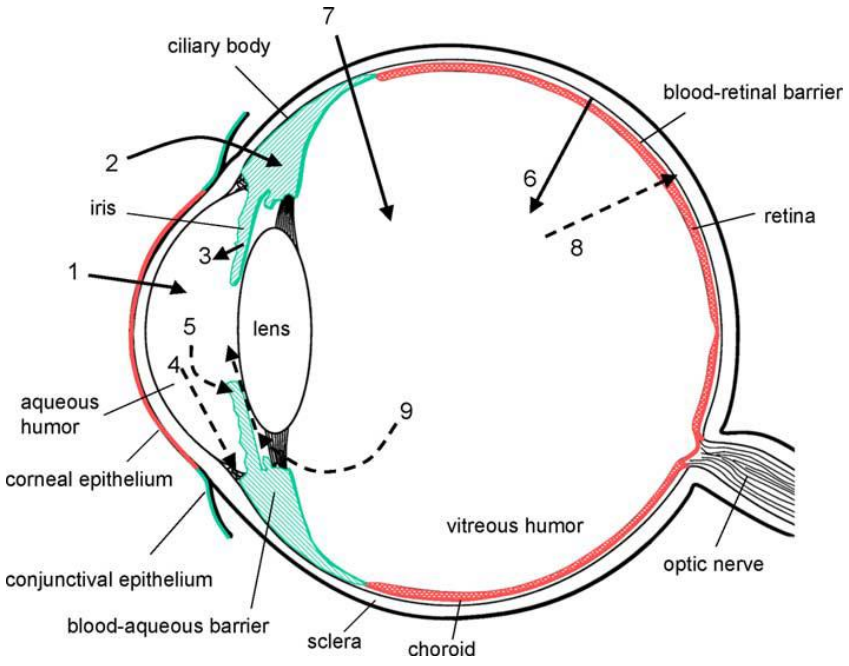

Figure 1. Physiological barriers to ocular drug delivery (diffusional barriers are indicated in red, elimination route is indicated in green). A major pathway for ocular penetration of topically administered therapeutic agents is via the cornea (1). Some large and hydrophilic drugs prefer

the conjunctival and scleral route, and then diffuse into the ciliary body (2). After systemic administration small compounds can diffuse from the iris blood vessels into the anterior segment (posterior chamber) (3). From the anterior segment the drugs are eliminated either by aqueous humor outflow (4) or by venous blood flow - diffusion across the iris surface (5). Systemically administered therapeutics agents must pass across the retinal pigment epithelium or the retinal capillary endothelium to reach the retina and vitreous humor (6). Alternatively, drugs can be administered by intravitreal injection (7). Drugs are eliminated from the vitreous via the blood–retinal barrier (8) or via diffusion into the anterior chamber (9).

Topical delivery is the preferred and patient-friendly technique for treating diseases of the anterior segment and involves instillation of the eye drops into the conjunctival cul-de-sac. A topically applied formulation, however, has to overcome multiple pre-corneal barrier mechanisms, such as dilution, overflow, tear-fluid enabled lacrimal drainage and conjunctival absorption resulting in elimination from the pre-corneal area.[17, 25-26] The ocular tissues maintain a highly regulated environment for visual cells and transparent tissues. Ocular barriers, namely the Blood-Aqueous Barrier (BAB) and the Blood-Retinal Barrier (BRB), play a vital role in the protection of the eye and the maintenance of ocular functions by restricting the entry of xenobiotics, consequently challenging the passage of therapeutic drug molecules into the ocular tissues.[27]

The cornea is the outermost tissue in the anterior ocular segment and consists of five layers: the epithelium, Bowman's membrane, the stroma, Descemet's membrane, and the endothelium.[28-29] The corneal epithelial cells are connected to each other via desmosomes and express tight-junctions that act as a rate-limiting barrier for hydrophilic molecules.[30-31] Lipophilic drugs, depending on biopharmaceutical characteristics such as solubility, partition coefficient, ionization

and charge and polar surface area, demonstrate better transcellular permeation compared to hydrophilic molecules.[32-33] The stroma underlying the corneal epithelium, however, is hydrophilic in nature.[34] Additionally, efflux pumps present on the corneal and conjunctival membranes restrict the entry of substrates (mostly lipophilic in nature) into the deeper ocular tissues.[29, 35-37] Thus, therapeutic agents must possess optimal physicochemical and biopharmaceutical characteristics to permeate efficiently across the total corneal membrane. The non-corneal route of absorption encompasses conjunctival pathways, and favors hydrophilic and large polar molecules.[14, 38-39] The BAB and the BRB also limit the passage of both hydrophilic and lipophilic molecules by virtue of the tight-junctions and efflux mechanisms present.[14, 36, 40-43] Both systemic and periocular delivery are affected by the presence of the BAB and BRB.

Designing a stable formulation delivering effective amounts of API to the desired site of action involved several steps, such as preformulation screening, stability and solubility of the API, determination of the route of delivery and an appropriate formulation strategy, excipient selection and compatibility, process parameters and scale up[44]. The drug product development process for any molecule is a multi-variate process and these variables could be interdependent, affecting the efficacy of the optimized formulation. In this situation, instead of running random trials, by changing single variable, using Quality by Design (QbD) principles for formulation and process development a more cost effective and time efficient technique. This process involves setting up a target product profile for the product, within its safety and efficacy limitations, identifying critical quality attributes (CQAs) that affect the final drug product properties, coming up with a manufacturing process that meets the CQAs for the final drug product, identifying the main effects or the critical process parameters (CPPs) that control the critical material attributes of the final product. The different tools utilized by QbD are Design of Experiment (DOE), process analytical

technologies (PAT) and risk assessment. Using DOE for formulation optimization is a systematic way of analyzing effects of independent variables and interactions on the final formulation properties (response variables). Constructing a robust model using these variables results in establishing a predictive design space, helping us design an optimum formulation as also establish the edge of failure.

QbD principles can also be applied to optimization of pharmaceutical manufacturing processes such as tableting or homogenization or even filling. A process optimization DOE would help establish equipment limits and optimum conditions for processing the material, in turn increasing process efficiency. Applying QbD principles to developing processes involves similar steps, keeping in mind a target product profile, identifying the CQAs for the product and establishing the CPPs for the process in concern. The design space constructed facilitates understanding of the relationship between CPPs and CQAs of the product in question. A pharmaceutical capping process is a critical process that ensures the optimized drug product is protected from external stresses. Depending on the equipment in use, there are various CPPs (main effects) that affect the CQA, which in this case would be an acceptable crimp ensuring container closure integrity through the product cycle. The final chapter would discuss one such process optimization for a stopper-vial combination for storage and shipping at frozen conditions.

The work described herewith would employ prodrug/analog strategy, formulation strategy and both to enhance ocular bioavailability of the target molecule. In entirety, the research chapters described henceforth would talk about various aspects of the path followed by a small molecule ophthalmic from the bench to the final product. The initial chapters would discuss work on the cannabinoids in early discovery phase: THC and CBD, their prodrugs and analogs respectively. The THC chapter aims at improving the ocular bioavailability of the molecule by means of

optimizing a novel formulation of its prodrug, THC-VHS. The therapeutic potential of this novel formulation was evaluated in a set of preclinical pharmacokinetic-pharmacodynamic (PK-PD) studies in a small animal model. The primary goal of the CBD chapter was to screen CBD analogs in an *in vitro* setup. Furthermore, the efficacy of a few lead candidates was evaluated in a small animal model. Apart from Cannabinoids, formulation optimization of anti-inflammatory agents (Triamcinolone Acetonide), antifungals (Voriconazole) and antimicrobial agents (Ciprofloxacin) was undertaken by statistical DOE. The final chapter discusses pharmaceutical capping process optimization for drug products meant for cold storage. This work tries to unify pharmaceutical unit operations such as capping and filling at a laboratory scale and a manufacturing scale by modeling a predictive design space for that operation.

Specific Aims

1. To evaluate ocular bioavailability of CBD analogs with a range of physicochemical properties and establish *in vitro-in vivo* correlation.
2. To evaluate the intra-ocular pressure (IOP) lowering efficacy and ocular tissue disposition of THC and its prodrug, THC-VHS in nanoemulsion and solid lipid nanoparticulate formulation.
3. To study the effect of surface modification of Triamcinolone Acetonide Nanostructured Lipid carriers with Chitosan and Chitosan derivatives on the permeation profile of the same
4. Anti-fungal & Anti-bacterial PEGylated-NLCs for ocular applications: Formulation Development, Characterization and In vitro Efficacy Testing
5. Optimization of Capping Parameters for Low Temperature Storage of a Plastic Vial-Rubber Stopper Combination

CHAPTER 2

ANALOG DERIVATIZATION OF CANNABIDIOL FOR IMPROVED OCULAR PERMEATION

Introduction

Non-inflammatory disorders such as diabetic retinopathy (DR) might occur as a result of inflammatory mediators, needing anti-inflammatory agents as a part of clinical therapy. [45] DR is one of the leading causes of vision loss in working age adults and the fifth most common cause of moderate to severe vision impairment. [46-47] Studies testing the global prevalence of DR reported 285 million people with diabetes, one third of whom show symptoms of DR. [48] DR involves leakage of the retinal blood vessels leading to distorted vision. Breakdown of the blood-retinal barrier leads to further vision loss through macular edema and retinal neovascularization. [49-50] Degeneration of the retinal cells may be caused by a mechanism involving tyrosine nitration and may include a vascular endothelial growth factor (VEGF) triggered breakdown component.[51-52] Diabetic retinas have shown an increase in the vascular permeability which can be associated with increase in VEGF and tumor necrosis factor alpha (TNFα) pointing towards pro-inflammatory roots of this disease.[53] High glucose conditions in diabetic retinas stimulates endothelial apoptosis by activation of p38 MAP kinase.[54]

Current treatment options for DR include laser photocoagulation, vitreoretinal surgery and intravitreal injections of anti-VEGF and steroids. Laser photocoagulation is the recommended

therapy for DR; however, laser photocoagulation is associated with neural tissue death raising the need for the development of non-invasive therapies for DR. [55] Intravitreal steroid therapy often leads to unwanted side effects such as elevated intra-ocular pressure, cataracts and advent of opportunistic infections. [56-57] Ophthalmic surgical procedures such as vitreoretinal surgeries are often accompanied by post-surgical complications such as elevated intra-ocular pressure, endopthalmitis and cataract formation.[58]

Discoveries pertaining to the involvement of the endocannabinoid system in modulation of ocular pain and inflammation open new avenues for targeting the cannabinoid receptor system (CB_1 and CB_2) for the management of ocular inflammatory conditions. [59-60] CB_1 are $G_{i/o}$-protein-coupled receptors expressed in the central nervous system (CNS) especially in the basal ganglia, cerebellum and hippocampus. They are also located in the periphery, including the retina, sperm cells, testis, colonic tissues and peripheral neurons. [61-63] While CB_2 receptors are located in the immune system; there have also been reports of localization of CB2 receptors in the retinal cells. [61, 64-67]

CBD is a major cannabinoid of the plant *Cannabis sativa*, free of cannabimimetic CNS activity, possessing neuroprotective, anti-emetic and anti-inflammatory properties [68]. Possible explanations for the anti-inflammatory activity of CBD could be its ability to interact with CB_2 receptors and inhibiting immune cell migration.[69] Moreover, CBD acts as an effective anti-oxidant by scavenging reactive oxygen species (ROS) and blocking NADPH oxidase [50]. CBD has been shown to decrease retinal inflammation by blocking ROS and TNFα formation and by p38 MAP kinase activation.[50] It has also been reported to exert anti-inflammatory activity by inhibiting adenosine re-uptake in rat retinal microglial cells. [70] Thus, CBD, by virtue of its anti-inflammatory

properties, might be a treatment option for DR induced pain and inflammation, by modulating the formation of TNFα and scavenging ROS.

El-Remessy et al. demonstrated neuroprotection in NMDA-induced retinal neurotoxicity in rats via the anti-oxidant effect of CBD [50]. They also determined the effect of blocking oxidative stress on the BRB preservation in diabetic rats [50]. The benefits of CBD, i.e. blocking oxidative stress and inhibiting adenosine reuptake to enhance a self-defense mechanism against retinal inflammation, potentially represents a novel therapeutic approach for the inflammatory complications of the eye. [70]

CBD (Figure 2A) is a lipophilic molecule with a Clog P of 5.91 making its topical delivery to treat retinal inflammation extremely challenging. In order for CBD to produce a therapeutic effect, the molecule has to transverse across the static ocular layers and the dynamic blood-ocular barriers to reach the back of the eye [71]. This work aims at improving ocular penetration of CBD by means of bio-engineered analog derivatization. Through structural modifications in the molecule, inherent molecular properties such as molecular size, structural conformation, lipophilicity, solubility etc. were optimized to increase the "druglikeness" of the molecule.

CBD-amino acid ester (CBD-AA) analogs are prepared by linking one or both of its hydroxyl groups to an amino acid such as L-Valine, via an ester linkage, to form CBD-monovalinate (CBD-Mono-Val) and CBD-divalinate (CBD-Di-Val), respectively (Figures 2B & C). L-Valine has previously been reported to improve the transport of the molecule acyclovir and ganciclovir [72]. The electron releasing-electron withdrawing properties of the side chain determine the stability of the bond. The parent molecule, as a virtue of its steric bulk is lipophilic and incorporation of an ionizable group in this structure attempts to increase its aqueous solubility. Hemi-esters of dicarboxylic acids have been known to enhance the solubility of

methylprednisolone, chloramphenicol, propranolol and a few other drugs [73-76]. CBD-dicarboxylic acid (CBD-DCA) analogs were synthesized (Figure 2D) by attaching a dicarboxylic acid, such as succinic acid to both hydroxyl groups of CBD (CBD-HS). Another derivatization approach employed synthesis of CBD-amino acid- dicarboxylic acid ester (CBD-AA-DCA) analogs by linking a dicarboxylic acid such as succinic acid to the free amino group of the CBD-AA to form CBD-monovalinate-monohemisuccinate (CBD-Mono-VHS) (Figure 2E) and CBD-divalinate-dihemisuccinate (CBD-Di-VHS) (Figure 2F), respectively. The rationale behind this modification was to impart the stability in biological matrix as achieved by the AA analogs and solubilize the molecule at physiological pH by including an ionizable group. Moreover, addition of an ester bond after the amide bond increases the stability of the amide bond. The physicochemical properties of the synthesized analogs are mentioned in Figure 2.

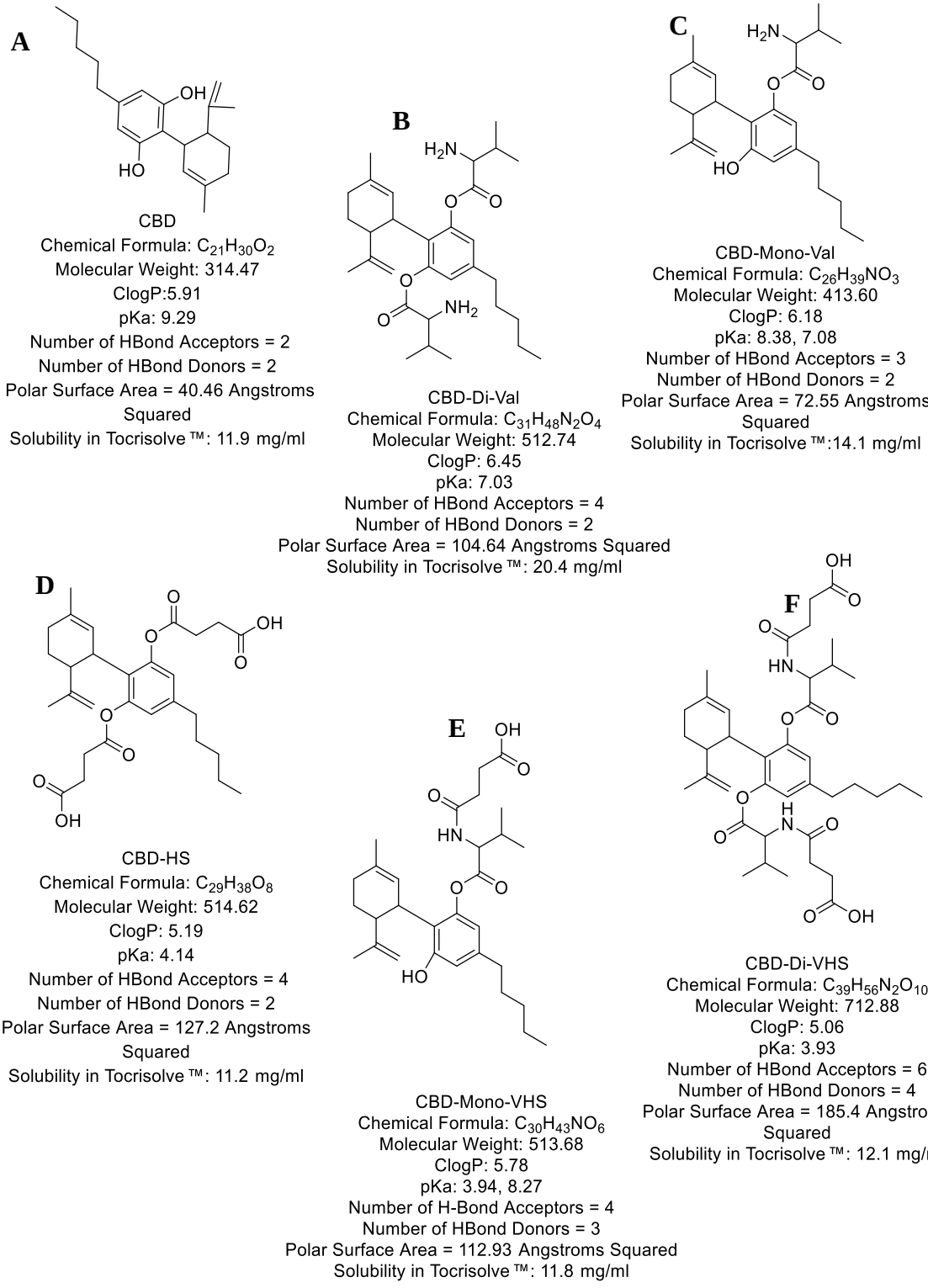

Figure 2. Structures, chemical formulae and physicochemical parameters of CBD and biologically active CBD-analogs

Materials

CBD analogs were synthesized by ElSohly Labs Inc. [77]. Tocrisolve™ was purchased from Tocris® Bioscience, Bristol, UK. High performance liquid chromatography (HPLC) - grade solvents, and other chemicals (analytical grade) were obtained from Fisher Scientific (Hampton, NH, USA).

Animals

Male New Zealand White rabbits (2-2.5 kg), obtained from Harlan laboratories® (Indianapolis, IN) were used in all studies. All animal experiments conformed to the tenets of the Association for Research in Vision and Ophthalmology statement on the use of animals in ophthalmic and vision research. All experiments followed the University of Mississippi Institutional Animal Care and Use Committee approved protocols.

Methods

Stability of CBD and Analogs in Ocular Tissue Homogenates

Tissue Preparation

The degradation of CBD analogs was determined in aqueous humor (AH), vitreous humor (VH), iris-ciliary bodies (IC), and retina-choroid (RC). The tissues were shipped on dry ice from Pel-Freez Biologicals; AR. Ice-cold isotonic phosphate buffer (IPBS) was used to homogenize the solid tissues, RC and IC, in an ice bath using a TISSUEMISER (Fisher Scientific). The homogenates were then centrifuged at 13,000 rpm at 4°C for 15 minutes. The protein contents of the supernatants were determined according to the method of Bradford and were adjusted to approximately 1 mg/mL. [78]

Hydrolysis Procedure

Enzymatic degradation of CBD and analogs was studied at 37°C in a shaking water bath. The tissue homogenates were equilibrated for 30 minutes at 37°C to activate the enzymes. To 1.9 mL

of the supernatant, 100 µL of the CBD/analog stock solution were added to make the final CBD/ analog concentration as 25 µg/mL (analog concentration spiked for CBD-di-Val was 50 µg/mL). At predetermined time-points, 100 µL aliquots of the sample were withdrawn up to 6 hours post initiation. An equal volume of ice-cold acetonitrile was added to each sample to arrest the enzymatic degradation. The samples were centrifuged at 13,000 rpm for 15 minutes and the supernatant was analyzed for analog/CBD content using HPLC-UV.

Chromatography methods

Analytical method for *in vitro* samples

The *in vitro* samples were analyzed for CBD and analogs using an HPLC-UV system comprising a Waters 717 plus Auto sampler, Waters 600E pump controller, Waters 2487 dual λ Absorbance detector and an Agilent 3395 integrator. Stock solutions of CBD and analogs were prepared in acetonitrile. A gradient method (Table 1.) was used for elution of CBD and analogs with the mobile phase consisting of Acetonitrile and 5 mM Phosphate buffer (pH 2.5). A Phenomenex® C18 (4.6 x 150 mm) column was used at a flow rate of 1 mL/min. Detection was carried out at 222 nm.

Table 1. HPLC gradient method for separation and quantification of CBD and analogs

Time (min)	Flow (mL/min)	% Acetonitrile	% Buffer
0	1	75	25
3-6	1	95	5
7-15	1	75	25

Preparation of topical ophthalmic nanoemulsion of CBD/analogs

CBD and the associated analogs were formulated into a soybean-oil based nanoemulsion composed of a 1:4 ratio of soya oil/water that was emulsified with the block co-polymer Pluronic F68 (Tocrisolve™). The formulations were prepared by adding the drug/analog to the blank emulsion. This mixture was vortexed for five minutes followed by sonication for ten minutes. For quantification of CBD and analogs in the nanoemulsion, the formulations were centrifuged at 9000 rpm for 5 min at 25°C. The solubility of CBD and the analogs is listed in Figure 2.

Distribution of CBD and analogs in ocular tissues after topical administration

In vivo bioavailability of CBD and analogs was determined in Male New Zealand White Albino (NZW) rabbits, weighing between 2 and 2.5 kg, procured from Charles River Labs. CBD and its analogs, namely CBD-Di-VHS, CBD-Di-Val, CBD-Mono-Val, CBD-Mono-VHS and CBD-HS were formulated in Tocrisolve™ emulsion. These formulations were evaluated *in vivo* in a conscious rabbit model, at least in triplicates (n = 3). The initial study compared ocular penetration of CBD-Di-VHS and CBD-Di-Val to that of CBD. The second study compared the ocular bioavailability of CBD-Mono-Val, CBD-Mono-VHS, CBD-HS and CBD. Concentration of the CBD analog as well as CBD were determined in the AH, VH, RC and IC. Fifty microliters of the above formulations were dosed topically (Dose: 250 μg CBD equivalent) - instilled in the conjunctival sac of the NZW rabbits. Ninety minutes after dosing the rabbits were anesthetized using a combination of ketamine (35 mg/kg) and xylazine (3.5 mg/kg) injected intramuscularly. The rabbits were euthanized with an overdose of pentobarbital injected through the marginal ear vein. The eyes of the rabbits were then enucleated and washed thoroughly with IPBS and the intraocular tissues such as IC, AH and VH were separated.

Tissue sample preparation and extractions

A protein precipitation technique was employed to determine the amount of CBD and analogs in the ocular tissue homogenates. The solid tissues, namely IC (50 mg) and RC (30 mg) were cut into small pieces and homogenized with ice-cold IPBS in an ice bath using a TISSUEMISER (Fisher Scientific), whereas, the liquid tissues, AH (50 µL) and VH (100 µL) were taken as they were. For the calibrators, standards were prepared by spiking the tissues with CBD and the analogs to yield final concentrations of 2.5, 5, 10, 25, 50, and 100 ng/ml. Twenty-five microliters ice-cold acetonitrile, precipitating proteins from individual tissues. Samples were vortexed and kept aside for 10 minutes. The supernatant was collected after centrifuging for 30 minutes at 13,000 rpm and analyzed using LC-MS/MS.

Bio-analytical quantification method

Analysis was performed on two LC-MS-MS systems consisting of a Shimadzu Prominence HPLC with a dual pump, a vacuum solvent micro degasser, a controlled-temperature autosampler, and an MS-MS detector (Applied Biosystems/MSD Sciex Qtrap 3200 and 4500 with a turbo-ion ESI source operating the positive-ion multiple reaction monitoring, or MRM, mode). Specific MRM transitions were monitored for each compound for maximum selectivity and sensitivity. Separation was achieved on a Synergi Hydro-RP column (50 x 3.00 mm; 2.5 µm; 100 Å) from Phenomenex (Torrance, CA, USA). Water with 0.1% Formic acid (Pump A) and Acetonitrile with 0.1% Formic acid (Pump B) were used as the mobile phase with a gradient elution. Data acquisition and processing were performed with Analyst™ 1.6.2 software (Applied Biosystems (AB Sciex), Foster City, CA).

Statistical analyses

Data is represented as the mean ± standard deviation, for a minimum of three independent experimental runs. Statistical comparisons of the means were performed using one-way analysis of variance (ANOVA) or Student's t-test. The differences were considered significant when the p-value was < 0.05.

Results and Discussion

Physicochemical characterization of analogs

To improve aqueous solubility and tissue permeability, the parent molecule was derivatized; the aim of analog design was to modify molecular properties in the desired direction. Physicochemical parameters such as molecular weight, log P, pKa, hydrogen bond donors and acceptors and polar surface area, were estimated using the ChemDraw software (PerkinElmer®) to obtain a better understanding of the membrane permeation characteristics of the molecule. Figure 1. lists the computed physicochemical parameters for CBD and analogs. Optimum physicochemical parameters would in turn prove to be efficient predictors of overall ocular bioavailability. The RO5 defined by Lipinski determines limitations for drug design for an oral targeted molecule to be successful through all the stages of drug development (molecular weight 500, log P 5, H-bond donors 5, H-bond acceptors 10). With a few modifications, we can utilize the Lipinski's RO5 in designing molecules for non-oral routes of delivery. [2-3]

Stability of CBD and analogs in ocular tissue homogenates

Stability of CBD in ocular tissue homogenates

The stability of CBD in the biological matrix and its resistance to enzymatic attack is shown in Table 2. CBD was stable in most of the ocular tissues tested. Some degradation is observed in the iris-ciliary bodies.

Table 2. Stability of Cannabidiol in ocular tissue/tissue homogenates.

Tissue	Time (min)	0	15	30	45	60	90	120	180	240	360
Aqueous Humor	**CBD (µg/mL)**	31.3	29.8	31.8	30.0	29.4	29.3	23.9	30.5	32.6	26.3
Vitreous Humor	**CBD (µg/mL)**	30.9	34.2	34.5	34.4	32.9	34.0	37.4	44.2	34.9	32.0
Retina Choroid	**CBD (µg/mL)**	30.0	19.9	34.3	34.2	31.9	34.5	36.2	28.4	34.1	32.0
Iris Ciliary bodies	**CBD (µg/mL)**	16.6	12.5	15.1	11.2	10.9	14.8	13.8	12.5	10.9	7.3

Stability of CBD-Di-Val in ocular tissue homogenates

The results (Figure 3) suggest that CBD-Di-Val is enzymatically hydrolyzed in some of the ocular tissues with detectable levels of CBD observed ninety minutes post initiation of the study. The half life of CBD-Di-Val in AH and VH was 5.78 h and 2.89 h respectively, with apparent first order degradation rate constants of $0.33x10^{-4}$ h^{-1} and $0.67x10^{-4}$ h^{-1}. The delayed and restricted generation of CBD could be explained by possible formation of intermediate degradation products such as CBD-Mono-Val. AA derivatives synthesized with promoeties such as valine, isoleucine, phenylalanine etc. have been reported to provide stability to hydrolytic attack in comparison to the DCA analogs due to the presence of steric groups such as branched aliphatic amino acid (valine) or aromatic amino acid (phenylalanine). [79-82] CBD-Di-Val is a lipophillic molecule with a clog P of 6.45 (Figure 1.), and shows limited dissolution in the homogenized tissues. Figure 3. depicts low initial concentrations of CBD-Di-Val followed by a slight increase and steady analog concentrations through the duration of the study. This behaviour could be attributed to the drug concentrations exceeding equilibrium solubility in the biological matrices, leading to possible precipitation of the analog followed by continual dissolution of the same in the tissue matrix leading to an equilbrium between the drug in solution and undissolved drug. In solid tissues, IC

and RC, no CBD as a breakdown product was observed. However,a decline in the analog levels were detected. This could again be attributed to generation of intermediate degradation products and the resistance of the analog to hydrolytic attack.

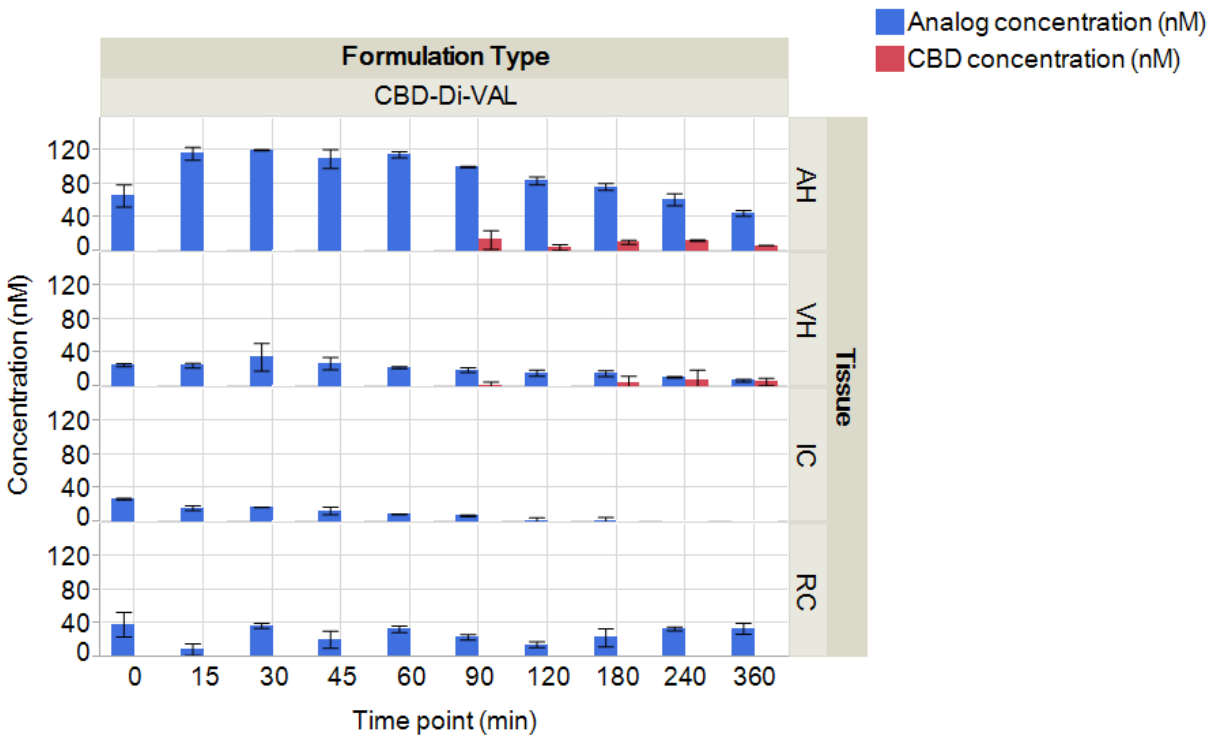

Figure 3. In vitro enzymatic stability of CBD-Di-Val in ocular tissue homogenates; Aqueous Humor, Vitreous Humor, Retina Choroid and Iris Ciliary Bodies. The blue bars represent CBD-Di-Val concentrations (nM) and the red bars represent regenerated CBD (nM) concentrations.

Stability of CBD-HS in ocular tissue homogenates

CBD-HS, like CBD-Di-Val, is enzymatically hydrolyzed in some of the ocular tissues (Figure 4). The half life of CBD-HS in AH and VH was 13.07 and 13.52 minutes, respectively, with apparent first order degradation rate constants of 0.053 and 0.051 min^{-1} respectively. Furthermore, the AH, VH and IC data shows constant CBD-HS levels initially with a sudden drop, below detection levels

hinting towards solubility issues of the analog and the stability of ester bond governing the overall rate of the reaction, with it changing from pseudo-zero to first-order degradation process. The delayed generation of CBD suggest formation of an intermediate degradation product, like CBD-Mono-HS, before generating CBD or a different degradation pathway.

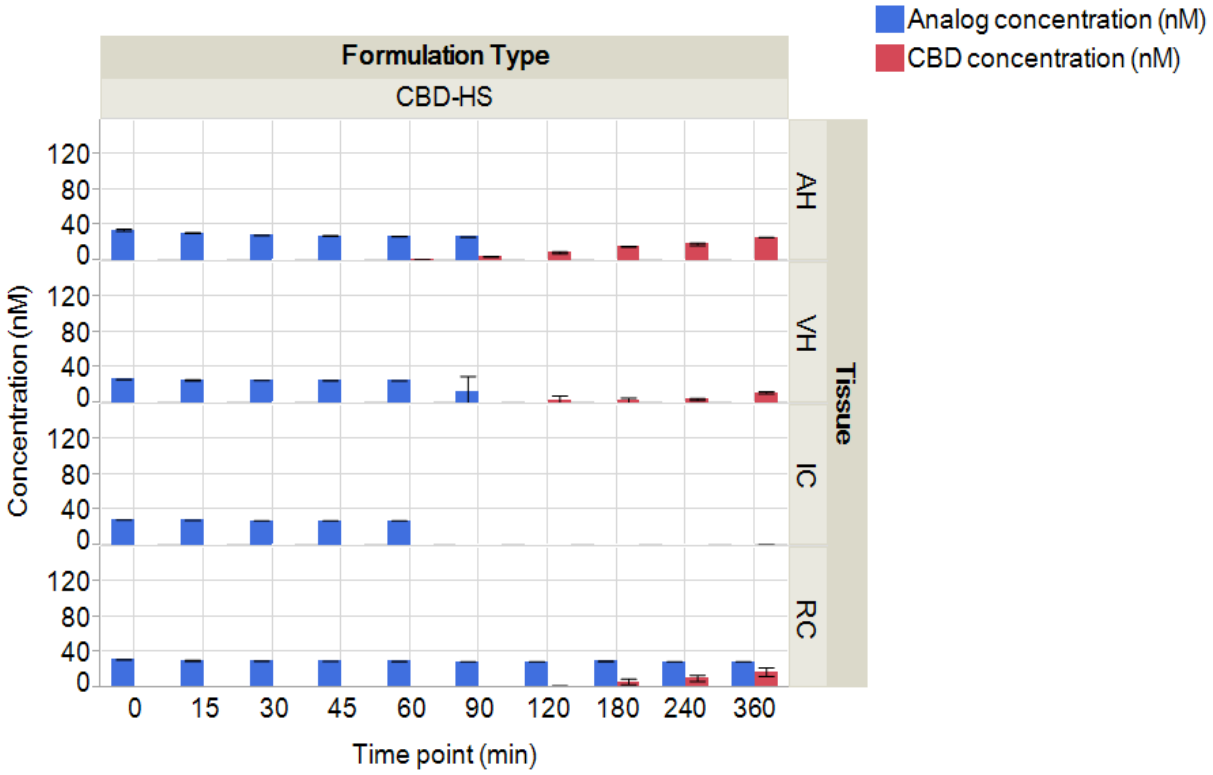

Figure.4. *In vitro* enzymatic stability of CBD-HS in ocular tissue homogenates; Aqueous Humor, Vitreous Humor, Retina Choroid and Iris Ciliary Bodies. The blue bars represent CBD-HS concentrations (nM) and the red bars represent regenerated CBD (nM) concentrations.

The half life of CBD-HS in IC was 16.5 minutes and the apparent first order degradation rate constant was 0.042 min^{-1}. The observed bioconversion in IC was similar to the results for bioconversion of CBD-Di-Val in IC; CBD-HS failed to regenerate CBD through the duration of

the study. We can attribute this phenomenon to secondary degradation products formed due to precence of multiple sites for hydrolytic attack and presence of unexplored degradation pathways. The results in RC point towards formation of an initial supersaturated solution followed by precipitation and generation of an equilibrium between the solid state and solution state as evidenced by CBD-HS levels remaining almost constant even though generation of CBD is observed two hours post initiation. [76, 82].

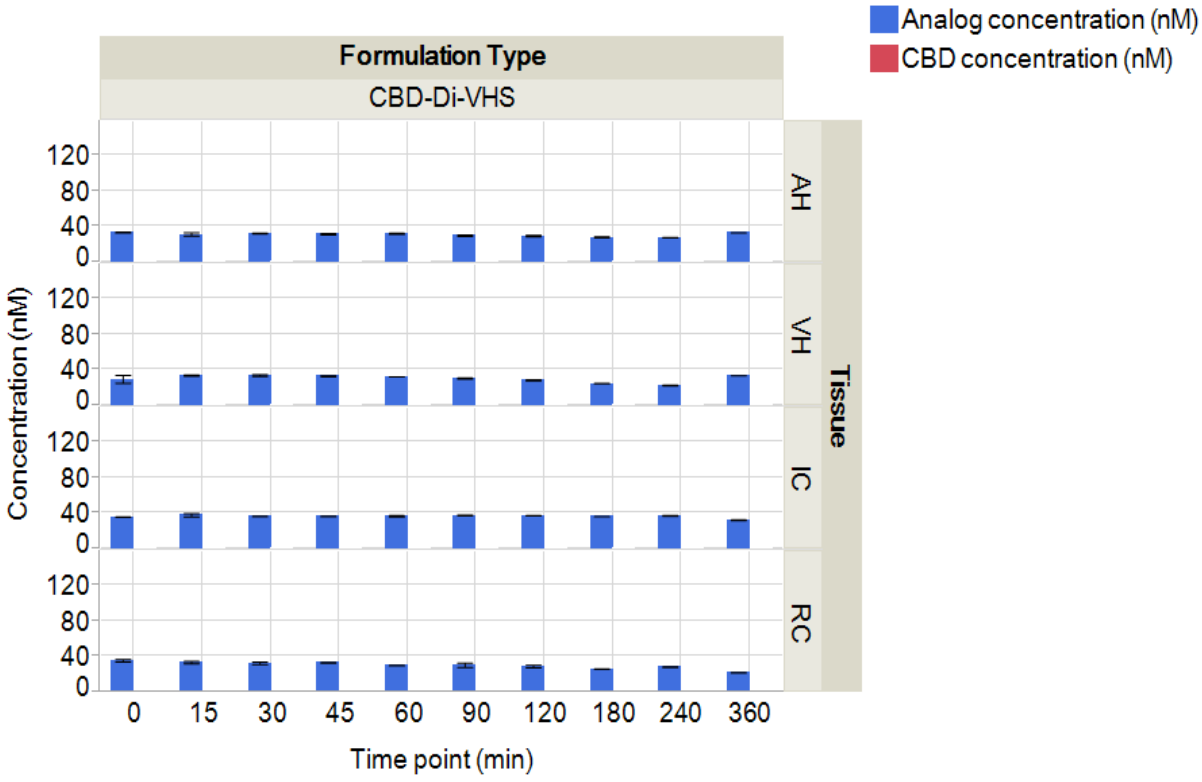

Figure.5. *In vitro* enzymatic stability of CBD-Di-VHS in ocular tissue homogenates; Aqueous Humor, Vitreous Humor, Retina Choroid and Iris Ciliary Bodies. The blue bars represent CBD-Di-VHS concentrations (nM) and the red bars represent regenerated CBD (nM) concentrations.

Stability of CBD-Di-VHS in ocular tissue homogenates

CBD-Di-VHS demonstrates excellent stability in the ocular tissues without any CBD generation even after a 6 h exposure (Figure 5.). This is consistent with the results observed with CBD-Di-Val and CBD-HS since the increased chain length leads to steric hindrance and provides greater protection from enzyme attack. Moreover, the number of intermediates that can form are double that with CBD-Di-Val and CBD-HS. Out of all the analogs tested, CBD-Di-VHS was observed to be the most stable, with no degradation within the study duration, whereas, CBD-Di-Val and CBD-HS regenerated CBD but at a slow rate.

The *in vitro* data points towards the solubility of the analogs, the stability of the ester bond, involvement of different degradation pathways and formation of multiple degradation intermediates as a possible explanation for the low rate of bioconversion observed in the biological matrices of the analogs and generation of CBD.

Distribution of CBD and Analogs in ocular tissues after topical administration

First PK Study

Fifty microliters of three formulations were dosed in the first study, CBD, CBD-Di-Val and CBD-Di-VHS (n=6) in Tocrisolve™ emulsion in NZW rabbits (n=3), with the dose being equivalent to 250 µg CBD (Figure 6). CBD, from CBD formulations, did not penetrate across the ocular tissues following topical instillation, with CBD being detected only in the RC tissues (17.35 ± 4.57 ng/g). This indicates that CBD, because of its physicochemical characteristics, is not suited for penetration across the ocular membranes. CBD-Di-Val formulations displaying a similar pattern - did not permeate significantly into the ocular tissues with about 9.11 ± 1.07 ng/g of the analog (equivalent to ng/g of CBD) being detected in the RC only. A potential explanation for this

phenomenon could be that CBD-Di-Val, being slightly more hydrophobic than the other analogs displays poor solubility in the tissue environment at physiological pH. In comparison to CBD, CBD-Di-Val is more lipophilic (clog P 6.45) and is a bulkier molecule, resulting in overall lower bioavailability in comparison to the parent molecule. Because of its lipophilic nature and high solubility in the oily emulsion (Figure 2), its dissolution in the tissue microenvironment serves as a rate-limiting step, preventing the molecule from partitioning into the hydrophilic tear fluid.

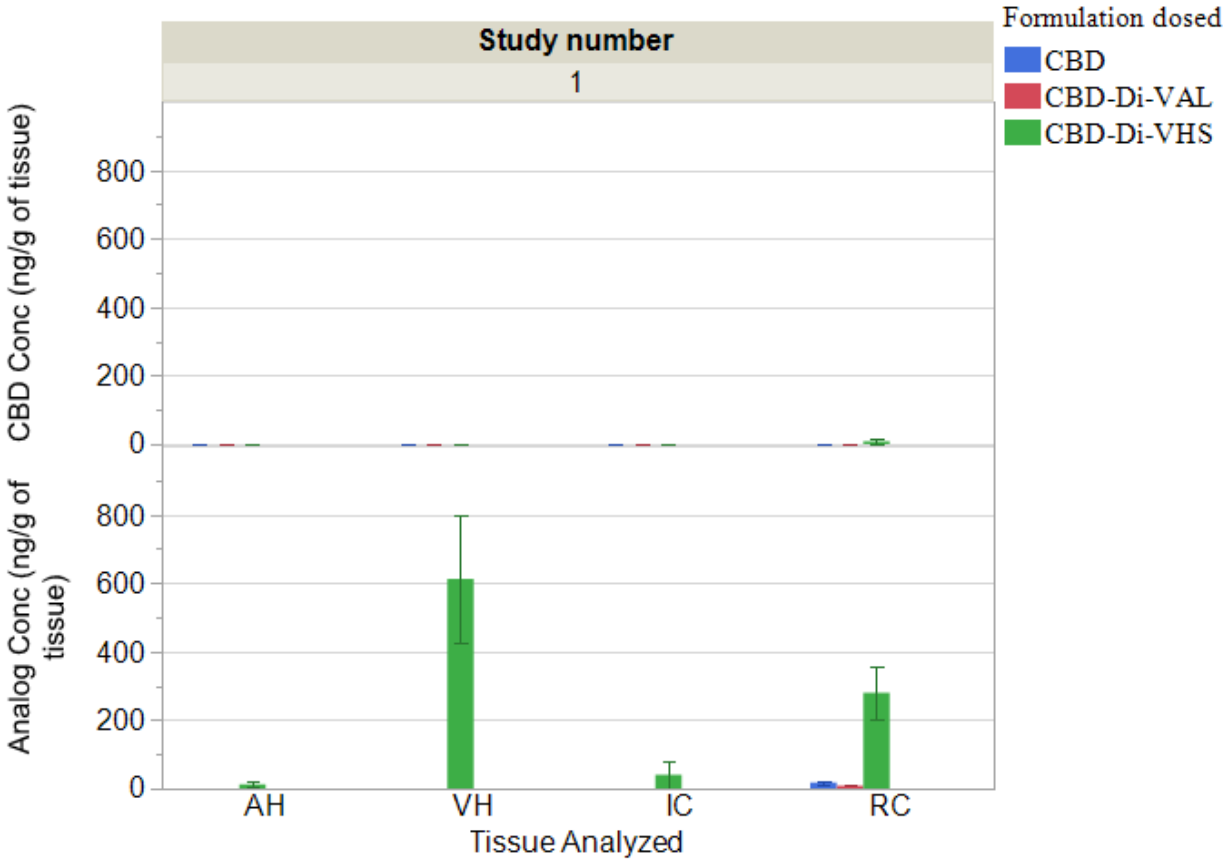

Figure 6. Ocular tissue concentrations of CBD, CBD-Di-Val and CBD-Di-VHS 90 min post topical application of CBD (0.47%), CBD-Di-Val (0.94%) or CBD-Di-VHS (1.2%) in Tocrisolve™

emulsion (Dose: 250 µg CBD; 50 µL instilled volume) respectively. Data represented is Mean ± SEM, the differences were considered significant when the p-value was < 0.05

CBD-Di-VHS, on the other hand, demonstrated significantly better ocular bioavailability. CBD-Di-VHS concentration were 612.48 ± 187.11 ng/mL (detected in three of the six test animals) in the VH and 279.77 ± 75.29 ng/g tissue weight in the RC. Concentrations in the front of the eye tissues were lower with 12.32 ± 7.53 ng/ mL in the AH and 160.31 ng/ g tissue weight in the IC (detected in IC of only one animal). The reason behind overall higher bioavailability of this compound could be its improved solubility at physiological pH. CBD-Di-VHS has a pKa of 3.93, and is charged at physiological pH, resulting in higher solubility of the analog, in turn increasing its partitioning into the tear and permeation. CBD-Di-VHS was not metabolized to CBD in the ocular tissues within the timeframe tested. This observation was consistent with the *in vitro* stability data in the tissue homogenates. The analog demonstrated surprisingly high penetration into the VH. The charge of the analog at physiological pH and the route of ocular permeation could possibly explain penetration of the analog from the RC into the VH. However, the overall tissue disposition profile of CBD and the analogs, from the nanoemulsion formulations, suggests a non-corneal route of absorption, with higher levels of the analogs present in the posterior tissues.

Second PK Study

Taking into consideration the *in vitro* and *in vivo* data of CBD, CBD-Di-Val and CBD-Di-VHS, mono derivatized AA and AA-DCA analogs of CBD (CBD-Mono-VHS, CBD-Mono-Val) were synthesized for *in vivo* evaluation, aiming to reduce the steric bulk of the molecule but retaining

the overall permeation/stability profile offered by an AA and AA-DCA analog. CBD and the DCA analog, CBD-HS, were also included in this set.

Fifty microliters of the four formulations were dosed in the second study: CBD, CBD-Mono-Val, CBD-Mono-VHS (n=6), and CBD-HS in Tocrisolve™ emulsion in NZW rabbits (n=3), with the dose being equivalent to 250 µg CBD (Figure 7). Following topical administration of CBD-HS, the analog concentrations were below detection levels in all the ocular tissues tested at the end of 90 minutes; however, bio-reversed CBD, 263.15 ± 93.33 ng/ g tissue weight in RC and 266.69 ± 35.52 ng/g in IC, were observed, consistent with the *in vitro* stability profile. CBD-HS, being a DCA analog has two ester bonds prone to hydrolysis rendering it susceptible to chemical and enzymatic hydrolysis.

Comparing the data obtained in both sets, following CBD administration, lower levels of CBD were observed in the RC in the first study, however the difference in the drug concentrations detected were not statistically significant and this variation could be attributed to biological system variability.

CBD-Mono-Val is a hydrophobic molecule with a clog P value of 6.18, (Figure 2). The lipophilic nature as well as other physicochemical characteristics of the molecule along with restricted solubility in the tissue microenvironment results in low ocular bioavailability (below detection limit in all tissues tested) as observed in the *in vivo* study.

CBD-Mono-VHS, in contrast, showed significantly higher levels of the analog in AH (94.5 ± 7.83 ng/ml), IC (728.18 ± 152.62 ng/g) and RC (603.92 ± 160.42 ng/ g tissue weight), in comparison to CBD-HS and CBD-Mono-Val (Figure 7).

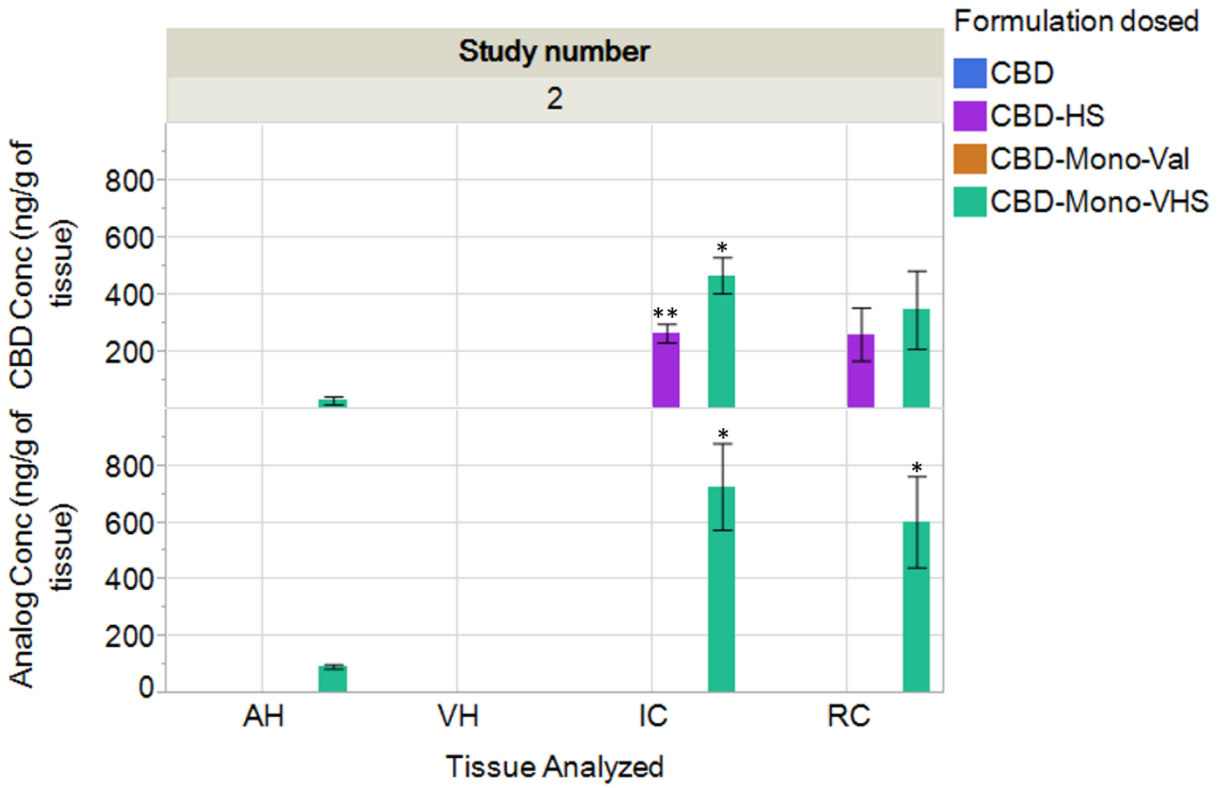

Figure 7. Ocular tissue concentrations of CBD- Mono-VHS, CBD-Mono-Val, CBD, CBD-HS 90 min post topical application in Tocrisolve™ emulsion (Dose: 250 µg; 50 µL instilled volume) respectively. Data represented is Mean ± SEM, the differences were considered significant when the p-value was < 0.05

*CBD-Mono-VHS > CBD, CBD-HS, CBD-Mono-Val

**CBD-HS > CBD & CBD-Mono-Val

The *in vivo* studies suggest that the mono derivatized form, CBD-Mono-VHS permeates more effectively than CBD-Di-VHS, with higher concentrations of the analog detected in the tissues. CBD-Mono-VHS levels are almost twice, four times and eight times higher in RC, IC and AH (Figure 7), respectively in comparison to CBD-Di-VHS (Figure 6). Looking at the ocular

bioavailability in relation to drug design, several features about the physicochemical properties of the molecule stand out (Figure 2.); CBD-Mono-VHS is a smaller molecule (M.W 513.68) in comparison to CBD-Di-VHS (M.W 712.88) and has one charged group at physiological pH, balancing its hydrophilic and lipophilic nature. The transmembrane permeation of CBD-Mono-VHS, which has a PSA of 112.93 $A^{2,}$ [is] comparatively more effective than that of CBD-Di-VHS, a more polar molecule with a PSA of 185.4 A^2. Looking at the total number of hydrogen bond donors and acceptors (Figure 2), even though both molecules follow Lipinski's RO5, CBD-Mono-VHS displays a better profile due to a lower number of donors and acceptors, giving it a comparatively better ADME profile. We also observe bio-converted CBD, following topical application of CBD-mono-VHS formulations, in RC (348.37 ± 131.17 ng/g), IC (469.09 ± 62.78 ng/g) and AH (30.66 ± 13.84 ng/ml) indicating that this analog was more prone to hydrolysis than CBD-Di-VHS.

Conclusion

The above results demonstrate that CBD displays poor ocular tissue permeation following topical application. When analogs are designed with a natural AA modification (e.g. CBD-Di-Val) or as a DCA ester (e.g. CBD-HS), penetration into the ocular tissues is not adequate. A combination of an AA and DCA (e.g. CBD-Di-VHS) strikes an effective balance between the hydrophilicity and lipophilicity and other physicochemical characteristics, effectively increasing ocular bioavailability.

CBD-mono-AA analogs, wherein one of the hydroxy groups is derivatized as a valine ester and the other hydroxyl group is unsubstituted, do not penetrate into the ocular tissues. On the other hand, when one of the hydroxyl groups is derivatized with a valine-hemisuccinate moiety and the other hydroxyl group is free (CBD-Mono-VHS), ocular bioavailability following topical application is significantly enhanced. The results suggest that the free –COOH group and stability

of the linkage plays an important role in the penetration across the ocular tissues. Amongst all the derivatives studied, the AA-DCA analog possessed optimum physicochemical properties, permeating effectively across ocular barriers.

Supporting data

Table 3**.** *In vitro* stability of CBD-Di-Val, CBD-Di-VHS and CBD-HS in ocular tissue homogenates; AH, VH, RC and IC. Analog and CBD concentrations (nM) monitored over a period of 6h.

			Analog concentration (nM)		**CBD concentration (nM)**	
Formulation Type	**Tissue**	**Time point**	**Mean**	**Std. Dev**	**Mean**	**Std. Dev**
CBD-HS	AH	0	34.9	1.15	0	0
		15	31.5	0.5	0	0
		30	29.1	0.25	0	0
		45	28.4	0.31	0	0
		60	27.6	0.17	1.19	0.23
		90	26.9	0.03	4.73	0.34
		120	0	0	9.18	1.07
		180	0	0	16.2	0.33
		240	0	0	18.8	1.43
		360	0	0	26.5	0.12
	VH	0	27	0.19	0	0
		15	26.2	0.56	0	0
		30	25.9	0.08	0	0
		45	25.8	0.1	0	0
		60	25.5	0.04	0	0
		90	12.6	17.9	0	0
		120	0	0	3.42	4.83
		180	0	0	2.5	3.54
		240	0	0	4.31	1.14
		360	0	0	12	1.31
	IC	0	29.2	0.06	0	0
		15	28.7	0.08	0	0
		30	28.4	0.02	0	0
		45	28.3	0.03	0	0
		60	28.2	0.02	0	0

		90	0	0	0	0
		120	0	0	0	0
		180	0	0	0	0
		240	0	0	0	0
		360	0	0	0.5	0.7
	RC	0	32.2	0.12	0	0
		15	31	0.74	0	0
		30	30.6	0.08	0	0
		45	30.4	0.05	0	0
		60	30.2	0.04	0	0
		90	29.9	0.01	0	0
		120	30	0.1	2.29	0.23
		180	30.3	0.49	7.14	3.09
		240	30	0.02	11.2	3.48
		360	29.9	0.01	18.2	4.85
CBD-Di-Val	AH	0	66.4	13.3	0	0
		15	117	7.76	0	0
		30	121	0.66	0	0
		45	111	11.3	0	0
		60	116	3.8	0	0
		90	101	0.9	13.9	11.1
		120	84.5	4.77	4.93	3.58
		180	77.4	4.12	11.1	2.54
		240	62.2	7.15	13.2	0.92
		360	45.7	3.28	7.31	0.2
	VH	0	26.1	1.93	0	0
		15	25.5	2.8	0	0
		30	35.4	16.5	0	0
		45	27.9	7.34	0	0
		60	23	1.3	0	0
		90	20.3	2.94	2.44	3.45
		120	16.5	3.74	0	0
		180	15.9	3.44	5.34	7.56
		240	11.7	0.72	8.36	11.8
		360	7.7	1.63	5.95	4.55
	IC	0	27.7	0.96	0	0
		15	16.9	2.69	0	0
		30	17.8	0.14	0	0
		45	13.8	4.43	0	0
		60	9.62	0.29	0	0
		90	7.66	1.1	0	0

		120	2.24	3.16	0	0
		180	2.4	3.4	0	0
		240	0	0	0	0
		360	0	0	0	0
	RC	0	39.4	14.5	0	0
		15	9.73	6.91	0	0
		30	37.8	2.98	0	0
		45	21.3	10.3	0	0
		60	33.7	3.85	0	0
		90	24.3	3.41	0	0
		120	15.4	3.57	0	0
		180	23.7	10.9	0	0
		240	34.3	2.2	0	0
		360	34.5	6.53	0	0
CBD-Di-VHS	AH	0	34	0.47	0	0
		15	31.8	1.91	0	0
		30	33	0.37	0	0
		45	32	0.86	0	0
		60	32.5	0.61	0	0
		90	30.5	0.71	0	0
		120	30.1	0.84	0	0
		180	28.6	0.49	0	0
		240	28.1	0.32	0	0
		360	33.6	0.03	0	0
	VH	0	30.1	4.38	0	0
		15	34.3	0.64	0	0
		30	34.3	0.96	0	0
		45	33.6	0.65	0	0
		60	32.8	0.11	0	0
		90	30.9	0.59	0	0
		120	29.1	0.69	0	0
		180	25.2	0.31	0	0
		240	23.1	0.29	0	0
		360	34.1	0.04	0	0
	IC	0	36.3	0.08	0	0
		15	38.4	1.83	0	0
		30	37.1	0.22	0	0
		45	37.1	0.33	0	0
		60	37.2	0.85	0	0
		90	38.3	0.39	0	0
		120	37.9	0.21	0	0

		180	36.8	0.1	0	0
		240	37.8	0.56	0	0
		360	32.7	0.34	0	0
	RC	0	35.8	1.49	0	0
		15	33.8	1.3	0	0
		30	32.9	1.45	0	0
		45	33.5	0.41	0	0
		60	30.4	0.22	0	0
		90	30.8	2.5	0	0
		120	29.5	1.3	0	0
		180	26.6	0.25	0	0
		240	28.7	0.34	0	0

Table 4**.** Ocular tissue concentrations of CBD, CBD-Di-Val, CBD-Di-VHS, CBD-HS, CBD-Mono-VHS compiling studies 1 and 2, **90 min** post topical application of CBD (0.47%), CBD-Di-Val (0.94%) or CBD-Di-VHS (1.2%) in Tocrisolve™ emulsion (Dose: 250 µg CBD; 50 µL instilled volume) respectively. Data represented is Mean ± SEM

*Concentrations detected in only one animal

**Concentrations detected in three of the six test animals

			Analog Conc (ng/g of tissue)		**CBD Conc (ng/g of tissue)**	
Study number	**Formulation dosed**	**Tissue Analyzed**	**Mean**	**Std Err**	**Mean**	**Std Err**
1	CBD	AH	0.00	0.00	0.00	0.00
		VH	0.00	0.00	0.00	0.00
		IC	0.00	0.00	0.00	0.00
		RC	17.35	4.57	0.00	0.00
	CBD-Di-Val	AH	0.00	0.00	0.00	0.00
		VH	0.00	0.00	0.00	0.00
		IC	0.00	0.00	0.00	0.00
		RC	9.11	1.07	0.00	0.00
	CBD-Di-VHS	AH	12.32	7.53	0.00	0.00
		VH	612.48**	187.11	0.00	0.00
		IC	160.31*	-	0.00	0.00
		RC	279.77	75.29	8.35	8.35

2	CBD	AH	0.00	0.00	0.00	0.00
		VH	0.00	0.00	0.00	0.00
		IC	0.00	0.00	0.00	0.00
		RC	0.00	0.00	0.00	0.00
	CBD-HS	AH	0.00	0.00	0.00	0.00
		VH	0.00	0.00	0.00	0.00
		IC	0.00	0.00	266.69	32.52
		RC	0.00	0.00	263.15	93.33
	CBD-Mono-Val	AH	0.00	0.00	0.00	0.00
		VH	0.00	0.00	0.00	0.00
		IC	0.00	0.00	0.00	0.00
		RC	0.00	0.00	0.00	0.00
	CBD-Mono-VHS	AH	94.50	7.83	30.66	13.84
		VH	0.00	0.00	0.00	0.00
		IC	728.18	152.62	469.10	62.78
		RC	603.92	160.42	348.37	137.2

CHAPTER 3

Δ^{9}-TETRAHYDROCANNABINOL DERIVATIVE LOADED NANO-FORMULATION LOWERS IOP IN NORMOTENSIVE RABBITS

Introduction

Glaucoma is a neurodegenerative disorder characterized by progressive peripheral vision loss due to structural and functional damage to the optic nerve head. [83-84] The latest statistics from the World Health Organization ranks glaucoma as the second leading cause of blindness, after cataracts, affecting almost 60 million people worldwide.[85] The 2010 report by the National Eye Institute stated that 2.72 million people in United States suffer from glaucoma, 23 percent higher than the 2.22 million affected in the year 2000, and projects almost 6.3 million to be affected by this illness by 2050. [85-88]

Glaucomatous optic neuropathy is caused by several factors that result in death of retinal ganglion cells (RGC) and their axons. The major risk factor for glaucoma is elevated intraocular pressure (IOP), normally regulated by AH hydrodynamics in the anterior chamber.[89] AH is a fluid secreted by the IC.[90] AH drains out via the trabecular meshwork (TM) through the Canal of Schlemm into venous circulation. The ciliary muscles maintain the tension on the TM structure and control the drainage of AH. The Goldmann equation can be used to describe AH hydrodynamics,[91]

$$IOP = P_e + \frac{(F-U)}{C_{trab}} \quad \text{.....(1)}$$

Wherein, P_e is the episcleral venous pressure (the pressure opposing the drainage of AH through the trabecular meshwork), F is the AH flow, U is the uveoscleral outflow and C_{trab} is the AH outflow from the TM and Schlemm canal.[89] The balance between AH production and drainage determines IOP, wherein increased AH production or inadequate AH drainage might result in increased pressure.[89, 92-94] Glaucoma medications target IOP reduction by acting on the aforementioned factors i.e. either decreasing the production of AH or increasing AH outflow through TM and through the uveoscleral pathway or both.[95-97]

Currently, there are five families of treatment governing the market as anti-glaucoma agents.[98] Adrenergic agonists, beta blockers, prostaglandin F2-α analogs, carbonic anhydrase inhibitors and cholinergic agents. The mechanism of action of each class and examples of some FDA approved agents are listed in Table 5.

Table 5. Classification and mechanisms of action of the currently used anti-glaucoma medications

Anti-glaucoma medications	Mechanism of Action	FDA approved therapy
Prostaglandin analogs	Reduction in hydraulic resistance to uveoscleral outflow, Increase in trabecular outflow facility	Xalatan® (latanoprost), Lumigan® (bimatoprost), Travatan Z® (travoprost), Zioptan™ (tafluprost)
Beta blockers	Reduce aqueous humor production by acting on the β_1 and β_2 receptors	Timoptic® (timolol maleate ophthalmic solution), Betagan® (levobunolol hydrochloride ophthalmic solution
Adrenergic agonists	Increases elimination by reducing episcleral venous pressure, increasing uveoscleral outflow by increasing prostaglandin synthesis	Alphagan®P (brimonidine), Iopidine® (apraclonidine hydrochloride, ophthalmic solution)
Carbonic anhydrase inhibitors	Inhibit the enzyme carbonic anhydrase, reduce production of aqueous humor	Trusopt® (dorzolamide), Azopt® (brinzolamide)

Cholinergic agents	Increases aqueous humor outflow by contracting longitudinal fibers in of the ciliary muscles	Isopto® Carpine (pilocarpine hydrochloride ophthalmic solution)[98-99]

Current glaucoma research is directed towards finding new lines of treatment pursuing novel mechanisms for lowering of the IOP. The recent FDA approvals on anti-glaucoma agents, Rhopressa (Netarsudil 0.02%), a rho-kinase inhibitor and Latanoprostene Bunod 0.024% (made of two components, Latanoprost and a nitrogen oxide donating component) are examples of drug products harnessing novel mechanisms of action for IOP reduction.[99] There are several investigational treatments such as a sustained release bimatoprost implant and ocular punctal plugs of travoprost and latanoprost, however all these approaches focus on a formulation-based approach.[99] A completely new class of agents would bring forth another perspective for anti-glaucoma medications.

Cannabinoids have been investigated for the past few decades for their IOP lowering capacity. Cannabinoids utilize several unique mechanisms for IOP reduction. There are reports suggesting that IOP reduction occurs due to decreased AH production, a result of curtailed release of noradrenaline in ocular tissues.[100] Δ^9-Tetrahydrocannabinol (THC) is an example of a cannabinoid that favors the opening of the endothelial-lined Schlemm' s channels draining the AH.[100-105] Another suggested mechanism involves the CB1 receptors in IOP reduction. Human ciliary bodies are rich in CB1 mRNA, and functional protein, supporting the hypothesis that cannabinoids such as THC, through their action on CB1 receptors, may act directly as vasodilators of the efferent blood vessels of the anterior uvea, favoring AH efflux.[63, 106] Taking into consideration the pathophysiology of glaucoma, along with increased IOP, there is also a neurodegenerative component to the disease. Increased IOP produces early injury in glaucomatous

optic atrophy resulting in structural changes in the lamina cribrosa, a membrane through which the RGC axons pass before condensing to form the optic nerve.[107-109] Moreover, overproduction of free radicals, such as nitric oxide, results in an excessive release of glutamate, which, by activating NMDA receptors results in apoptotic ganglionic cell death.[110-112] Findings suggest that THC can inhibit glutamic acid release by increasing K^+ and decreasing Ca^{2+} permeability.[111, 113-114] It also exhibits antioxidant properties and prevents neuronal cell death by reactive oxygen species (ROS) scavenging action.[104, 115] Reportedly, in an animal glaucoma model, treatment with THC for 20 weeks decreased IOP and reduces death of RGCs by approximately 75%. [116] The neuroprotective effect of THC on the RGC makes it one of the very few agents tackling not only IOP reduction but also halting progressive vision loss.[104, 117]

Hepler and Frank reported about 25-30% drop in IOP after smoking marijuana, in a small number of subjects with a duration of action of 3-4 hours.[118-119] Crawford and Merritt in the late 1970's conducted clinical studies to determine a relationship between changes in heart rate, blood pressure, IOP in normotensive (n=8) and hypertensive volunteers (n=8) and also patients diagnosed with open- angle glaucoma (n=16) and they observed decreased IOP (6-21mm of Hg lower than control) along with intense cardiovascular effects.[120] Overall, it has been observed that smoking of marijuana is accompanied with a drop in both systolic pressure as well as IOP; however, cardiovascular effects such as tachycardia and postural hypotension outweighs the IOP lowering effects, giving rise to the need of investigating the effect of topical application THC on lowering of IOP.[119-120] Several reports can be found on the topical administration of THC formulated in various oily vehicles.[121-124] However, for THC to show both an IOP reducing and a neuroprotective effect, it is important for it to permeate through initial layers of the eye, to the target tissues.[63, 125] Previously, a prodrug approach was devised aiming to improve the ocular

bioavailability of THC.[126] Adelli et al. evaluated the pharmacokinetic and pharmacodynamic efficacy of a hydrophilic prodrug of THC, Δ^9-Tetrahydrocannabinol-Valine-Hemisuccinate (THC-VHS) in an elevated IOP model (Figure 8.). THC-VHS demonstrated a better permeation profile in comparison to THC, penetrating to the IC and RC, and a corresponding IOP drop for about 180 minutes. [76, 86]

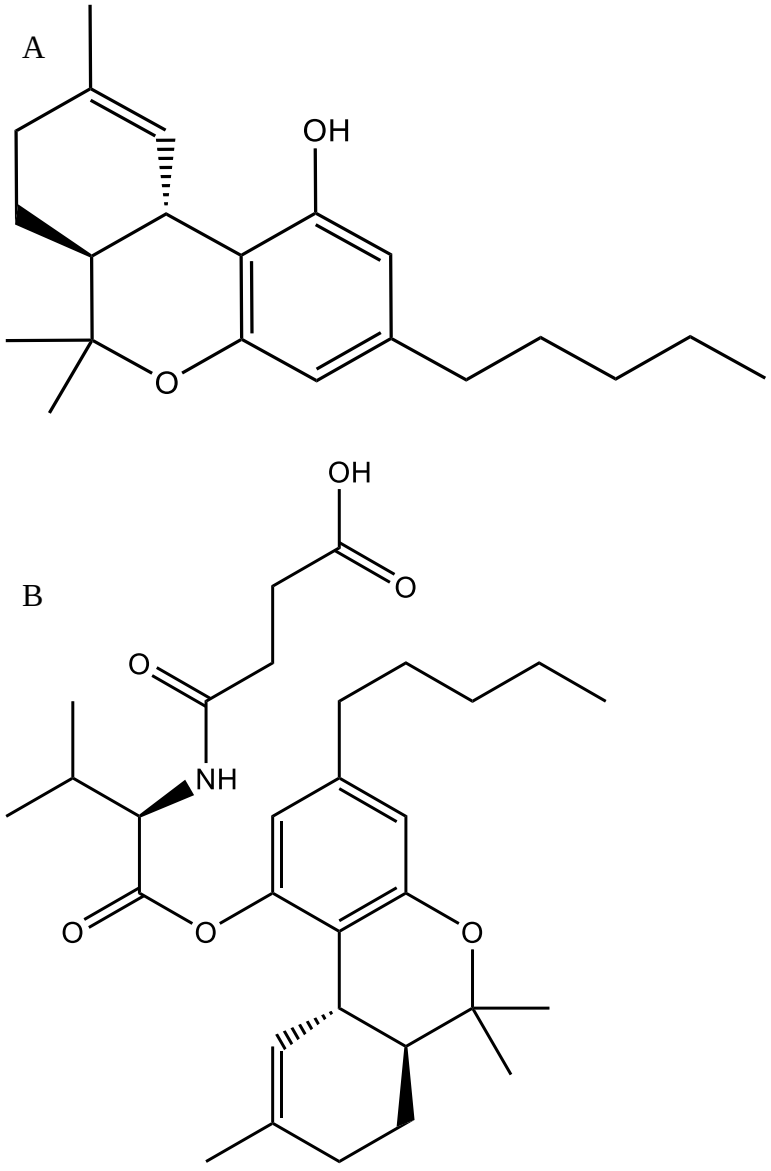

Figure 8. Chemical structures of (A) Δ^9-Tetrahydrocannabinol and (B) Δ^9-Tetrahydrocannabinol Valine Hemisuccinate (THC-VHS).

To understand the IOP lowering mechanisms of THC-VHS in an intact eye with all the production and drainage mechanisms unimpaired, a normotensive IOP model was opted for in the current set of studies. The goals of this project were to formulate a lipid-based vehicle, SLNs, to improve the delivery of the prodrug, THC-VHS, to the target tissues. SLNs have been reported to enhance ocular bioavailability by prolonging the residence time of the formulation in the *cul-de-sac,* forming a lipid-based drug reservoir interacting with the ocular mucosa.[127]

The formulation was characterized in terms of drug content (% w/v), particle size (d. nm), polydispersity index and scanning transmission electron microscopy (STEM). Stability of the formulations in terms of particle size growth under different storage conditions was investigated. A comparative PK-PD profile of the THC-VHS-SLN formulations was established post single and multiple topical applications in a normotensive rabbit model. The PK-PD profile of THC-VHS-SLN was compared to that of THC-VHS formulated in a soybean oil-based emulsion and THC-SLN to delineate the effect of prodrug derivatization and the effect of vehicle in improving ocular bioavailability. IOP lowering efficacy (PD profile) of the formulations were also compared against marketed ophthalmic formulations of pilocarpine and timolol maleate in the same model (single dose).

Materials

THC-VHS was synthesized by ElSohly Laboratories, Inc. according to previously established protocols.[128] Compritol® 888 ATO (glyceryl behenate) was obtained as a gift sample from Gattefossé (Paramus, NJ, USA), glycerin was purchased from Acros Organics (NJ, USA), Pluronic® F68 (poloxamer 188) was purchased from Spectrum Pharmaceuticals (Henderson, NV), Tween™ 80 was received as a gift sample from Croda Inc. (Mill Hall, PA), Tocrisolve™ 100 was purchased from Tocris® biosciences (Bristol, UK). HPLC - grade solvents, and other chemicals

(analytical grade) were obtained from Fisher Scientific (Hampton, NH, USA). Amicon® Ultra centrifugal filter devices, regenerated cellulose membrane (MWCO 100 kDa) were purchased from EMD Millipore (Billerica, MA). Formalin was purchased from Thermo Scientific™. Timolol maleate eye drops (0.25 % w/v) and pilocarpine HCl eye drops (2 %w/v) are commercially available formulations obtained from The University of Mississippi, Health Center.

Animals

Male New Zealand White rabbits (2-2.5 kg), obtained from Harlan laboratories® (Indianapolis, IN) were used in all studies. All animal experiments conformed to the Association for Research in Vision and Ophthalmology statement, "Use of Animals in Ophthalmic and Vision Research" and followed the University of Mississippi Institutional Animal Care and Use Committee approved protocols.

Development of SLNs and Emulsion

THC-VHS-SLNs and THC-SLNs

THC-VHS or THC loaded SLNs were prepared by the ultra-sonication technique. Compritol® 888 ATO constituted the lipid phase of the SLNs. THC-VHS (equivalent to 0.6% of THC) and 0.6% of THC was mixed with Compritol® 888 ATO to obtain a clear lipid phase. The aqueous phase comprising of Pluronic® F-68 (0.25% w/v), Tween™ 80 (0.75% w/v) and glycerin (2.25% w/v) was simultaneously heated in bi-distilled water. The hot aqueous phase was added to the melted lipid phase under constant stirring. A coarse emulsion from this pre-mix was formed by emulsification at 11,000 rpm for 5 min using T 25 digital Ultra-Turrax™. This coarse emulsion was subjected to ultrasonification using SONICS® Vibra-Cell™ Ultrasonic Liquid Processor using previously optimized parameters (Amplitude: 40%; Pulse on: 10 seconds, Pulse off: 15 seconds;

Time: 10 minutes). The temperature during this entire process was maintained at 70°C. The hot emulsion was slowly cooled to room temperature to form THC-VHS or THC SLNs.

THC-VHS and THC emulsion

THC-VHS and THC emulsion were prepared by dispersing weighed amount of THC (0.6% w/v) or THC-VHS (0.98% w/v, equivalent to 0.6% w/v THC) in the Tocrisolve™ emulsion vehicle (THC-TOC and THC-VHS-TOC), a soya-bean oil emulsion composed of a 1:4 ratio of soya oil/water, purchased from Tocris Bioscience. Tocrisolve™ is a water-soluble emulsion used for formulating hydrophobic moieties such as cannabinoids. The soybean oil solubilizes the cannabinoid molecule and the emulsion is stabilized by the block co-polymer, Pluronic-F68, preventing the lipid droplets from coalescing in the dispersion. This mixture was vortexed for 5 minutes on Ultra Cylone™ and sonicated for 10 minutes.

Formulation Characterization

Drug content

To determine the drug content in the SLNs and the emulsion, the lipid/oil was precipitated using ethanol. An accurately measured volume of the formulation was extracted in 1 mL ethanol and this suspension was centrifuged at 13,000 rpm for 15 minutes. The drug content in the supernatant was analyzed using the following HPLC-UV method.

In-vitro sample analysis

The samples were analyzed for THC and THC-VHS using an HPLC-UV system comprising a Waters 717 plus Autosampler, Waters 600E pump controller, Waters 2487 dual λ Absorbance detector and an Agilent 3395 integrator. Stock solutions of THC-VHS and THC were prepared in acetonitrile and used immediately. A mobile phase consisting of 60: 40 Acetonitrile: Water with

0.1% glacial acetic acid was used on a Phenomenex® C18 (4.6 x 250 mm) column at a flow rate of 1 mL/min. Detection was carried out at 226 nm.

Particle size, Polydispersity Index (PDI), Zeta Potential

The mean particle size and the PDI of the THC-VHS-SLN, THC-SLN, and THC-VHS-TOC formulations were determined by Dynamic Light Scattering (DLS) technique using the Zetasizer Nano ZS Zen3600 (Malvern Instruments, Inc.) at 25°C and 173° detection optics using the Non-Invasive-Back-Scatter technology. The cells used were disposable folded capillary clear cells. The measurements were obtained using a helium-neon laser of 633 nm, and the particle-size analysis data was evaluated using intensity distributions. Zeta potential was measured at 25°C in folded capillary cells using the same instrument. To measure the particle size distribution, the samples were diluted (1:500) with bidistilled water filtered using 0.2-micron filters.

Scanning transmission electron microscopy studies

A negative staining procedure was used to conduct the STEM studies. THC-VHS-SLNs were characterized by scanning transmission electron microscope Zeiss Auriga®-40 dual beam using 1%w/v uranyl acetate as a stain. Twenty microliters of the sample was placed on a piece of parafilm and a glow discharged 200 mesh copper grid with a thin carbon film was floated on top of the sample (film side down) for 30 seconds. After taking the grid off the drop, excess sample was blotted using a piece of filter paper. The grid was then floated on a drop of distilled water for a couple of seconds. Once excess water was removed, the grid, sample side down was floated on a drop of 1% uranyl acetate for 1 minute. After blotting and drying, the samples were imaged in a Zeiss Libra operating at 30 kV and in STEM mode.

Physical and Chemical Stability

THC-VHS-SLNs were evaluated for changes in % drug content, particle size and PDI on storage at conditions of 40°C/60% RH, 25°C/75% RH and 4°C.

Corneal Histology

Six NZW rabbits were used for comparison of corneal histology after treatment with Placebo-SLNs or with IPBS as control (n=3). The placebo-SLNs were topically administered to the eye of normotensive New Zealand White rabbits to observe the effect of the vehicle on the histological characteristics of the cornea. Rabbit corneas dosed with IPBS, under similar experimental conditions, were used as controls. The study was conducted for 120 minutes, after which the animals were euthanized, and the corneas were excised. Extracted corneas were fixed in 10% Neutral Buffered Formalin. Histological evaluation was carried out at Excalibur Pathology Inc. (Oklahoma City, OK) as per previously reported protocols. Corneas embedded in paraffin were sliced into 5µm cross sections using a microtome (American Optical® 820 Rotary Microtome). These sections were placed on a slide and dried overnight in an oven at 68 °C. The slide was washed with xylene to remove paraffin and washed with alcohol and water to hydrate the tissue. This was then stained with nuclear dye Gill III hematoxylin (StatLab medical) for 10 min and rinsed, and then counterstained with eosin. These slides were then washed in reverse manner (running water, alcohol, and xylene), cover slipped and examined under microscope (ChromaVision ACIS II).

Efficacy studies

Multiple Dose studies

The rabbits were acclimatized to the environment, personnel and IOP measurements using a Tono-Pen Vet™ (Reichert® Technologies) for a period of 2-3 weeks. The formulations THC-VHS-

SLNs, THC-VHS-TOC, THC-SLNs were dosed topically, conforming to a predetermined multiple dosing protocol in eighteen NZW rabbits (n=6). Fifty microliters of SLNs or nanoemulsion (in Tocrisolve™), was instilled topically in the cul-de sac of the left eye of normotensive rabbits, twice a day, for five consecutive days. The right eye served as the control. To avoid spillage, the eyelid was closed for 10 seconds. On Day 1, for the single dose IOP-Time profiling, IOP was measured before (baseline IOP), and, every 30 minutes after administration until IOP returned to 90 % of the baseline. From Day 2 onwards the IOP was measured before (baseline) and 60-90 min after administration of the dose. The IOP value displayed by the TONO-PEN VET™ (Reichert, Inc.) was an average of five concurrent IOP measurements, and each time point was measured in triplicates. The decrease in IOP was recorded as a function of single dose and multiple dosing, i.e. an intra-day as well as an inter-day IOP trend was monitored. On Day 5, IOP-Time profiling was done similar to Day 1. On Day 6, the animals were sacrificed at two time points, the first time point, which showed the lowest drop in IOP on day 5, and the second time point right before the IOP returned to 90% IOP from the baseline.

Eye Dissection and Tissue collection

At the time points mentioned before, the rabbits were administered Ketamine (35 mg/kg) and Xylazine (3.5 mg/kg) intramuscularly and euthanized under anesthesia with an overdose of pentobarbital administered through the marginal ear vein. The eyes were immediately enucleated after washing with ice-cold IPBS. Enucleated eyeballs were then dissected and the AH, VH, IC and RC tissues were collected. All samples were weighed and stored at −80°C until further processing.

Bioanalytical methods for quantification

An AB Sciex QTrap 4500 (Framingham, MA, USA) LC-MS/MS quadrupole interfaced with Shimadzu Nexera HPLC (Kyoto, Japan) was used to analyze both the THC and THC-VHS content. Calibration curves were prepared by spiking THC and THC-VHS into blank ocular tissues along with the internal standard, D3-THC. The tissues analyzed were AH, VH, IC, RC and plasma (PL). Protein precipitation took place after addition of ice-cold acetonitrile followed by extraction of THC and THC-VHS. The samples were vortexed and then centrifuged at 13,000 rpm, for 30 minutes. The supernatant was filtered through a 0.2-µm filter, and the filtrate was analyzed for THC and THC-VHS content. The calibration curves were prepared with both THC and THC-VHS in AH (2.5–100 ng/ml), VH (2.5–100 ng/ml), IC (2.5–100 ng/ml), RC (2.5–100 ng/ml), and plasma (2.5–100 ng/ml). Tissues collected from the multiple dosing studies were also prepared per this protocol. A Phenomenex Synergi Hydro Reverse Phase, 100 A, 50 x 3 mm, 2.5-µm column was used with a gradient elution method; the solvent phase was composed of water and acetonitrile with 0.1% w/v formic acid.

Single Dose studies

Single dose IOP-lowering efficacy studies were conducted with the marketed ophthalmic formulations of timolol maleate (0.25 % w/v) and pilocarpine HCl (2 %w/v) in NZW rabbits (n=4). Fifty microliters of each test formulation were instilled into the lower *cul de sac* of the left eye of the rabbits, while the right eye acted as the control. The eyelids were closed after the instillation for 10 seconds to avoid spillage. IOP was measured before instillation (baseline IOP) and every 30 min post instillation until the IOP returned to 90% of baseline IOP. The drop in IOP was also expressed as ΔIOP or percent baseline IOP (± SEM) i.e. (measured IOP/baseline IOP) x 100.

Statistical Analysis

To assess the effect of formulation on change in IOP over time a repeated measures model was used. Between and within group differences were modeled using the *proc mixed* procedure in SAS with treatment, time and interaction of treatment and time as independent factors in the model. A two-tailed p-value of ≤ 0.05 was considered statistically significant. Data analysis was conducted using Statistical Analysis System 9.4 software (SAS Institute; Cary, NC). Furthermore, using JMP® 12 (SAS Institute, NC, USA) data analyses software, a Standard Least Squares personality was used to fit the time-based IOP-drop from the baseline IOP for each of the formulations to study the comparative IOP trend across treated and untreated eyes. A p-value of less than 0.05 was considered statistically significant.

Results

Formulation characterization

A detailed description of the compositions of these formulations has been listed in Table 6.

The homogenization-ultrasonification process yielded SLNs with hydrodynamic radii less than 300 d. nm and a narrow distribution range. However, their particle size was slightly greater than that of Tocrisolve™ emulsion. Tocris Bioscience reports the mean droplet size of the emulsion as 182 nm and our investigated values for THC-VHS-TOC particle size fall along similar lines (189.75 ± 22.7 d. nm). Physicochemical properties of the test formulations have been listed in Table 7. A consistent negative zeta potential was observed in all the formulations. That, along with a narrow PDI suggests no aggregation/ coalescence of the nano-colloidal formulations.

Table 6. Optimized composition of THC-VHS-SLN, THC-VHS-TOC and THC-SLN formulations

Content (% w/v)			
Ingredients	**THC-VHS-SLN**	**THC-VHS-TOC**	**THC-SLN**
Compritol	3	-	3
Glycerin	2.25	-	2.25
Poloxamer 188	0.25	-	0.25
THC	-	-	0.6
THC-VHS (0.6% THC equivalent)	0.98	0.98	-
Tocrisolve™ emulsion	-	Q.S	-
Tween 80	0.75	-	0.75
Water, HPLC grade	Q.S	-	Q.S

Table 7. Particle size (d. nm), polydispersity index (PDI), zeta potential (mV) and drug content (%w/v) of test formulations THC-VHS-SLN, THC-VHS-TOC and THC-SLN

Formulation	Particle size (d. nm) (± Std. deviation)	Polydispersity Index (PDI) (± Std. deviation)	Drug content (% w/v) (± Std. deviation)
THC-VHS-SLN	287.80 ± 7.35	0.29 ± 0.01	93.57 ± 4.68
THC-VHS-TOC	189.75 ± 22.7	0.15 ± 0.06	87.74 ± 3.6
THC-SLN	269.2 ± 5.66	0.32 ± 0.15	96.84 ± 0.02

Scanning transmission electron microscopy studies

Morphological characteristics of THC-VHS-SLNs were studied using STEM (Figure.9). STEM technique images samples based on absorption of an electron beam as it passes through ultra-thin layer of sample. The transmitted beam is then projected on a phosphorescent screen or detector, providing us with information regarding the morphological characteristics of the particles as well as the hydrodynamic radius. The electron microscopy pictures at different magnifications (Figure. 9) show the presence of spherical nanoparticles with a smooth well-defined periphery.

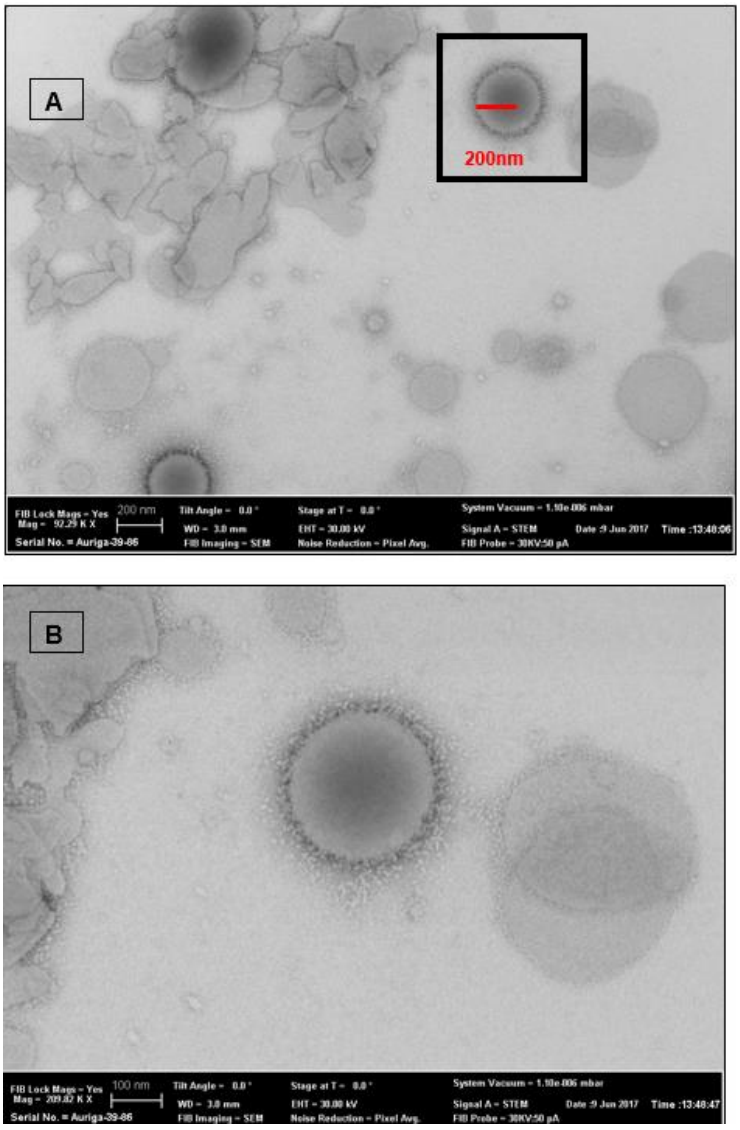

Figure 9. STEM images of THC-VHS-SLN at A. 92.29 KX and B. 209.82 KX magnification

Physical and Chemical Stability

The particle size and polydispersity index of THC-VHS-SLNs was observed for 6 months at 40°C/60% RH, 25°C/75% RH and 4°C. The formulations were stable over a period of six months at both 4°C and 25°C with particle size remaining around 200 to 300 d.nm and a PDI of 0.3 [129] (Figure 10.). However, after 1 month at 40°C, a 95% increase in particle size was observed from the original diameter of 248.9 nm and a PDI of 0.4. In terms of drug content, the THC-VHS-SLN was stable with a change in % drug content of ± 1.5% when stored at 4°C and 25°C over a period of 23 days (the last timepoint checked).

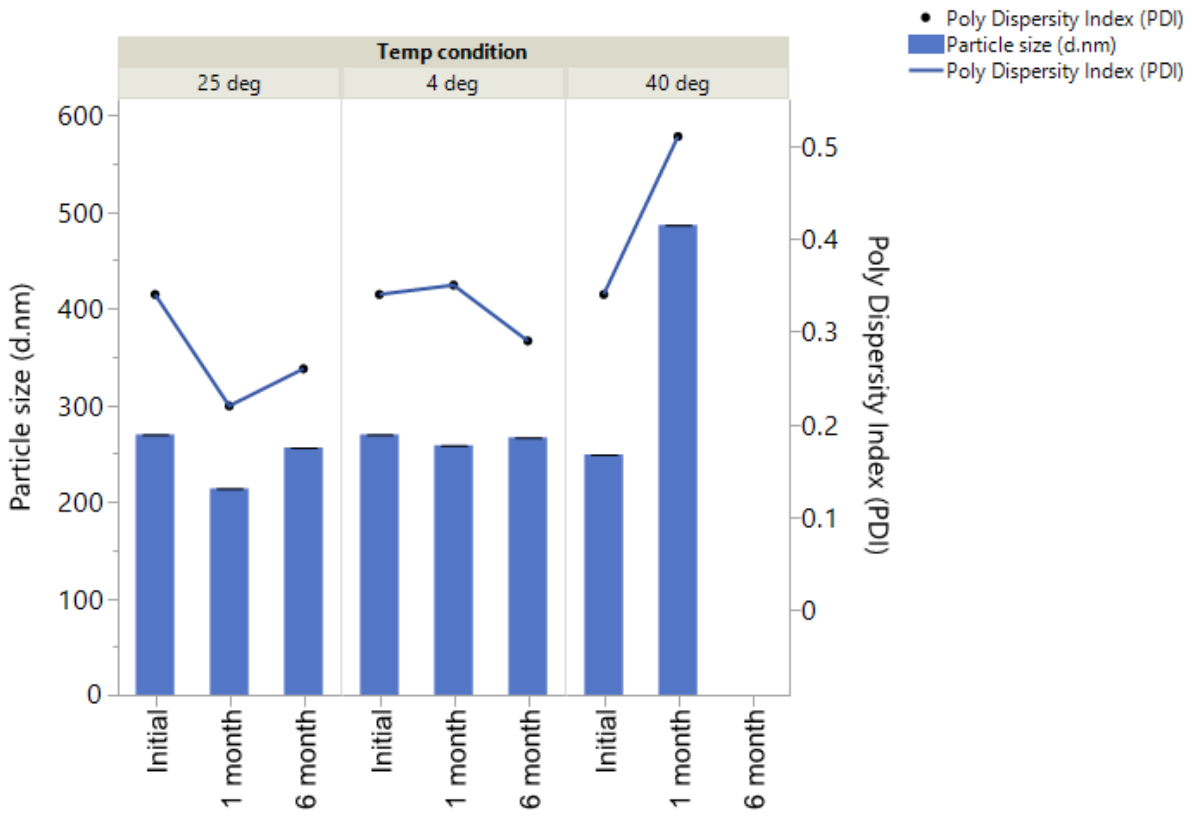

Figure 10. Particle size and polydispersity index of THC-VHS-SLNs stored at conditions of 40°C/60% RH, 25°C/75% RH and 4°C over a period of six months.

Corneal Histology

To observe the effect of formulation on the corneal histology, cross-sections of rabbit corneas treated with placebo-SLNs (Figure 11. A, B, C) and IPBS (control) were studied (Figure 11. D, E, F). The cornea is composed of five membranes; the corneal stratified squamous epithelium (1), Bowman's membrane (2), stroma consisting of collagen fibers and keratocytes (3), Descemet's membrane (4) and the endothelium (5), as marked in Figure 11. A. The corneal epithelium of all the rabbits, treated with control or placebo-SLNs looked intact, and attached to the Bowman's membrane, without any signs of edema.

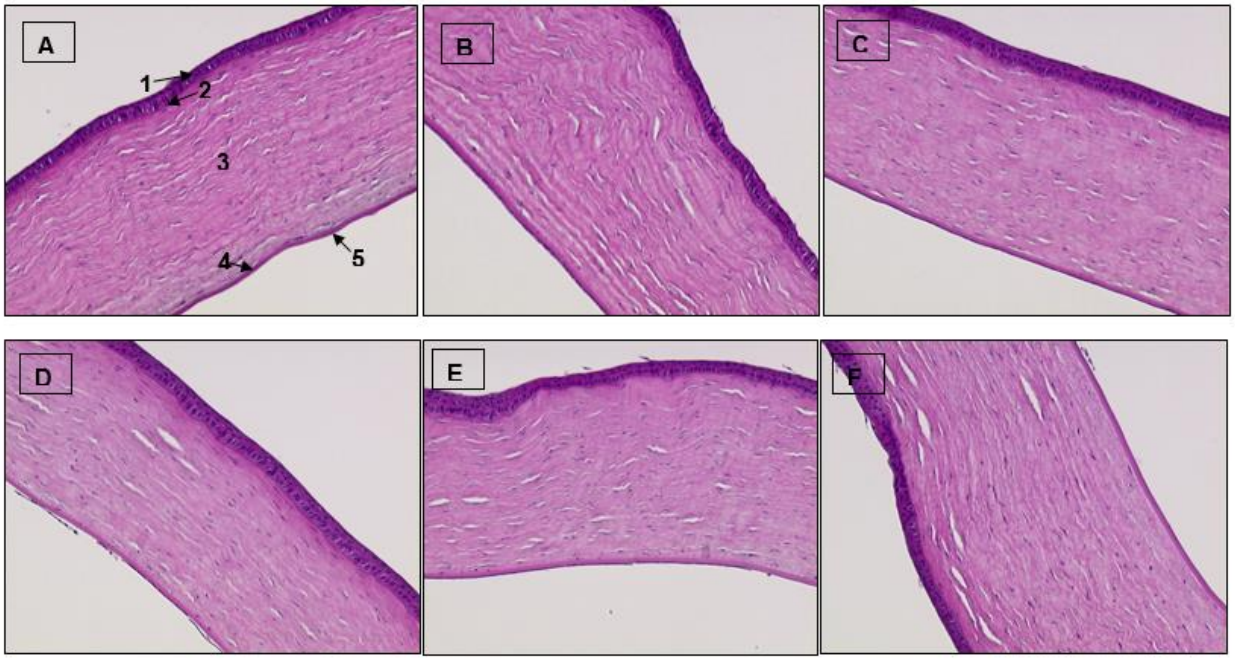

Figure 11**.** Histological sections of rabbit corneas (Magnification 10x) excised from NZW rabbits (n=3) treated with placebo-SLNs (A, B, C) and IPBS (control) (D, E, F) 120 minutes after application

Efficacy studies

Multiple dosing regimen for THC-VHS-SLN

It has been previously reported that THC fails to lower IOP of normotensive rabbits. The data obtained on normotensive rabbits for studies with THC-VHS-SLN formulations show a significant IOP lowering effect by THC-VHS when formulated in SLNs. Figure 12 depicts the 5-day mean IOP vs Time profile for treated eye after dosing with THC-VHS-SLN over the five-day dosing regimen in comparison to the contralateral eye IOP (untreated eye). IOP of the treated eye was significantly lower than the untreated eye from the 30 minutes time-point, and this effect lasted until 360 minutes.

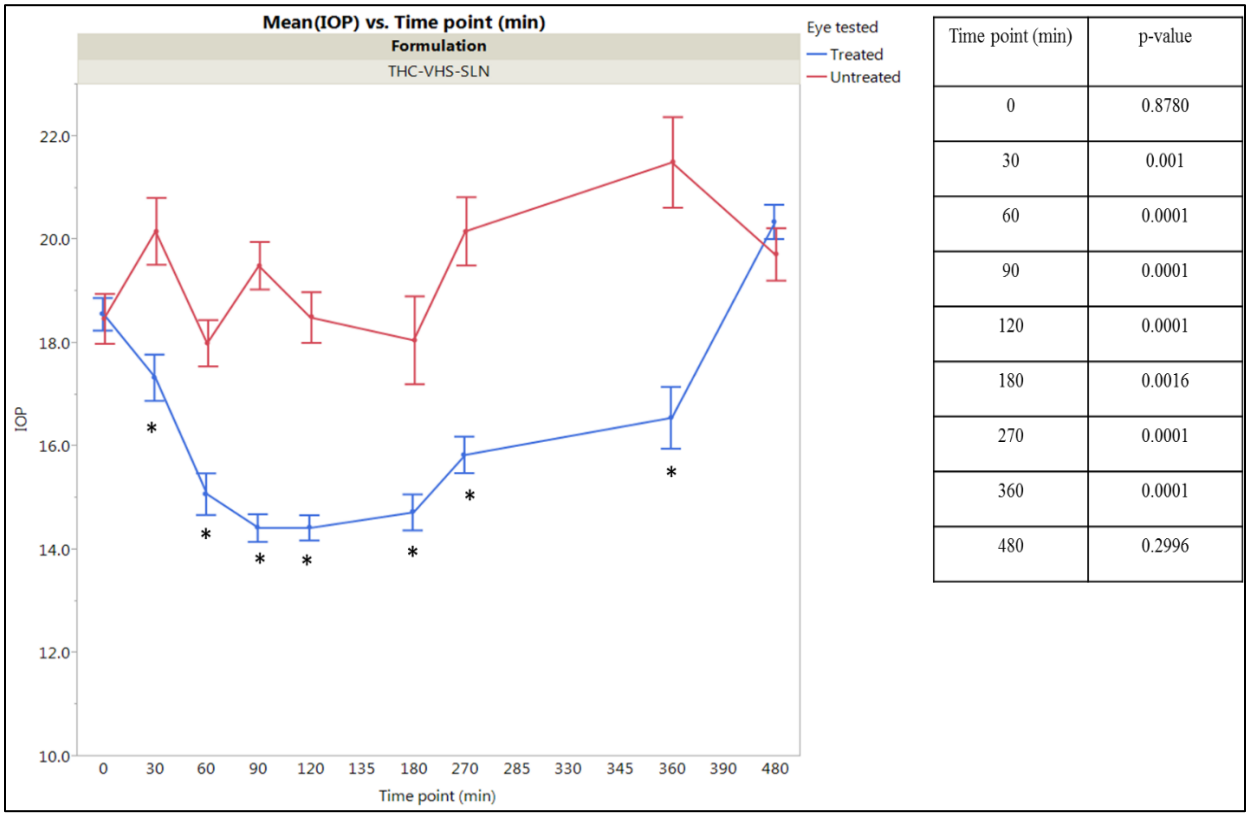

Time point (min)	p-value
0	0.8780
30	0.001
60	0.0001
90	0.0001
120	0.0001
180	0.0016
270	0.0001
360	0.0001
480	0.2996

Figure 12**.** Mean IOP vs time profile for treated (blue line) and untreated (red line) eyes in normotensive rabbits (n=6) dosed with 50 µL of 0.98 % THC-VHS-SLN twice a day for five

consecutive days. The line represents the mean of these data points at each time point (± SEM). The IOP profile of the Treated vs contralateral rabbit eyes were compared using *proc mixed* repeated measures model. The p-values for treated vs untreated eyes are also listed.

Multiple dosing regimen for THC-VHS-TOC

The THC-VHS-TOC emulsion formulation did not have a significant effect on the IOP of normotensive rabbits. The 5-day mean IOP vs Time profile for the eye treated with THC-VHS TOC in comparison to the contralateral eye is shown in Figure 13. The IOP drop in the treated eye lasts for about 90 minutes with IOP significantly lower than the contalateral eye at the 30, 60 and 90 minute time points.

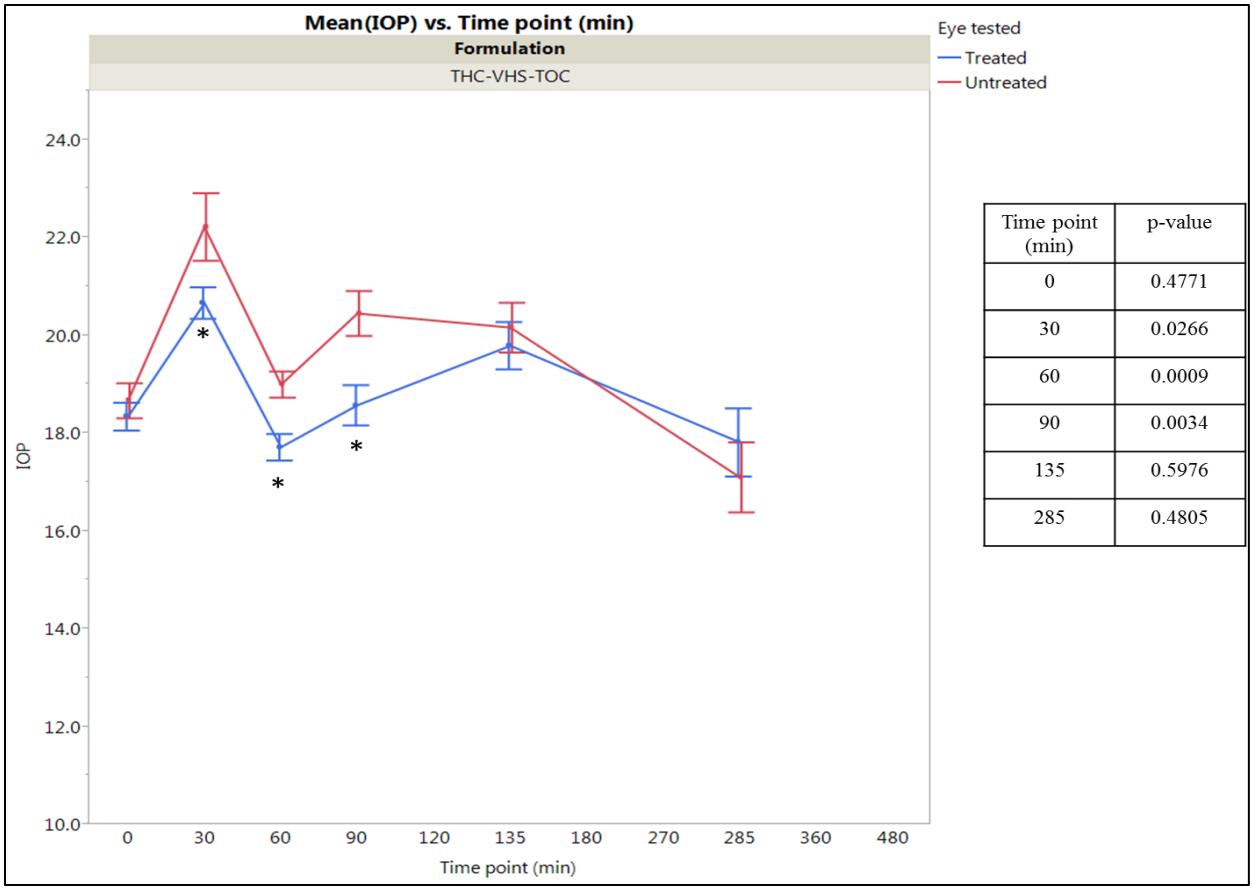

Time point (min)	p-value
0	0.4771
30	0.0266
60	0.0009
90	0.0034
135	0.5976
285	0.4805

Figure 13**.** Mean IOP vs time profile for treated (blue line) and untreated (red line) eyes in normotensive rabbits (n=6) dosed with 50 μL of 0.98 % THC-VHS-TOC twice a day for five consecutive days. The lines represent the mean of these data points at each time point (± SEM). The IOP profile of the Treated vs contralateral rabbit eyes were compared using *proc mixed* repeated measures model. The p-values for treated vs untreated eyes are listed in figure.

Multiple dosing regimen for THC-SLN

To elucidate the effect of prodrug derivatization, the efficacy of the THC-SLN formulations were also tested. The mean 5-day IOP vs Time profile comparing the THC SLN treated and contralateral eyes is shown in Figure. 14. The eyes receiving THC-SLNs did not show a significant drop in IOP in comparison to the contralateral eye upto 90 minutes. However, at the 135 minute time-point the IOP of the treated eye was significantly lower than the contralateral eye. After a period of 2.5 hours, at the 285 minute time-point, this effect was reversed and the contralateral eye showed significantly lower IOP in comparison to the treated eye.

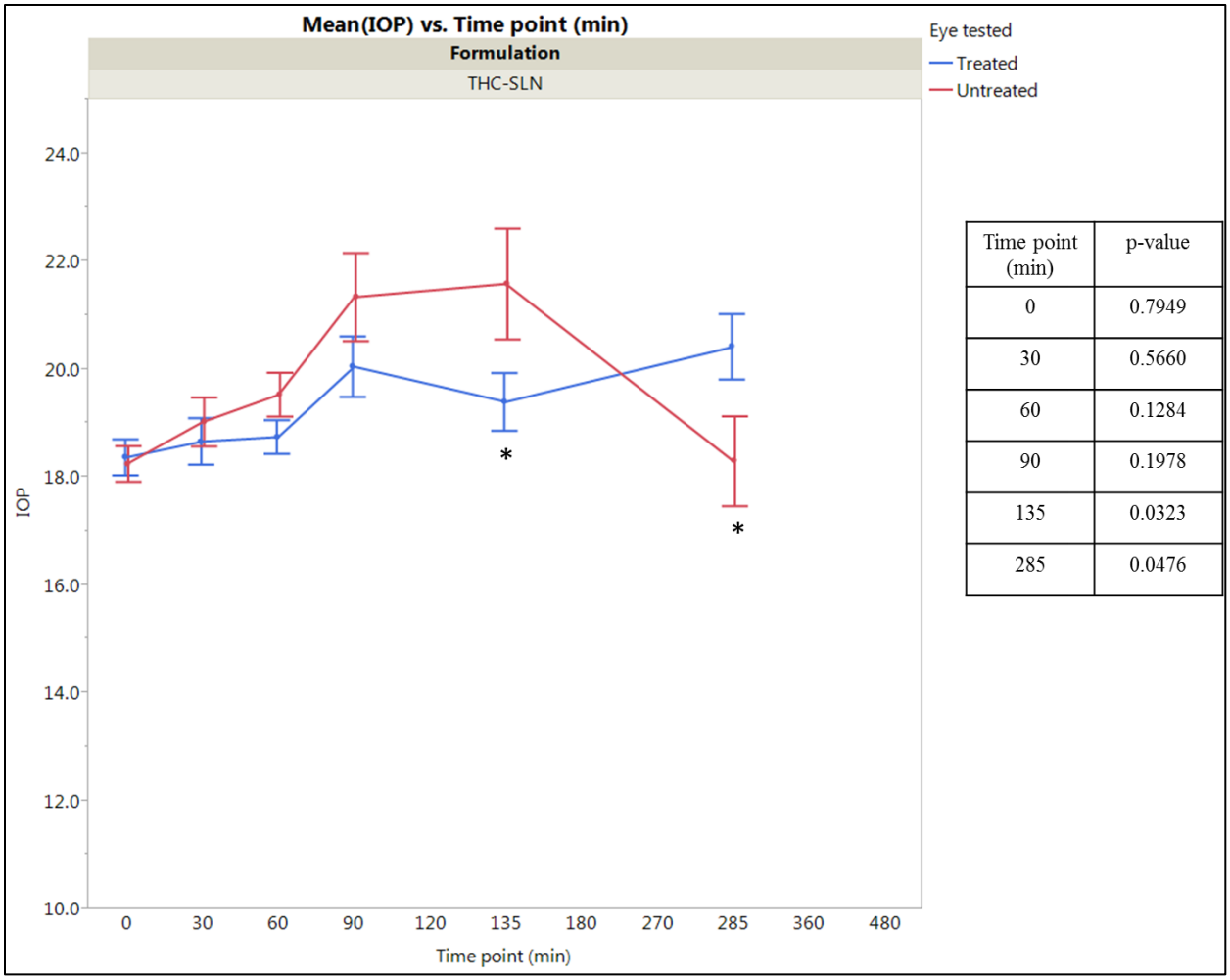

Time point (min)	p-value
0	0.7949
30	0.5660
60	0.1284
90	0.1978
135	0.0323
285	0.0476

Figure 14**.** Mean IOP vs time profile for treated (blue line) and contralateral (red line) eyes in normotensive rabbits (n=6) dosed with 50 µL of 0.6% THC-SLNs twice a day for five consecutive days. The line represents the mean of these data points at each time point (± SEM). The IOP profiles of the Treated vs contralateral rabbit eyes were compared using *proc mixed* repeated measures model. The p-values for treated vs untreated eyes are listed in the figure.

Figure 15. illustrates statistically significant within-group differences, comparing IOP for the same treatment with baseline IOP (time-point 0), and between-group differences for different formulations at various time points. The within-group differences for treatment THC-VHS-SLNs the drop in IOP at time-points 60, 90, 120 and 180 minutes are significantly lower than baseline

IOP (time-point 0 min) with p-values 0.011, <.0001, <.0001, 0.0021 respectively. A *proc mixed* repeated measures model was used with a Tukey Kramer adjustment to assess these differences. Other treatment formulations, THC-VHS-TOC and THC-SLNs do not show significantly lower IOP in comparison to baseline IOP. Analyzing between group differences, THC-VHS-SLNs demonstrated significantly lower IOP than THC-SLNs (p-value <.0001) and THC-VHS-TOC (p-value 0.0019) at time-points 60 and 90 minutes and 90 minutes, respectively.

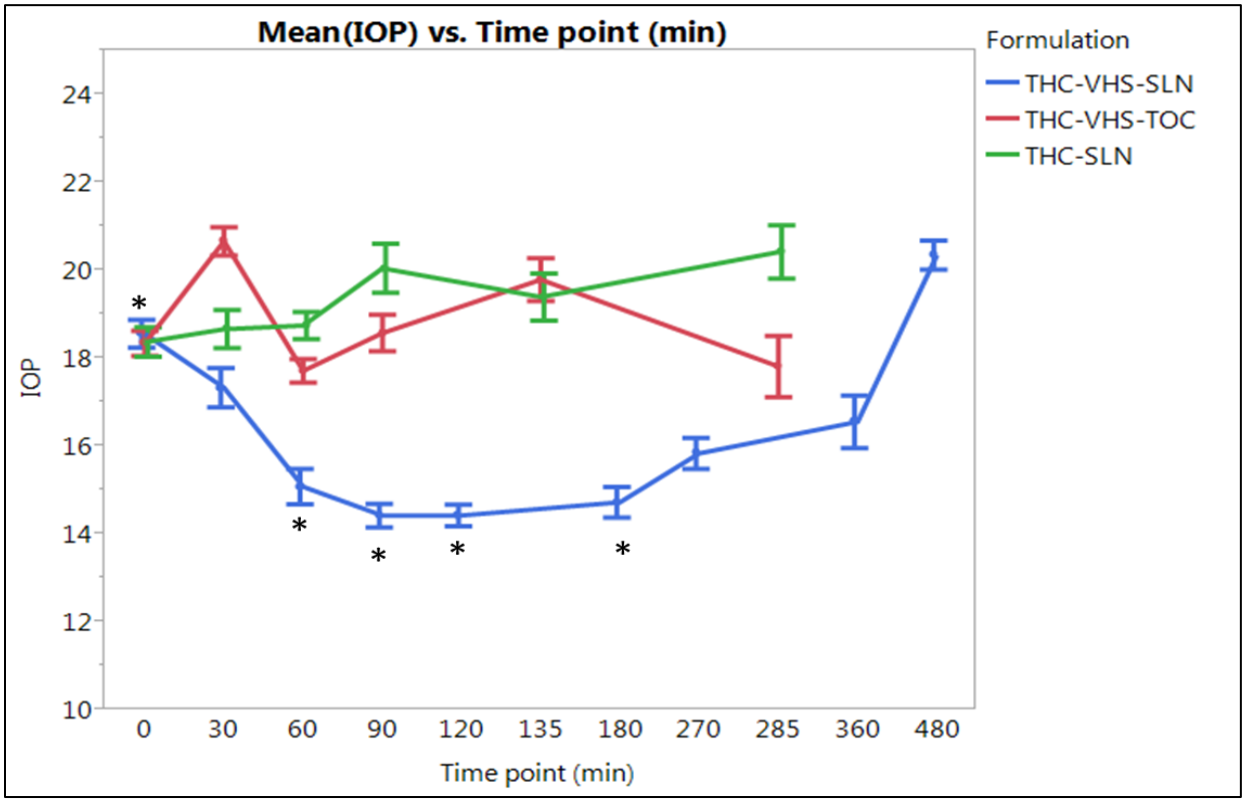

Figure 15**.** Comparative mean IOP vs time profiles for rabbits treated with 50 µL of 0.98 % THC-VHS-SLN, 0.98 % THC-VHS-TOC or 0.6 % THC-SLNs (n=6) twice a day for five consecutive days. The line represents the mean of these data points at each time point (± SEM). The rabbit eyes receiving the different formulations were compared using *proc mixed* repeated measures model.

Ocular Bioavailability

For THC-VHS-SLN, the maximum drop in the IOP from the baseline (ΔIOP_{max}) was 31% and 29.3 % on Day 1 and Day 5, respectively. The time to achieve ΔIOP_{max}, T_{max} on Day 1 and Day 5 was 90 minutes and the duration of action for THC-VHS-SLN, or the time required for ΔIOP to reach 90% of baseline IOP was 480 minutes on both Days 1 and 5. The two-sacrificial time-points, determined based on the IOP data, were 90 and 360 minutes. Table 8. displays the concentration of both THC-VHS and the parent molecule at the two-sacrificial time-points. At 90 minutes, THC-VHS concentrations were 10.67 ± 2.28 ng/50 mg in AH and decreased to 3.84 ± 0.53 ng/50 mg at 360 minutes. In comparison to AH, higher levels of the prodrug were observed in the IC and RC with 1466 ± 514.5 ng/50 mg and 902 ± 372 ng/50 mg observed at 90 minutes and 77.6 ± 69.5 ng/50 mg and 238.3 ± 143.3 ng/50 mg observed at the 360 minutes time points, respectively. At 360 minutes, 6.36 ± 3.83 ng/50 mg of bio-reversed THC was observed. Significant amounts of drug permeated to the RC and IC tissues, both important from the point of view of neuroprotection and IOP lowering and a corresponding IOP drop was observed as the pharmacodynamic response. THC-VHS was not observed in the plasma even after multiple administration, which helps rule out CNS involvement through systemic exposure.

Table 8. Tissue concentrations (ng/50 mg) of THC-VHS and THC on Day 6, post instillation of 50 μL of 0.98 % THC-VHS-SLNs, at 90 minutes (n=3) & 360 minutes (n=3) in Aqueous Humor, Vitreous Humor, Retina Choroid and Iris Ciliary Bodies. Dose equivalent to 300 μg THC.

ND: below limits of detection

			ng / 50 mg			
			THC-VHS		**THC**	
Formulation	**Tissue Analyzed**	**Time point (min)**	**Mean**	**Standard Error**	**Mean**	**Standard Error**
THC-VHS-SLN	Aqueous Humor	90	10.7	2.3	ND	ND
		360	3.8	0.5	ND	ND
	Vitreous Humor	90	ND	ND	ND	ND
		360	ND	ND	ND	ND
	Iris Ciliary Bodies	90	1466	514.5	ND	ND
		360	77.6	69.5	6.4	3.8
	Retina Choroid	90	902	372	ND	ND
		360	238.3	143.3	ND	ND

For THC-VHS-TOC, the ΔIOP_{max} for Day 1 and Day 5 of dosing was 11.7 and 10.9% respectively and the T_{max} was 60 minutes. The sacrifice time-points thus determined for this formulation were 60 and 120 minutes. The ocular concentrations of THC-VHS obtained with the THC-VHS-TOC formulation were significantly lower than those obtained with the THC-VHS SLN formulation (Table 9).

Table 9. Tissue concentrations (ng/ 50 mg) of THC-VHS and THC on Day 6, post administration of 50 μL of 0.98 % THC-VHS-TOC, at 60 minutes (n=3) & 120 minutes (n=3) in Aqueous Humor, Vitreous Humor, Retina Choroid and Iris Ciliary Bodies. Dose equivalent to 300 μg THC.

ND: below limits of detection

*Drug levels observed in a single animal only

			ng / 50 mg			
			THC-VHS		**THC**	
Formulation	**Tissue Analyzed**	**Time point (min)**	**Mean**	**Standard Error**	**Mean**	**Standard Error**
THC-VHS-TOC	Aqueous Humor	60	91.2	1.85	ND	ND
		120	ND	ND	ND	ND
	Vitreous Humor	60	ND	ND	ND	ND
		120	ND	ND	ND	ND
	Iris Ciliary Bodies	60	24.2	5.06	53	28.9
		120	11.3	0.50	57.4	18.5
	Retina Choroid	60	15.5	6.70	5.2	0.2
		120	7.5*	NA	5.3^	NA

Consistent with the previously reported data, THC did not produce as intense or as prolonged an IOP drop from baseline IOP in comparison to the THC-VHS formulations [86]. A 6.9% drop in IOP in comparison to the baseline IOP was observed with THC-SLNs at 60 minutes on Day 5. Animals were sacrificed at two time points on Day 6 at 60 and 120 minutes (Table 10). THC levels of 12.53 ± 3.51 ng/50 mg and 9.87 ± 3.22 ng/50 mg were observed in the IC at 60 and 120 minutes, respectively.

Table 10. Tissue concentrations (ng/ 50 mg) of THC on Day 6, post administration of 50 µL of 0.6 % THC-SLN, at 60 minutes (n=3) & 120 minutes (n=3) in Aqueous Humor, Vitreous Humor, Retina Choroid and Iris Ciliary Bodies. Dose equivalent to 300 µg THC.

ND: below limits of detection

			ng / 50 mg THC	
Formulation	**Tissue Analyzed**	**Time point (min)**	**Mean**	**Standard Error**
THC-SLN	Aqueous Humor	60	ND	ND
		120	ND	ND
	Vitreous Humor	60	ND	ND
		120	ND	ND
	Iris Ciliary Bodies	60	12.5	3.5
		120	9.9	3.2
	Retina Choroid	60	ND	ND
		120	ND	ND

Single dose efficacy studies

Pilocarpine HCl (2 %w/v) exhibited a ΔIOP_{max} of 15.9% at 30 minutes and its IOP lowering effect lasted for 120 minutes (Fig. 16). The graphs represent %IOP drop from the baseline IOP. Timolol maleate (0.25 % w/v) resulted in a more intense ΔIOP_{max} of 23.1% at 60 minutes with duration of action of 180 minutes for the IOP to reach 90% of the baseline IOP. THC-TOC emulsion or the placebo-SLNs did not result in any reduction in IOP (Data not shown). The IOP vs Time profiles of the marketed preparations are compared to that of the THC-VHS-SLNs, THC-VHS-TOC and THC-SLNs in Figure 16.

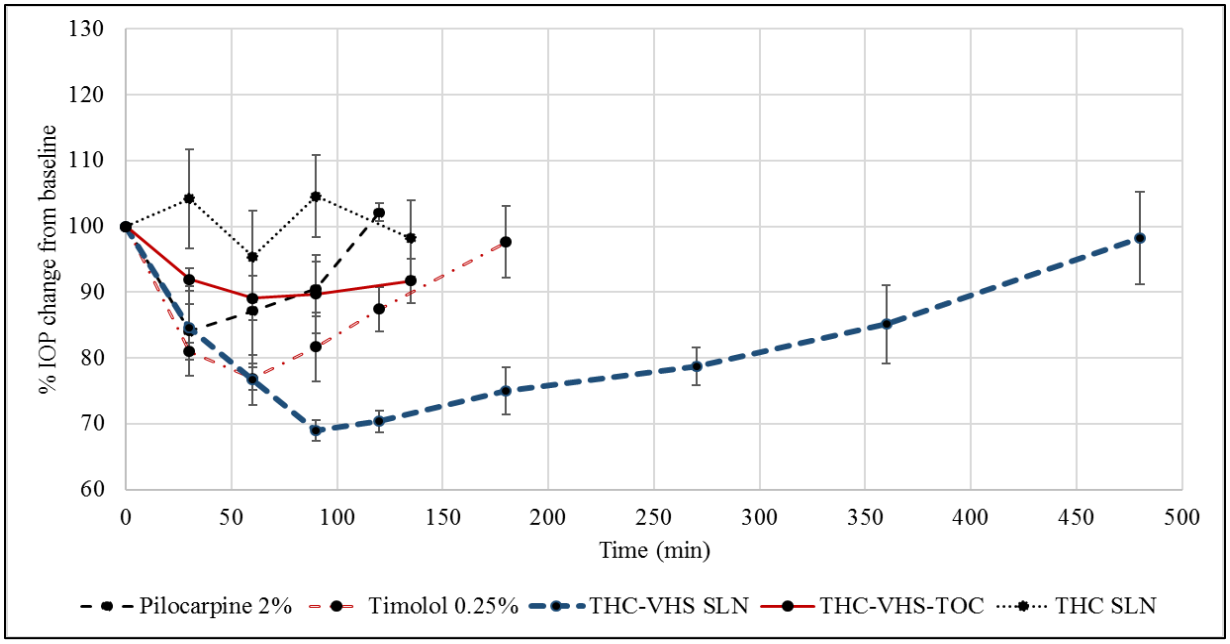

Figure 16. Percent IOP change from baseline vs Time profile for THC-VHS-SLN, THC-VHS-TOC and THC-SLN and 2% pilocarpine, 0.25% timolol maleate marketed formulations. A single drop (50 µL) was instilled. Data represents mean ± SE.

Discussion

In 1977, Green et al. reported a seventeen percent drop in the IOP, sixty minutes post dosing, using light mineral oil as the vehicle in adult albino rabbits. The tissue concentrations obtained were extremely low, about one ng of ^{14}C-labelled THC/ mg of wet tissue weight four hours post dosing in the cornea and IC. [130] Hingorani et al. observed that the amount of THC permeating into the ocular tissues was below levels of detection in rabbit AH, VH, RC and IC, one hour post administration of THC in light mineral oil (0.1% w/v), emulsion (0.37% w/v) or micellar solutions (0.125 % w/v THC, 0.5% Cremophor RH 40) in New Zealand White rabbits with detectable levels only in the cornea and sclera. [131] Such findings suggest that the lipophilic nature of THC prevents its partitioning from the oily vehicle into the tear film, in turn affecting its overall ocular

bioavailability. THC has poor aqueous solubility (1–2 μg/mL) and high log P (6.42), which makes the development of an eye drop for the molecule challenging. The lack of activity through the topical route of application, as observed in the above-mentioned reports, could be due to the ineffective delivery of THC to the target ocular tissues rather than absence of local pharmacological activity. Delivery of a therapeutic agent to the deeper ocular tissues depends on the type of formulation, physicochemical properties of the molecule and absorption pathway.[17] These properties determine the permeation profile of the molecule across alternating lipophilic and hydrophilic tissue layers and through the corneal tight junctions. For targeting a molecule to the back-of-the eye, it should possess optimum physicochemical properties and be formulated in appropriate dosage forms.[132]

To improve the intrinsic solubility of THC, a prodrug strategy was employed by Hingorani et al. by using a hemiglutarate (dicarboxylic acid) ester (THC-HG), which, being ionized at physiological pH would have better aqueous solubility (19 μg/mL). [131, 133] One hour post instillation of 50 μL of THC-HG, formulated in 0.5% w/v Cremophor RH 40, 35.6 ± 12.5 ng of THC /50 mg of tissue was observed in the IC and 32.1 ± 12.6 ng of THC / 100 μL was detected in AH of New Zealand White rabbits, whereas, the THC tissue concentrations obtained post dosing of 50 μL THC formulated in 0.5% w/v Cremophor RH 40 were below detection levels. This finding suggested that hydrophilic prodrug derivatization is an efficient method to improve the ocular bioavailability of THC.[131] However, in terms of chemical stability, THC-HG was extremely unstable and underwent rapid degradation at acidic and alkaline pH conditions, as well as at physiological pH. [133-134]

In subsequent studies, THC-VHS was designed as an amino acid- dicarboxylic acid prodrug, the amide linkage enhancing its stability. In terms of the physicochemical properties,

THC-VHS is stable from pH 5 to pH 9.[128] Adelli et al. observed the efficacy of THC-VHS in a soybean oil-based emulsion in an elevated IOP-glaucoma model. THC-VHS demonstrated an IOP drop comparable to the marketed ophthalmic solution of 2% Pilocarpine HCl.[76, 86] However, the IOP vs time profile indicated that frequent dosing would be necessary. Thus, developing a formulation strategy that could increase the amount of THC-VHS that could enhance the bioavailability as well as retention of the therapeutic agent at the ocular surface would be desirable.

Post topical application, a molecule has to overcome significant barriers, such as vascular and lymphatic drainage in the conjunctiva, sclera and choroid, restricting its passage from the ocular surface to posterior ocular tissues. [135] SLNs enhance ocular bioavailability of poorly soluble compounds by acting as unit carriers of the target molecules and prolonging its residence time in the *cul-de-sac* and forming a lipid-based drug reservoir that interacts with the ocular mucosa.[127, 132, 136-137] SLNs, being solid at room temperature have a modulated drug release profile in comparison to a liquid based-formulation.[138] Punyamurthula et al. demonstrated enhanced delivery of Δ^8 THC-SLNs to all ocular tissues attributed to the probable uptake of the SLNs by the conjunctival and corneal membranes - resulting in sustained release of the drug.[127]

However, in order to develop a SLN formulation of THC-VHS, thermal stability of the prodrug would play an important role during formulation development. Both molecules, THC and THC-VHS, are amorphous with absence of a definite crystal lattice structure making them susceptible to atmospheric degradation.[134, 139] THC undergoes rapid thermo-oxidative degradation into its metabolite cannabinol. The use of polymeric stabilizers and cross-linked matrices can be considered as a way of controlling the oxidative degradation of amorphous molecules such as THC.[139-141] Compritol 888 ATO is a crystalline amphiphilic material with a melting point of about 70°C. The crystalline structure of the bulk lipid can form protective barriers increasing the storage

stability of the formulation. [142] The high solubility of THC and THC-VHS in Compritol 888 ATO, along with the stabilizing effect provided by the crystalline lipid make it a good choice of lipid for development of the SLN formulation. Previous reports show that THC-VHS shows only about 3 % degradation of drug when heated at 120°C for 10 minutes.[128] Taking into consideration this along with the melting point of Compritol® 888 ATO, a temperature of 70°C was chosen to formulate the SLNs.

The physicochemical data suggests that a structured lipid phase comprising of Compritol® 888 ATO (stabilized by a Poloxamer 188 - Tween 80 surfactant system) resulted in a stable nano-particulate system. The data obtained from the STEM indicates that the size of the well-rounded nanoparticles is slightly greater than 200 nm, also consistent with the results obtained from DLS. In case of multimodal data, particle size may not agree across different measurement techniques, however, for a monodisperse formulation the particle size data might be comparable.[143] [144] Introduction of any form of energy such as temperature to the nanoparticulate system can lead to particle growth and subsequent gelation[145]. The increase in the particle size at the storage condition of 40°C/60% RH can be attributed to increase in the entropy of the system because of the high temperature, resulting in coalescence of the SLNs and a corresponding particle size growth. At the six-month time point, complete gelation of the SLN formulation was observed (Figure 10.).

Histological analysis of the rabbit corneas treated with the SLNs helps understand the toxicity profile of the SLNs; edema results into separation of structural elements and accumulation of edematous fluid in the stroma results into empty spaces formed between keratocytes and corneal collagen fibers.[146] Figure 12. (D, E, F), corneas treated with control, portray a more generalized and widespread edema with detachment of Descemet's membrane. We also observe structurally disturbed collagen bonds in areas close to the Descemet membrane invagination. However, taking

into consideration the exclusivity of this event, the damage to this cornea can be attributed to mechanical stress during the enucleation and the fixing of the cornea. Figure 12. (A, B, C), for corneas treated with Placebo-SLNs, the stroma is present as even layers with signs of edema ranging from slight to none.

Topical THC-VHS-SLNs produced a prolonged and intense drop in the IOP in normotensive rabbits in comparison to the THC-VHS-TOC as well as THC-SLNs. THC-VHS-SLNs lowered the IOP of the treated eye in comparison to the untreated eye and maintained IOP below baseline until 360 minutes. In comparison, rabbit eyes treated with THC-VHS-TOC produced a significant drop in IOP in comparison to the untreated eye at 30, 60 and 90 minutes only. Comparing the p-values for differences in the IOP for treated and untreated eyes, the IOP drop produced by THC-VHS-TOC was not as significant as THC-VHS-SLN. SLNs, being colloidal carriers have advantages of better penetration, stability, drug loading and sustained release of the drug.[147] The large surface area provided by the nanoparticulate system increased the contact area, ensuring close contact with the ocular mucosa after instillation. Lipid based nanoparticles have an occlusive effect and forms a depot in the *cul de sac*, slowly releasing the drug over prolonged duration of time.[148-149] The additives present in the formulations, such as surfactants, also play a role in permeation enhancement via fluidization of the lipid bilayers of the ocular membranes.[150]

The THC-SLN treated eyes showed a statistically significant lower IOP in comparison to the untreated eyes at the 135 minutes time point only. Based on the IOP data, THC-VHS was effectively delivered to the target tissues within the first 30 minutes from both the SLN and emulsion-based formulations, whereas the parent molecule required about 2 hours to demonstrate a pharmacodynamic response.

The pharmacokinetic data suggests that the SLN formulations deliver an almost 60 times greater concentration of THC-VHS in the IC in comparison to the emulsion formulation. THC levels in the ocular tissues from the THC-VHS-SLN formulations were extremely low (below detection levels in most cases) in comparison to that obtained from the THC-VHS-TOC or THC-SLN formulations. However, the duration of IOP drop observed with the THC-VHS-SLNs was significantly more prolonged. A possible explanation for this disconnect between the pharmacokinetic and pharmacodynamic observations could be that the site of action might not be the IC. It could also be possible that the prodrug being more permeable could be distributing deeper into the tissues better than THC (administered as such or THC generated from THC-VHS). As a result, a correlation between the prodrug concentration, rather than THC concentration, and IOP lowering effect is observed. The lack of a pharmacodynamic response even though the ocular tissues exhibited significant THC concentrations (with the THC-VHS-TOC and THC-SLN formulations) could be because of THC forming a depot in the ocular tissues, rather than penetrating and distributing across the ocular tissues (e.g. IC). As a result concentrations at the site of action maybe low even though the overall tissue concentrations are high..[104] The reason why THC-VHS-TOC is not as effective as THC-VHS-SLN could be because the emulsion formulation is not protecting the prodrug from bio-reversion (chemical or enzymatic) as a result of which higher THC tissue concentrations are observed from THC-VHS-TOC, thus decreasing the concentration deeper in the tissues. On the other hand, the SLN formulation protects against bioreversion of THC-VHS to THC, as evidenced by the lack of detectable THC concentrations from the THC-VHS-SLN formulations.

The overall tissue distribution profile indicates a non-corneal route of absorption. With THC-VHS-SLN, we observe 1466 ± 514.50 ng/50 mg tissue of THC-VHS in the IC at 90 minutes.

The prodrug concentrations dropped almost 20-fold at 360 minutes, which can be explained by elimination and slow conversion into THC, which was also detected then. We also observe THC-VHS partitioning into the RC, from both THC-VHS-TOC and THC-VHS-SLN formulations, which is important for neuroprotective action. With THC-SLNs however, we observe THC levels in the IC at both sacrifice time points, but THC fails to distribute itself across other tissues. The preferential accumulation of THC in the IC could indicate binding of THC to an IC specific protein.

The IOP lowering duration with THC-VHS-SLNs lasted almost twice as long as the marketed formulations, 2.5% w/v pilocarpine or 0.2 % w/v timolol maleate. A combined effect of prodrug derivatization and the dosage form can be attributed to this effect as the prodrug alone (in an emulsion formulation) or the parent compound THC in an SLN formulation, were not effective. The molecule design facilitated easy passage of the parent molecule across the ocular tissues and the lipid-based nano-carrier system acted as a long acting depot, resulting in a formulation with better pharmacokinetic and pharmacodynamic profile.

Conclusion

These studies suggest that formulation development efforts along with prodrug derivatization can effectively improve overall ocular bioavailability. THC-VHS-SLNs were successfully formulated and tested in a normotensive rabbit model. Results suggested that the prodrug, THC-VHS has a better permeation profile than THC due to its modified structure. Solid lipid nanoparticles are efficient in delivery of THC-VHS to the RC, important from the point of view of neuroprotection. THC-VHS-SLNs, on multiple dosing were able to achieve an intense IOP drop with its effect lasting for a longer duration than the marketed solutions of 2.5% w/v pilocarpine HCl and 0.2% timolol maleate. Thus, THC-Val-HS has the potential of bringing forth

cannabinoids as another line of therapy as anti-glaucoma agents at par with the anti-cholinergic, beta-blockers and carbonic anhydrase inhibitors, with the added advantage of its neuroprotective activity

CHAPTER 4

TRIAMCINOLONE ACETONIDE-NLCS FOR OCULAR DELIVERY: EFFECT OF CHITOSAN AND CHITOSAN DERIVATIVE

Introduction

Corticosteroids have been used for the treatment of ocular inflammation since the past few decades. Triamcinolone Acetonide (TA) is a corticosteroid administered intravitreally for the management of ocular inflammatory conditions such as diabetic retinopathy, cystoid macular edema, and choroidal neovascularization [151-152]. The use of TA has been prevalent in conditions of posterior uveitis to reduce intraocular inflammation and extravasation of blood vessels. Currently, the marketed products for ophthalmic use (e.g. Kenalog®, Tricinolon®, Flutex® and Kenacort®) are intravitreally administered ophthalmic suspensions containing TA [151, 153]. However, intravitreal injections are often associated with defects such as intraocular pressure elevation, retinal detachment, cataract formation, subconjunctival bleeding, vitreous hemorrhage and endopthalmitis. In addition, repeated administration of corticosteroid intravitreal injections results in lower patient compliance in comparison to a sustained release device therapy and implants [154-155]. Chemically, TA is a lipophilic molecule and has a Log P of 2.5 (Figure 17.), making it an unfavorable candidate for back of the eye delivery via topical administration. There arises a need for the development of a novel formulation of TA dosed topically, designed to achieve drug levels at the back of the eye.

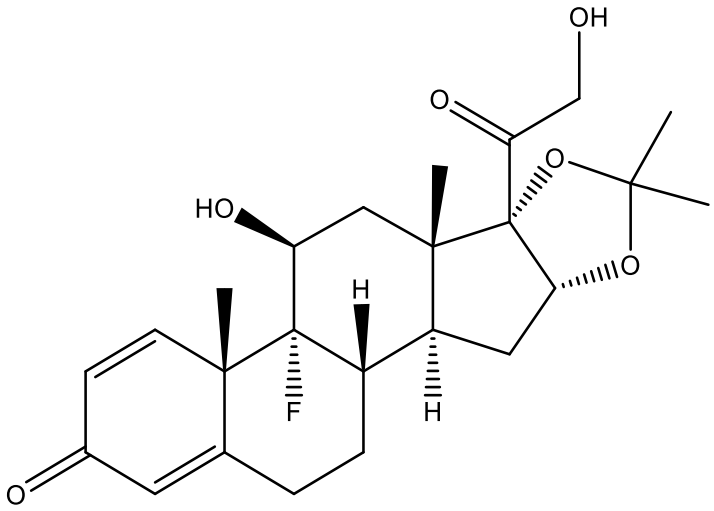

Triamcinolone Acetonide

Figure.17. Chemical structure of Triamcinolone Acetonide

Bioavailability can be enhanced by modification of physicochemical properties of the drug by attaching a promoiety, formation of ion-pairs, use of permeation enhancers or by formulation approaches aiming at increasing the pre-corneal residence time [76, 86, 156-157]. In the past few years, research focus on the use of colloidal nanoparticulate systems as a promising ocular drug delivery platform has increased [137-138, 158]. Lipid based colloidal nanocarriers such as SLNs and NLCs are nanoparticulate systems efficient in targeted and controlled delivery of lipophilic drugs [159]. These nanoparticulate carriers may demonstrate superior ocular bioavailability of the encapsulated therapeutic agent because of improved retention in the *cul-de-sac* resulting in sustained release for prolonged duration of time. [97]

Chitosan (CH) is a biodegradable polymer known to interact with the mucin protein and extend retention time of the formulation.[160-162] It also behaves as mucoadhesive, increasing the contact time with the membrane and acts as an absorption enhancer across biological membranes. It helps in opening of the tight junctions between the epithelial cells enhancing transport of molecules.[160-

[161, 163-164] The predicted mechanism for this absorption enhancement is interaction of the positively charged amino groups on the C-2 position of chitosan with the negatively charged sites on the cell membranes [160-161, 163, 165-166]. Protonated chitosan is also known to interact with the glycoproteins of the mucous membrane covering the cornea and with the lipid bilayer of the corneal cell membrane resulting in permeability enhancement. The pKa value of chitosan is between 5.5 and 6.5 and thus is insoluble at physiological pH, losing its positive charge [166-167]. Derivatization of chitosan to its quarternized form, tri-methyl chitosan (TMC) is an effort in solubilizing chitosan at all pH ranges [168]. TMC has been known to interact with the epithelial cell monolayers by the same mechanism as chitosan [164]. The use of permeation enhancers such as TMC and CH as nanoparticle surface modifiers may further improve the retention of the nanoparticles on the epithelial surface and increase cellular uptake of the nanoparticles. [162, 166]

This research aims at optimizing a colloidal formulation for the topical delivery of TA. The studies also investigate the effect of CH and TMC on the permeation characteristics of TA. Primarily, TMC was synthesized using previously reported protocols from deacetylated CH [169]. Lipid based nanoparticles of TA were formulated selecting a combination of solid and liquid lipids. The rationale behind selection of lipid-based nanoparticles, NLCs, was development of a topically dosed nano-colloidal based depot system sustaining the release of TA, thus reducing the overall frequency of administration. Transcorneal permeation of 0.1% TA encapsulated in CH and TMC nanoparticles was compared to that of the optimized TA-NLC system, 0.1% w/v TA-Randomly methylated β cyclodextrin (RMβCD) solution (TA-SOL). In addition, the effect of surface modification of NLCs using polymers CH and TA was evaluated; a 0.25% CH and 0.25% TMC surface modified TA-NLC system was evaluated for the precorneal retention and overall ocular bioavailability of TA.

Materials and methods

Materials

TA and sodium tripolyphosphate (TPP) was procured from Alfa Aesar™, Chitosan chloride (CH-Cl) < 200 kDa was received from Novamatrix (Philadelphia, PA, USA), Trimethyl Chitosan Chloride was synthesized using method detailed in the following section. Precirol® 888 ATO (glyceryl behenate) was obtained as a gift sample from Gattefossé (Paramus, NJ, USA), Glycerin was purchased from Acros Organics (NJ, USA), Pluronic® F68 (Poloxamer 188) was purchased from Spectrum Pharmaceuticals (Henderson, NV). Castor oil and Tween® 80 were purchased from Acros Organics (NJ, USA). HPLC - grade solvents, and other chemicals (analytical grade) were obtained from Fisher Scientific (Hampton, NH, USA). Amicon® Ultra centrifugal filter devices, regenerated cellulose membrane (MWCO 100 kDa) were purchased from EMD Millipore (Billerica, MA). Corneas for the transcorneal studies were purchased from Pel Freez, AK.

Animals

Male New Zealand White rabbits (2-2.5 kg), obtained from Harlan laboratories® (Indianapolis, IN) were used in all studies. All animal experiments conformed to the Association for Research in Vision and Ophthalmology statement, "Use of Animals in Ophthalmic and Vision Research" and followed the University of Mississippi Institutional Animal Care and Use Committee approved protocols.

Methods

Synthesis of Trimethyl chitosan chloride

To prepare TMC, a two-step synthesis described by Sieval et al. was employed. [169] Initially, 2g of 91% deacetylated chitosan, 4.8 g sodium iodide, 11 mL of 15% aqueous sodium hydroxide solution and 11.5 mL of methyl iodide was added to 80 mL of 1- methyl-2-pyrrolidinone. This

mixture was stirred on a water bath at 60°C for 1 hour. The product, N-methyl chitosan iodide, obtained hereby was precipitated using ethanol and further centrifuged for isolation. To completely remove the ethanol post centrifugation, the product was subjected to multiple washings with ether. The substance thus obtained was dissolved in 80 mL of 1-methyl-2-pyrrolidinone and heated to 60°C. 5.4 g of sodium iodide, 11 mL of 15% NaOH solution and 9 mL of methyl iodide was added, the reaction mixture heated on a water bath with the temperature maintained at 60°C for 30 min. The product obtained was dissolved in 40 mL of 10% NaCl solution. ^{1}H NMR were measured in D_2O at 400MHz.

The degree of quaternization (DQ) and the degree of dimethylation (DM) were calculated by using the following equations:

$$DQ = [(CH_3)_3]/[H]*1/9] * 100$$

$$DM= [(CH_3)_2]/[H]*1/6] * 100$$

Saturation solubility studies

Solubility of TA was studied in IPBS at pH 7.4. Effect of addition of solubility enhancers such as cyclodextrins; 5% HPβCD and 5% RMβCD was also evaluated. The experiment was conducted by adding excess amount of TA to centrifuge tubes containing 1 mL of the above-mentioned solutions. To achieve uniform mixing, samples were shaken overnight at 100 rpm, 25°C in a reciprocating water bath (Fisher Scientific). After 24hrs, the samples were centrifuged using the AccuSpin 17R at 13,000 rpm for 30 minutes and the supernatant was analyzed for TA using HPLC-UV analytical method.

Synthesis of TA formulations

TA-SOL solution

TA-SOL solution was prepared by dissolving TA (0.1% w/v) in 2.5% w/v RMβCD solution prepared in IPBS at pH 7.4. TA was added to the solution and the mixture was vortexed for 2-5 minutes and sonicated until a clear solution was obtained.

TA-NLCs

Lipid excipient screening study

The solubility of TA was observed in solid lipids; Compritol® 888 ATO with a melting point (MP) of 70°C–72°C, Precirol® 888 ATO (MP: 56°C), Coco butter (MP: 34–38 °C), and Geleol™ Mono and Diglycerides NF (MP: 54°C–64°C) and Gelucire® 50/13 was studied. Liquid lipids castor oil, Miglyol 812, Oleic acid and Sesame oil were scanned similarly. The solid and liquid lipids were heated to 80°C and TA (100 mg) was added to the heated lipids (100 mg) under constant magnetic stirring at 2000 rpm. The different TA-lipid mixtures were then cooled and observed for precipitation of the API. The lipids devoid of any precipitation were further selected for synthesis of the NLCs.

Selection of a binary lipid phase

To determine the best solubilizing potential of the solid-lipid-liquid-lipid mixture, 100 mg of TA was mixed with three different ratios, (i.e.; 2:3, 1:1, 3:2) of select solid and the liquid lipids, those showing maximum solubilizing potential for TA in the solubility study. TA was added to the lipid mixtures under magnetic stirring at 600-800 rpm at 80°C for 30 minutes. The miscibility of the binary lipid phase was observed by spreading the mixture on a glass slide followed by visual observation. Mixtures which presented with least to no bleeding of the oil from the solid lipid were selected from preparation of the NLCs.

Preparation of TA-NLCs

TA-NLCs were prepared by an ultrasound sonication method using Vibra-Cell™ Ultrasonic Liquid Processor, SONICS™. Based on lipid screening studies, Precirol® 888 ATO (glyceryl palmitostearate) was the choice of solid lipid and castor oil was chosen to be the liquid lipid. The aqueous phase composed of surfactants such as Poloxamer 188 (0.25% w/v), Tween® 80 (0.75% w/v) and glycerin (2.25% w/v) in bidistilled water, was heated at 80 ± 2°C and added to the molten lipid phase under stirring (2000 rpm) to form a coarse emulsion, the temperature during the entire process maintained at 80 ± 2°C. The premix was then homogenized at 11,600 rpm for 10 mins using T 25 digital Ultra-Turrax to form a pre-emulsion. This pre-emulsion was further subjected to probe sonication resulting in further particle size reduction and formation of a hot nanoemulsion. Further cooling resulted in the formation of TA-NLCs; a lipid based nanocolloidal suspension.

Preparation of TMC/CH surface modified NLCs

For the TMC/CH surface modification of TA-NLCs, TMC synthesized by the previously described protocols and CH-Cl (mol. wt. < 200 kDa) were used. Accurately weighed amounts of TMC/CH corresponding to 0.25% w/v were incorporated in the TA-NLC formulation once prepared and cooled. These surface modified formulations were then stirred at 800-900 rpm for 10-12hrs to ensure optimum surface interaction of TMC/CH to the NLCs. A pre and post-modification measurement of the hydrodynamic radius as well as zeta potential could confirm the effectiveness of the surface modification.

Preparation of TMC/ CH-TA nanoparticles

TMC/ CH nanoparticles (NP) were prepared by cross-linking with TPP by ionotropic gelation method. Primarily, TMC/CH solution (0.5 % w/v) was prepared by dissolving TMC/ the chloride salt of CH in bi-distilled water. TA (0.1% w/v) was dissolved in ethanol and added to the TMC/CH

solution under vigorous stirring. Further, for cross-linking, TPP was added under probe sonication to form TMC/ CH NPs. The TMC/CH to TPP weight ratio used was 5:1.

Physicochemical characterization

Assay and Entrapment

Methanol was used for the precipitation of lipids in the TA-NLC systems. An accurately measured volume of the TA-NLC (10 μL) was extracted with methanol (990 μL). For estimating the % Assay of TA in the CH-NP and TMC-NP formulations, the extracting solvent used was a 1:1 ratio of methanol: 0.1% Acetic acid for CH-NP and methanol: bidistilled water for TMC-NP. The supernatant was analyzed after centrifugation (13,000 rpm for 20 min) as such or with further required dilutions for TA content using a HPLC-UV method described later.

For estimating the % Entrapment Efficiency (%EE), five hundred μL of all the formulations centrifuged using a 100 kDa centrifugal unit made of regenerated cellulose membrane (Amicon Ultra) and the sample was centrifuged at 13,000 rpm, for 20 mins, following which the filtrate was analyzed for free TA content. Percentage EE was calculated using the formula,

$$\% EE = \frac{(Total\ drug\ content - Amount\ of\ free\ drug\ in\ aqueous\ phase) * 100}{Total\ drug\ content}$$

Chromatography

Samples were analyzed for TA using an HPLC-UV system comprising a Waters 717 plus Autosampler, Waters 600E pump controller, Waters 2487 dual λ Absorbance detector and an Agilent 3395 integrator. Stock solutions of TA were prepared in acetonitrile and used immediately. A mobile phase consisting of 50: 50 Acetonitrile: Water was used on a Phenomenex® C18 (4.6 x 250 mm) column at a flow rate of 1 mL/min. Detection was carried out at 254 nm.

Dynamic light scattering (DLS)

The hydrodynamic radius and the PDI of the TA-NLCs, TMC/CH coated NLCs and CH/ TMC NPs was determined by photon correlation spectroscopy using a Zetasizer Nano ZS Zen3600 (Malvern Instruments, Inc.) at 25°C and with 173° backscatter detection in disposable folded capillary clear cells. The same equipment was used to determine the zeta potential of the formulations at 25°C in folded capillary cells using the same instrument. To measure the particle size distribution and zeta potential, the samples were diluted (1:100) with bidistilled water filtered using 0.2 µ syringe filters.

Scanning transmission electron microscopy (STEM)

TA-NLCs were characterized using a 40-dual beam scanning transmission electron microscope by Zeiss Auriga®. A negative staining procedure was employed wherein 1% w/v uranyl acetate was used as a staining agent. A drop of the sample, about 20 µL was placed on a piece of parafilm. A 200-mesh glow discharged copper grid coated with a thin film made of carbon was floated on top of the sample with the film facing the sample. The contact between the grid and the sample was maintained for 30 s, after which the grid was displaced and excess sample on the grid was blotted using a filter paper. The grid was then subjected to washing using ultrapure water; the grid was placed on a drop of the ultrapure water, after which the excess water was blotted out. The grid then was placed sample side down on a drop of 1% uranyl acetate for 1 minute. The excess stain was then removed, and the sample was dried completely. After blotting and drying, the samples were imaged in a Zeiss Libra operating at 30 kV and in STEM mode. (The STEM studies were performed at University of Tennessee, Knoxville).

In vitro drug release of TA from formulations

The *in vitro* release kinetics of TA from TA-NLCs, TMC/CH coated TA NLCs and TA-SOL were evaluated across dialysis membranes (10K molecular weight cut-off) using Slide-A-Lyzer® Mini Dialysis Devices. The dialysis devices were placed in scintillation vials containing 20 milliliters of the release medium; IPBS at pH 7.4, containing 5% w/v HPβCD, the temperature of which was maintained at 34°C. The donor chamber was filled with 1 mL of each of the formulations and the cross-sectional area of diffusion was 0.64 cm^2. At regular time intervals up to a total duration of 5 hours, 600-µL of the release medium was aliquoted and replaced with an equal amount of fresh IPBS solution containing 5% HPβC. The aliquots were analyzed for TA content using a HPLC UV method.

The *in vitro* release profile of TA from TA-NLC, TMC/CH coated TA NLCs and TA-SOL was fitted to different mathematical models to analyze the release kinetics quantitatively. Models such as zero order, first order, Korsmeyer-Peppas, Higuchi and Hixson- Crowell release model were evaluated for linear regression of the release data. The best fit model was determined based on the regression coefficient (r^2) and the best fit model was considered the one with the highest r^2.

In vitro transcorneal permeability

A vertical Franz diffusion cell setup from PermeGear®, Inc. was used to evaluate trans-corneal permeability of formulations across isolated rabbit corneas. The corneas were excised from whole eyes obtained from Pel-Freez Biologicals, AK shipped overnight in Hanks' balanced salt solution over wet ice. The corneas were excised so that they had scleral lining of about 2-3 mm thickness to help secure the membrane between the diffusion cells. The cornea was clamped in between the two half-cells with the epithelial surface facing upwards toward the donor chamber. A jacketed circulating water bath helped maintain the temperatures of the diffusion half-cells at 34°C.

Permeability of TA from formulations TA-NLCs (0.1% w/v), TA-SOL (0.1% w/v), TMC-TA-NLC (0.1% w/v) and CH-TA-NLC (0.1% w/v) across the excised corneas was studied. The receiver medium comprised of 5 mL of 2.5% solution of RMβCD in DPBS. The contents of the receiver chamber were stirred continuously with a magnetic stirrer and aliquots of 600 µL were withdrawn from the receiver chamber at predetermined time points and replaced with an equal volume of receiver medium. TA was quantified using the previously mentioned HPLC-UV chromatography method.

Mucoadhesion study

To study the mucoadhesion of the coated NLCs, the interaction of the coated CH and TMC with mucin was studied in an *in vitro* setup. Zeta potential was used as a measure of the interaction between the surface modified NLCs and different concentrations of mucin solution. A 0.25% w/v solution of mucin stock solution was prepared by dispersing the mucin in Milli-Q® water. Dilutions of the stock were prepared at concentrations of 0.025 mg/mL, 0.125 mg/mL, 0.25 mg/mL, 0.5 mg/mL, 1.25 mg/mL, 2.5 mg/mL and 5 mg/mL. A 25 µL aliquot of each of the test formulations (TA-NLC, TMC-TA-NLC, CH-TA-NLC) was admixed with each of the mucin concentrations individually. The zeta potential of the resulting mixture was monitored. All the measurements were performed in triplicates.

Ocular pharmacokinetics

The ocular retention of TA-NLC, TMC-TA-NLC, CH-TA-NLC and TA SOL was determined by tear sample analysis of male New Zealand white rabbits, weighing between 2 and 2.5 kg. The experiment was carried out in 12 male rabbits, four groups comprising of three animals per group. A single instillation of 50 µL of each of the formulations (Dose: 50 µg) was made into the lower conjunctival sac of the rabbits, after which the test eye was manually closed for 10 s. Tear samples

were collected using Whatman™ Quantitative filter paper. A dry, pre-weighed triangular piece of filter paper (11 x 6 x 11mm) was angled using a pair of forceps into the cul-de-sac of the rabbit, making sure that the filter paper does not poke the eye of the rabbit. Tear samples were collected at time intervals of 1, 15, 30, 60, 90, 120 minutes after instillation. A pre and post sampling weight check was recorded for the filter paper in centrifuge tubes to quantify the amount of tear collected. TA was then extracted from the filter papers by adding 600 µL of acetonitrile to the centrifuge tube, followed by vortexing the sample for 30 to 45 s and centrifugation at 13,000 rpm for 15 min. Non-compartmental analysis of the collected tear fluid concentrations was performed to compute the ocular pharmacokinetic parameters using the software PK Solver 2. TA was quantified from the supernatant using the HPLC-UV method.

***In vivo* bioavailability**

In vivo bioavailability of TA was determined in male New Zealand white rabbits, weighing between 2 and 2.5 kg, procured from Charles River Labs. The formulations TA-NLC, TMC-TA-NLC, CH-TA-NLC, TA-SOL were evaluated *in vivo* in a conscious rabbit model in triplicates (n = 3); the ocular penetration of TA was evaluated as a function of the vehicle. Concentration of TA was determined in the Cornea (Cor), AH, VH, RC, IC and sclera (SC). Fifty microliters of the above formulations were dosed twice, with a 5-minute gap between the two doses (Dose: 100 µg TA). The formulations were instilled in the conjunctival sac of the rabbits; the eyelid of the rabbit was shut manually by the personnel for 10 to 15 seconds post dosing. Three hours after dosing, the rabbits were anesthetized using a combination of ketamine (35 mg/kg) and xylazine (3.5 mg/kg) injected intramuscularly. The rabbits were euthanized with an overdose of pentobarbital injected through a marginal ear vein. The eyes of the rabbits were then enucleated and washed

thoroughly with IPBS and the intraocular tissues such as Cor, RC, SC, IC, AH and VH were separated.

Tissue sample preparation and extractions

The amount of TA permeated through the ocular tissues was determined by precipitating the proteins in the ocular tissues. The solid tissues, namely, Cor (50 mg), Sc (250 mg), IC (50 mg) and RC (30 mg) were cut into small pieces, whereas, the liquid tissues, AH (100 µL) and VH (500 µL) were used as is. The calibrators were prepared by spiking the tissues with TA to yield final concentrations of 0.5, 1, 5, 10, 20, 50, and 100 ng/mL. Fifty ng/mL of internal standard (Fluocinolone Acetonide) was added to the samples. Volume was made up with ice-cold acetonitrile, precipitating proteins from individual tissues. Samples were vortexed and kept aside for 10 minutes. The supernatant was collected after centrifuging for 30 minutes at 13,000 rpm and analyzed using LC-MS/MS quadrupole.

Quantification of TA from biological matrices

TA quantification post tissue extractions was performed using a Waters Xevo TQ-S triple quadrupole tandem mass spectrometer with an electrospray ionization (ESI) source, equipped with the ACQUITY UPLC® I-ClassSystem, was used (Waters Corporation, Milford, MA). A Waters Xevo TQ-S quantitative analysis TargetLynx software was used for data acquisition which was processed using the MassLynx mass spectrometry software.

A C18 column (Acquity UPLC®BEH C18 100mm 2.1 m, 1.7-mm particle size) was used for the chromatographic separations with a gradient elution method. A mobile phase made up of components (A) Water + 0.1% formic acid and (B) acetonitrile + 0.1% formic acid at a flow rate of 0.7 mL/min was used. The gradient elution protocol was as follows; at 0 min, a ratio of 98% A/2% B which was held for 0.2 min, switching over to 100% B in next 2.3 min. This composition

was held for 1 min and switched over again to 98% A/2% B in the next 0.2 min. The system was then equilibrated with this composition over the next 2 min for the next injection. The column and sample temperature were maintained at 50°C and 10°C, respectively. After the chromatographic separations, the effluent passed into the ESI probe. The ESI source conditions were optimized for the molecule of interest; source temperature 150°C, desolvation temperature 600°C, capillary voltage 0.6 kV, cone voltage 26 V, nebulizer pressure 7 bar, and nebulizer gas 1000 $Lh^{-1}N2$. The mass spectra were acquired in positive mode and multiple reactions monitoring mode. Instrument control and data processing were performed by using MassLynx software (version 4.1; Waters, Milford, MA). The multiple reactions monitoring mode was applied to monitor the transitions parent to daughter compound; from 435.24 m/z to 339.153 m/z, 357.155 m/z and 397.190 m/z for TA and from 453.17 m/z to 121.02 m/z, 337.11 m/z and 413.16 m/z for the internal standard, Fluocinolone Acetonide.

Statistical analysis

Statistical analysis was performed using JMP® 14, SAS. Statistical significance was tested for using ANOVA followed by Tukey HSD test to analyze for inter-group differences (formulation dependent). Differences were statistically significant at a level of $p \leq 0.05$.

Results and Discussion

Synthesis of TMC

Chitosan was methylated with CH_3I to yield TMC. The yield of TMC obtained was 4.5 grams and the compound was freely soluble in water up to concentrations of 5% w/v. As per the peak assignments by Sieval et al [169], ^1H NMR data (Figure 18.) depicts a tertiary amino $N(CH_3)_2$ peak at 3.13 ppm and a quaternary amino peak at 3.36 ppm. The DQ of the product computed as per the

previously mentioned formula was 56.76% and the DM was 8.41%. TMC was prepared by a two-step synthesis with a high % DQ as per protocols elucidated by Sieval et al [169].

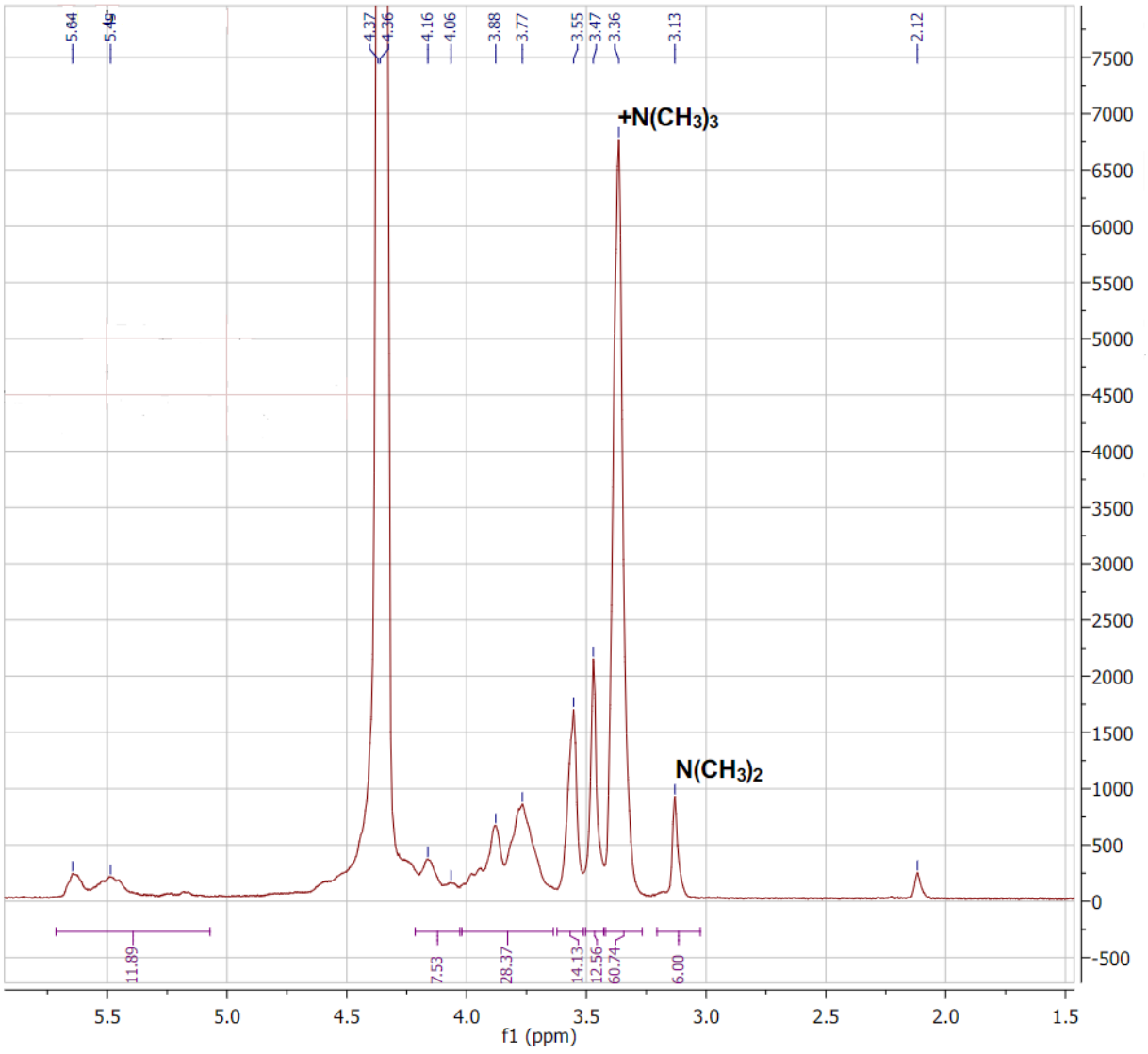

Figure.18. NMR spectra of the compound synthesized, N-Trimethyl Chitosan Chloride

Saturation solubility studies

Cyclodextrins have been known to enhance the solubility of poorly soluble compounds in ophthalmic and topical products. The solubility of TA was observed in 5% cyclodextrin solutions of HPβCD and RMβCD (Figure 19.). In HPβCD, the observed solubility of TA was 0.97 ± 0.03 mg/mL whereas in RMβCD saturation solubility of 1.6 ± 0.15 mg/mL was observed. Solubility of TA was extremely low in IPBS and was found to be 0.029 ± 0.004 mg/mL. The use of cyclodextrins led to 30-50 times enhancement of solubility of TA at pH 7.4. Based on the solubility data, RMβCD was selected as the solubility enhancer in the receiver medium for *in vitro* transcorneal permeation studies described previously.

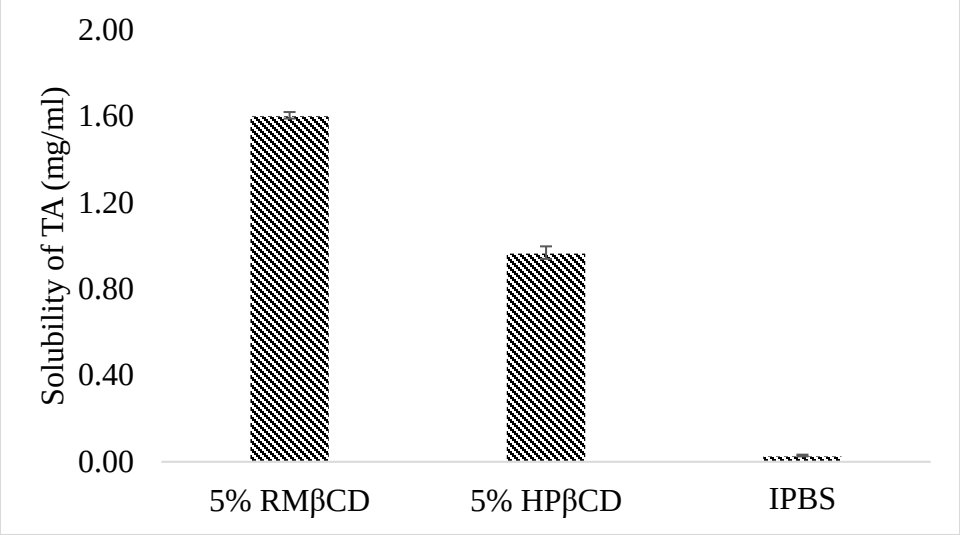

Figure 19. Saturation solubility of TA in phosphate buffer, 5% w/v HPβCD in phosphate buffer, and 5% w/v RMβCD in phosphate buffer (mg/mL). The results are depicted as the mean ± SD (n=3).

Lipid excipient screening study

Solubility of TA in both solid and liquid lipids has been illustrated in Figure 20. The lipids presenting with maximum solubility for TA were chosen to formulate the TA-NLCs. In the solid lipids tested TA demonstrated superior solubility in Precirol® 888 ATO and Compritol® 888 ATO whereas amongst the liquid lipids tested, castor oil was the best. At a ratio of 1:1 of TA: individual solid/liquid lipids, no undissolved drug was observed at an elevated temperature of 80°C. Furthermore, no precipitation was observed on cooling the lipid melt to room temperature.

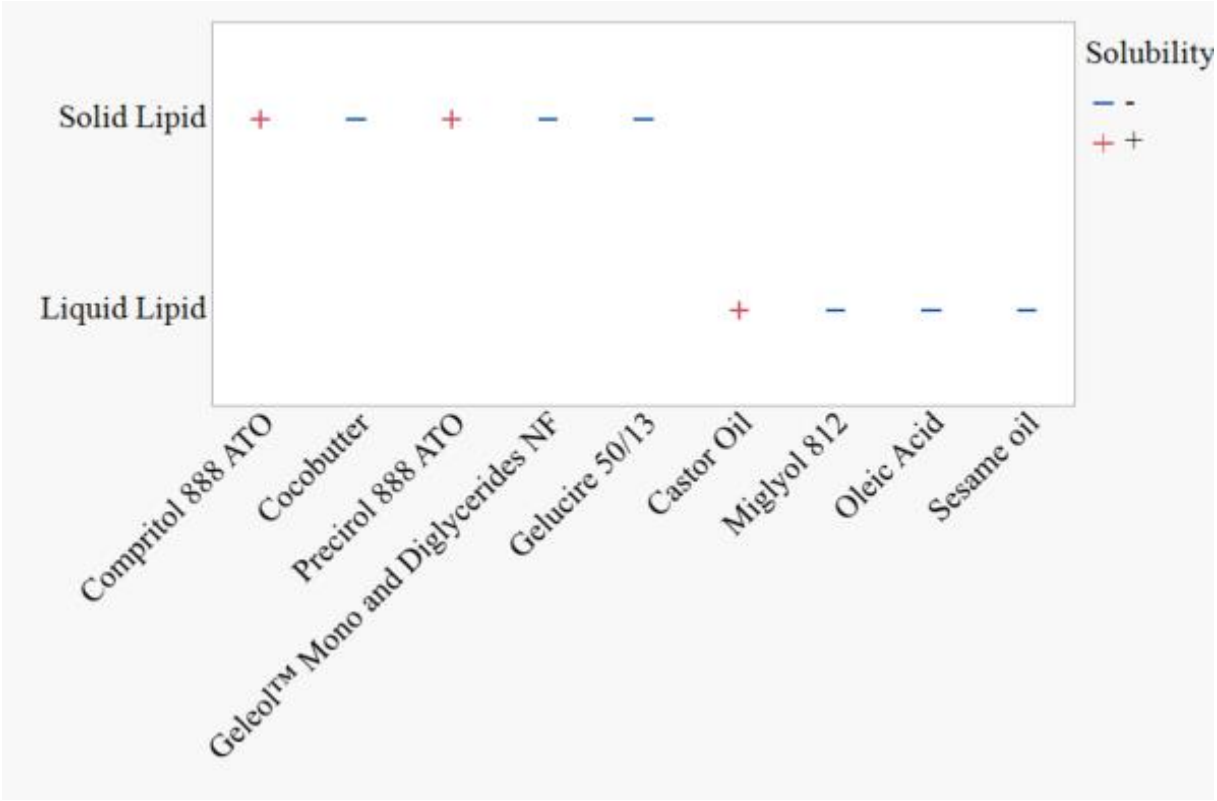

Figure 20. Solubility of TA in solid and liquid lipids.

Selection of a binary lipid phase

Solid lipids, Precirol® 888 ATO and Compritol® 888 ATO were tested individually at three different ratios for miscibility liquid lipid castor oil. Clear bleeding of castor oil from the solid phase was observed for both solid lipids at a 2:3 ratio of solid lipid: liquid lipid. However, when mixed at a 1:1 ratio Precirol® 888 ATO and castor oil demonstrated better stability in comparison to a combination of Compritol® 888 ATO and castor oil. Presence of higher amounts of liquid lipid permits for a better drug load and fluidity of the API within the particle. The goal behind formulation of these NLCs was to allow almost an equal amount of solid and liquid lipid which would further affect the partition and release characteristics of TA. Keeping this in mind, Precirol® 888 ATO and castor oil were chosen to formulation the NLCs at a ratio of 1:1.

Physicochemical characterization of all the formulations

The % Assay and % EE of TA-NLC, TMC-TA NP and CH-TA NPs was found to be 96.5 ± 8.1%, 85.76 ± 3%, 89.01 ± 0.86% and 99.01 ± 0.69%, 80 ± 0.07% and 88.14 ± 0.02%, respectively. The NLCs prove to be a superior nano-carrier for TA in terms of % Assay and % EE, which could be a virtue of the lipophilic nature of TA having increased affinity for the lipids used for the encapsulation of TA in the TA-NLCs. Table 11. compares the particle size (d. nm), PDI and zeta potential (mV) of the TA-NLCs and the surface modified NLCs. TA NLCs have a particle size of 192.27 ± 5.05 d. nm and a narrow PDI of 0.23 ± 0.001. On modification of the TA-NLC surface with different concentrations of TMC, the particle size of the NLC system increased up to 500 d. nm indicating that TMC had adhered to surface of the NLCs. The negatively charged (-37 mV) surface of the TA-NLCs provided a favorable setup for this surface modification. This surface modification can also be backed up by the ZP data, increase in the ZP of the TA-NLCs after surface modification indicated that TMC has accumulated on the NLC surface. Coating the NLCs with

concentration of 0.5% TMC or higher could possibly result in particle aggregation and an unstable formulation. Based on formulation stability, a 0.25% polymeric coating was chosen to coat the TA-NLCs for *in vitro* and *in vivo* evaluation. Table.11. provides a summary of the physicochemical characterization of the formulations.

Table 11. Particle size (d. nm), PDI and zeta potential (mV) values for each formulation

	Particle size (d. nm)		**Polydispersity Index**		**Zeta Potential (mV)**
Formulation	**Mean**	**Std Err**	**Mean**	**Std Err**	
0.1% TMC COATED NLC	515.90	7.58	0.22	0.02	20.10
0.25% TMC COATED NLC	531.10	11.44	0.24	0.00	26.80
0.5% TMC COATED NLC	325.23	2.82	0.47	0.02	24.10

Scanning transmission electron microscopy (STEM)

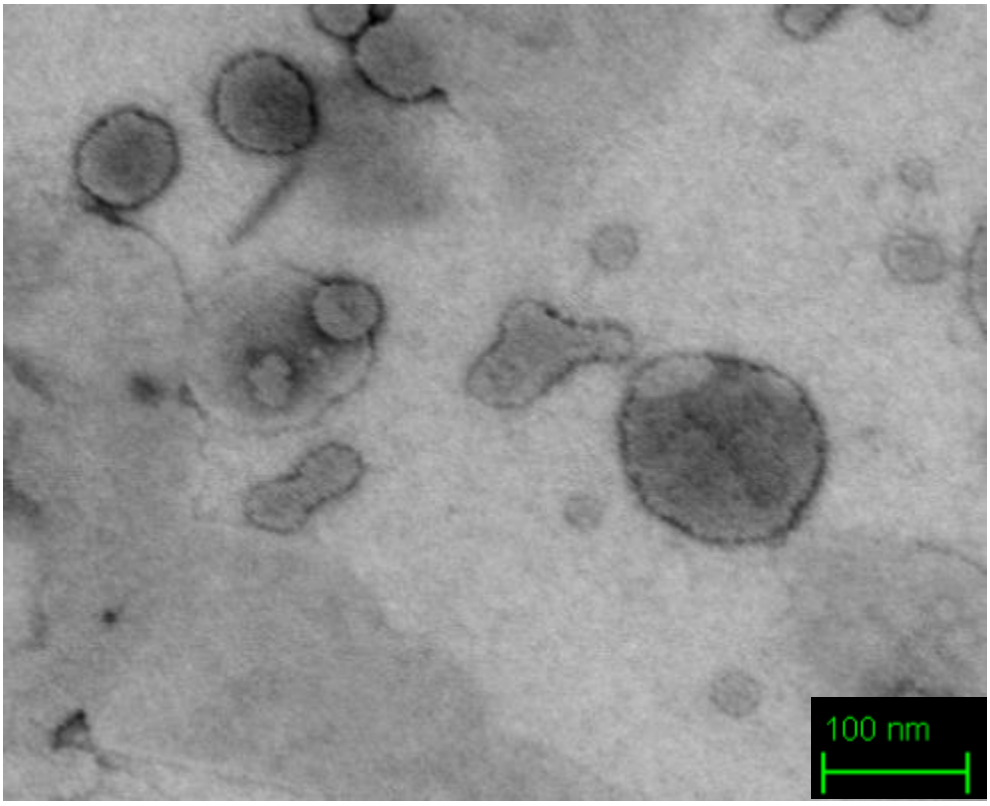

Figure 21. STEM image of the optimized TA-NLC formulation

To visualize the optimized NLCs for morphological characterization, STEM imaging was employed. (Figure. 21.) An electron beam is passed through a thin layer of prepared sample. The transmitted beam is then projected on a phosphorescent screen or detector. Figure 21. depicts spherical NLCs formed with a smooth periphery, the particle size of which is around 100 d.nm. DLS describes the particles to have a particle size of 192 d. nm, with a PDI of 0.23, and presence of a slightly polydisperse particle size distribution could be a possible reason for the discrepancy between the particle sizes reported by DLS and STEM imaging. [143-144]

In vitro drug release of TA from formulations

TA release from the formulations was observed in a simulated ocular tissue environment. The release curves were obtained by plotting the cumulative % drug release against the time of the study in minutes, Figure 22. To analyze the drug release rate kinetics, the *in vitro* drug release profiles were fit into mathematical models. The model that best fit the release data was determined by the r^2. The r^2 values for all the formulations are listed in Table 12. The zero-order model fit the release profile of TA NLC best, which meant that the nanoparticles did not disintegrate; rather they released the drug slowly. The release profile of TA from TA-NLCs (Figure.22.) depicts a slow and gradual increase in release of TA, from 1 to 7% over a period of 5h. Comparing the release profile of TA from the NLCs to the polymeric coated nanoparticles (Figure. 22.), the presence of the polymeric coat controlled the release of TA through the duration of the study. Percent cumulative drug lease from TA NLC was significantly greater than the coated NLCs at 60, 180 and 300 minutes. We observe a burst in release of TA from the TA-NLCs from the 30 minutes to 60-minute time-point. This can be attributed to release of TA from the external surface of the nanoparticles, following by gradual release from the lipid core. The kinetic model that best fit the drug release from the coated NLCs was the first order model with a r^2 value of 0.96 and 0.99 for TMC-TA-NLC and CH-TA-NLC respectively. Looking at the n values for the Korsmeyer-Peppas fit for the coated nanoparticles, CH-TA-NLC and TMC-TA-NLC had n values of 0.73 and 0.54 respectively, which meant that the coated NLCs demonstrated a non-Fickian transport mechanism, involving swelling of the polymeric coat and diffusion of the drug from the lipidic core, through the polymer into the release medium.

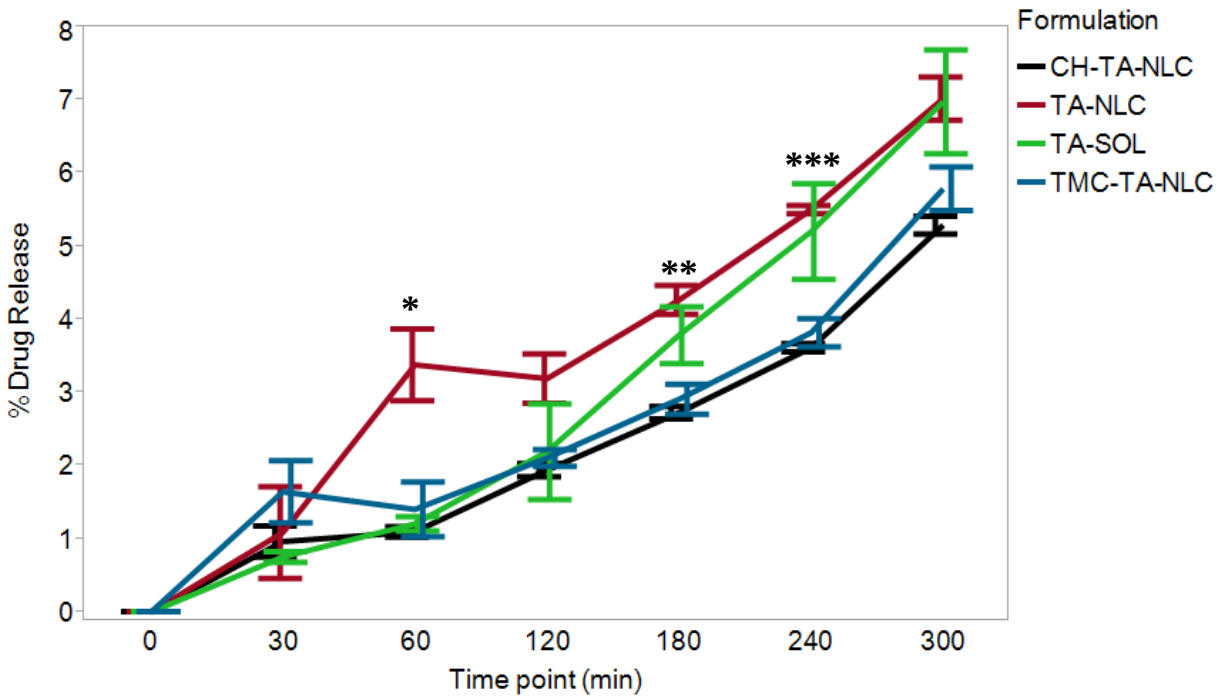

Figure.22. *In vitro* release profile of TA from nano-formulations in phosphate buffer, pH 7.4 over a period of 5h

*% Drug release from TA-NLC significantly greater than CH-TA-NLC, TMC-TA-NLC and TA-SOL

** Drug release from TA-NLC significantly greater than CH-TA-NLC, TMC-TA-NLC

*** Drug release from TA-NLC and TA-SOL significantly greater than CH-TA-NLC, TMA-TA-NLC

Table 12. *In vitro* release kinetic parameters for TA formulations; r^2 is the regression coefficient

Model fitted	Equation	r^2 value			
		TA-NLC	TA-SOL	CH-TA-NLC	TMC-TA-NLC
Zero Order	$C_t = C_0 + Kt$	0.90	0.93	0.97	0.91
First Order	$C_t = C_0\, e^{-Kt}$	0.73	0.95	0.99	0.96

Korsmeyer-Peppas	$\frac{C_t}{C_\infty} = Kt^n$	0.88 n=0.69	0.97 n=0.92	0.94 n=0.73	0.80 n=0.54
Higuchi	$C_t=Kt^{1/2}$	0.86	0.58	0.72	0.75

Mucoadhesion study

Ocular mucus is composed of mucin as one of its many components, protecting the corneal epithelium from desiccation and bacterial contamination. The mucin is negatively charged due to the presence of sialic acid residues, which helps the eye repel pathogens [170]. A positively charged particle would interact with the mucin layer and reside in the *cul-de-sac* and corneal epithelium for a longer duration of time. While targeting the delivery of TA to the back of the eye, on topical application, enhanced ocular retention would in turn increase the overall permeation of the molecule [76, 86]. This mucoadhesion study was conducted to study the electrostatic interaction between the positively charged coated TA-NLCs and the negatively charged mucin in an *in vitro* setup. Zeta Potential of TA-NLC, TMC-TA-NLC, CH-TA-NLC was monitored at increasing concentrations of mucin to investigate the electrostatic interaction (Figure.23.). On increasing the mucin concentration from 0.5 mg/mL up to 2.5 mg/mL, there was a sharp drop in the zeta potential of the TMC coated NLC, from 16.8 ± 4.02 mV to -1.47 ± 3.94 mV, indicating a strong interaction between the polymer and the mucin. For the CH-NLC, we observe this interaction at a higher concentration of mucin, with a sharp drop in the zeta potential from 19.3 ± 3.78 mV to 10 ± 5.16 mV at mucin concentrations of 1.25 mg/mL to 2.5 mg/mL. Increasing the mucin concentration further resulted in a negative zeta potential of both the coated formulations. Through all the increasing concentrations of mucin, TA-NLC had a negative zeta potential from about -30 mV to -40 mV, indicating no interaction between the uncoated particles and mucin. The interaction between the polymer coated NLC and the mucin

could result in retention of the nanoparticles in the ocular mucosa, improving the overall permeation profile of the formulation. The fact that TMC interacts with a mucin concentration 5 times lower than the mucin concentration CH interacts with is indicative that TMC is a better mucoadhesive agent in comparison to CH.

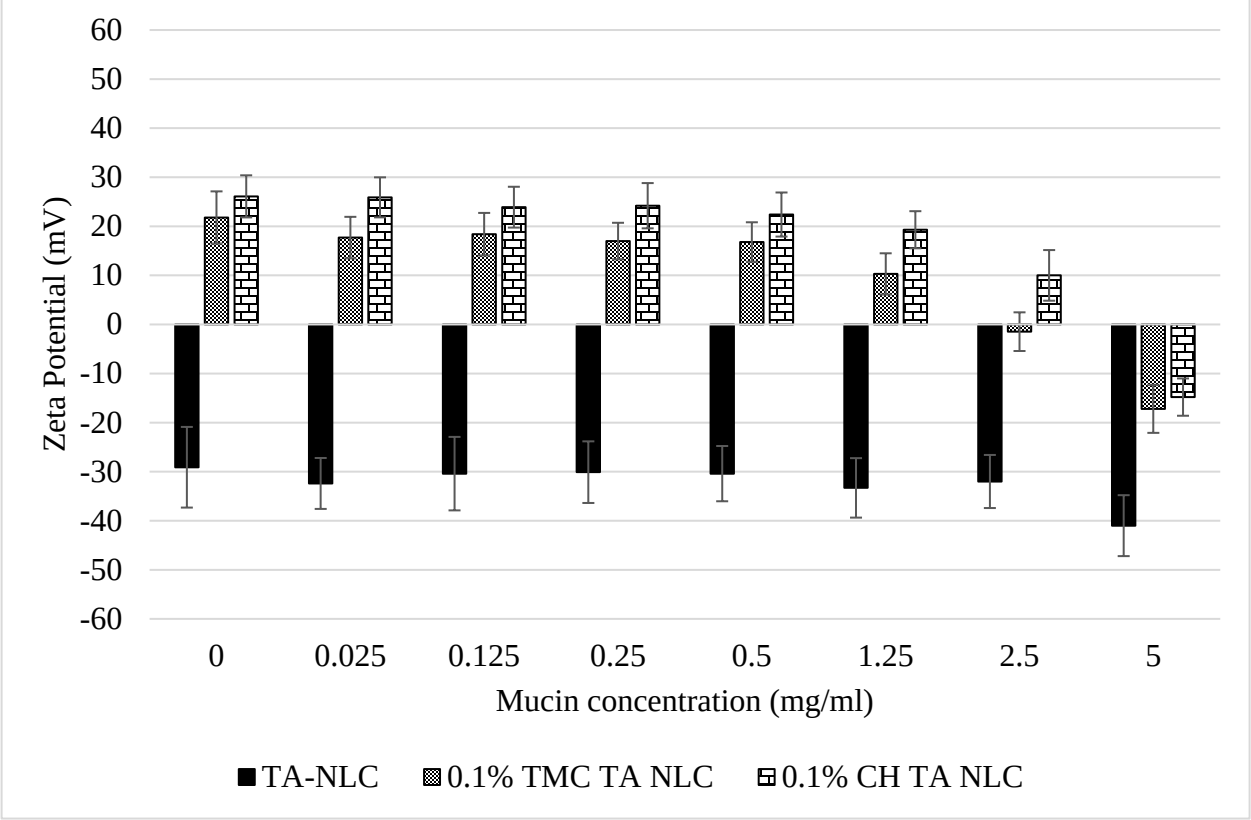

Figure.23. Zeta potential of TA-NLCs, TMC-TA-NLC, CH-TA-NLC formulations at increasing concentrations of mucin (0.025 to 5 mg/mL)

In vitro transcorneal permeation

The transcorneal permeation profile of TA-NLC, TA-SOL, TMC NP and CH NP solution was observed over 180 minutes at 34°C across isolated rabbit corneas. The 0.1% TA- SOL demonstrates an enhanced permeation profile (Figure.24.) with significantly high amounts of

permeated TA by the 180 min time-point and a permeability of 6.30 ± 0.9 x 10^{-6} cm/sec and a transcorneal flux of 0.378 ± 0.054 µg/min/cm^2 (Table 13.). Cyclodextrins have been previously reported to affect the barrier characteristics of rabbit corneas.[171] Cyclodextrins orient perpendicularly on the surface of the phospholipid monolayer and extract the cholesterol molecule and result in damage to the corneal membrane, increasing overall transmembrane permeation. CH/ CH derivatives are also known for their ability to interact with the corneal surface; CH/ CH derivatives interact with the mucin layer increasing the transcellular transport of molecules and increase the pre-corneal retention time. In terms of flux and permeability, TA-NLC demonstrate a slightly better permeation profile than the coated nanoparticles (Table.13.). This can be attributed to the presence of a hydrophilic polymeric barrier on the surface of the NLCs for the coated nanoparticles. This could possibly hinder the partitioning of the molecule from the lipophilic core into the external hydrophilic environment. The presence of CH and CH derivatives, along with mucoadhesion, also affect the dynamic transport mechanisms of molecules. The *in vitro* mucoadhesion study provides us with information that both TMC and CH interact with the negatively charged mucin at different concentrations, indicating that mucoadhesion is one of the inherent properties of the polymers that would affect the permeation of TA. However, to further elucidate the effect of polymeric coating on the TA-NLC, a dynamic *in vivo* environment would prove to be a better predictor over effect of CH and CH derivatives on overall ocular bioavailability. The comparable permeation profiles by CH-TA-NLC and TMC-TA-NLC indicate that despite increased adhesion and retention, the partition of TA from the lipophilic core is probably hindered and is a vital step that governs the transport mechanisms of TA.

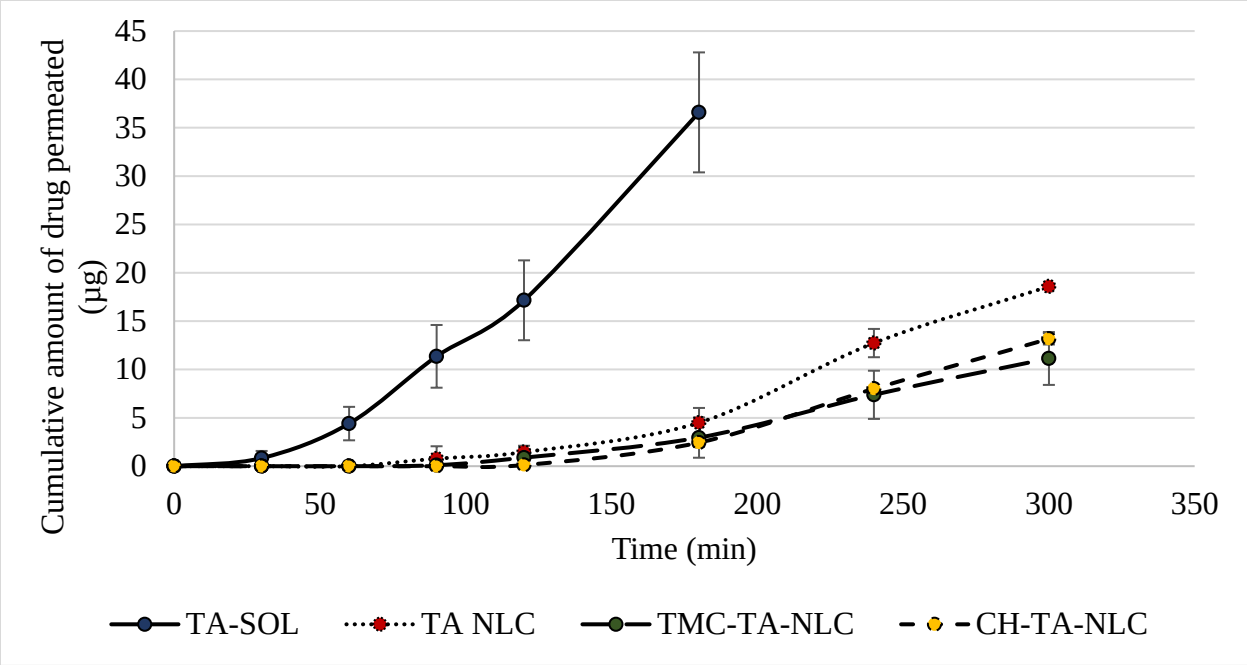

Figure 24. Transcorneal permeation profile across isolated rabbit cornea from TA-NLC, TA-SOL, TMC-TA-NLC, CH-TA-NLC at 34ºC. The receiver solution consisted of DPBS containing 2.5% w/v RMβCD (pH 7.4). The results are depicted as the mean ± S.D (n=3)

Table 13. Permeability (cm/sec) and transcorneal flux (µg/min/cm^2) of TA-NLC, TMC-TA-NLC, CH-TA-NLC and TA-SOL across isolated rabbit cornea. The results are depicted as the mean ± S.D (n=3)

Formulations	Permeability x 10^{-6} (cm/sec)	Flux (µg/min/cm^2)
TMC-TA-NLC	1.12 ± 0.25	0.067 ± 0.015
CH-TA-NLC	1.29 ± 0.04	0.077 ± 0.002
TA-NLC	1.88 ± 0.07	0.234 ± 0.106
TA-SOL	6.30 ± 0.9	0.378 ± 0.054

Ocular pharmacokinetics

Tear fluid kinetics of TA-NLCs and polymer coated NLCs in comparison to TA-SOL post single instillation (Dose: 50 µg) of each of the formulations was studied in NZW rabbits. Achieving suitable concentrations of the drug in the pre-corneal area and increasing its retention time is the first limiting step of achieving tissue concentrations at the back of the eye. Ocular barriers such as blinking, and tear clearance reduce the precorneal residence time of the drug. The concentration of drug present in the tear fluid is a measure of its availability to further permeate in the tissue layers. A higher mean residence time (MRT) indicates a longer residence of TA in the pre-corneal tissues. TMC-TA-NLC demonstrates an MRT of 49.50 minutes (Table 14.), with the MRT of the all the formulations ordered as TMC-TA-NLC > CH-TA-NLC> TA-NLC> TA-SOL. TMC-TA-NLC also demonstrated a 1.73, 1.63 and 1.72 times higher $AUC_{0-\infty}$ in comparison to the other tested formulations, TA-SOL, CH-TA-NLC and TA-NLC respectively. TMC-TA-NLC retain TA in the precorneal area and show significantly higher concentrations (264.12 ± 59.74 ng/mg tear weight). Ocular pharmacokinetics of TA-SOL demonstrates quick drainage and minimum retention of the formulation in the pre-corneal tissues. Figure.25. is a graphical representation of the tear fluid concentrations; TA-SOL demonstrates a high concentration of TA, 2821.33 ± 78.31 ng/mg tear weight significantly greater than all other formulations at the 0-time point. This observation can be attributed to the free TA present in solution at the first-time point. However, a sharp drop in TA concentrations was observed post the 0-minute time point signifying absence of precorneal retention from this solution formulation; the MRT for TA-SOL is 1.08 minutes. Due to the colloidal system, TA-NLCs does increase the overall precorneal retention of TA, and the MRT of the TA-NLCs is 28 times greater than the solution formulation. Presence of a positive charge on the particles does show a slight improvement in the MRT and $AUC_{0-\infty}$ of the NLCs. Looking

at the Clearance (Cl) of the TA formulations, TMC-TA-NLC depicts the lowest CL values of 0.0013 mL/min, in comparison to the other formulations. The Cl values of the formulations can be ordered as TA NLC>TA-SOL>CH-TA-NLC>TMC-TA-NLC. Low Cl values of the coated nanoparticles can be indicative of the mucoadhesive properties of the positively charged polymers, CH and TMC and interaction of the same with the negatively charged ocular mucosa. The results of ocular pharmacokinetics agree with *in vitro* findings stating that presence of a charged polymeric coating enhances the residence of TA in the eye. The TMC and CH interact with the negatively charged corneal surface, impacting the retention of the NLC formulation in the pre-corneal area.

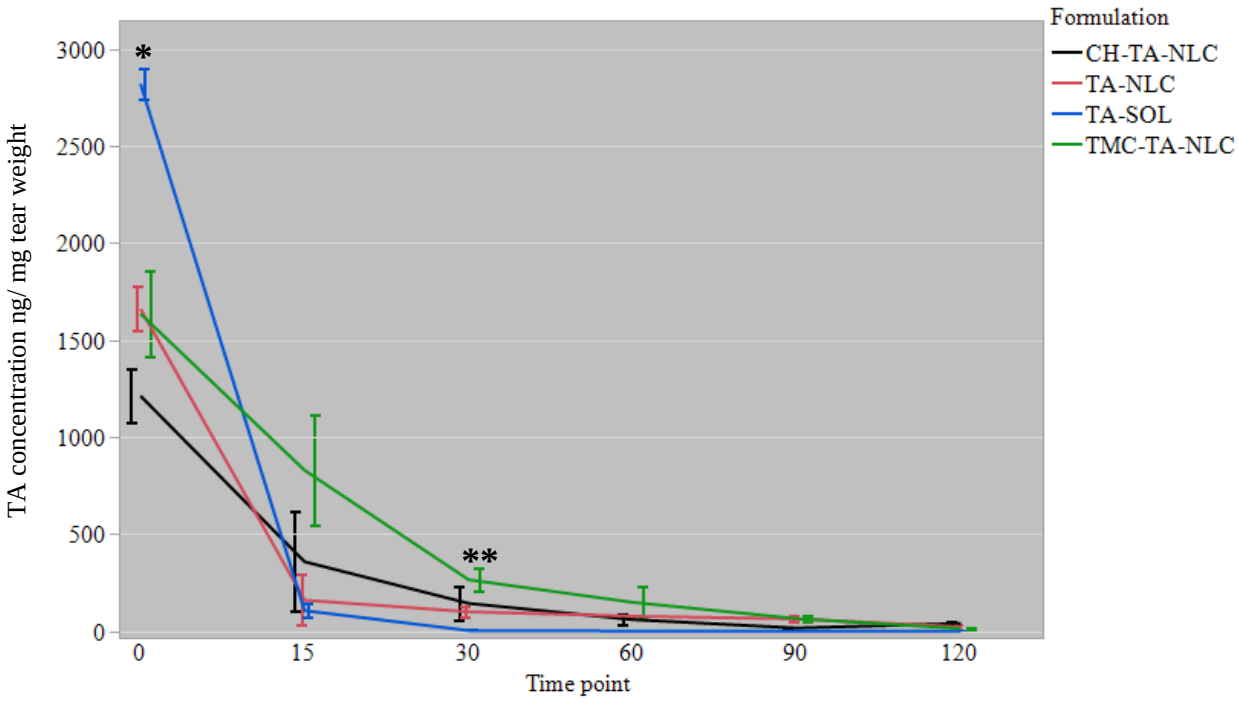

Figure.25. Tear concentration (ng/mg tear weight) vs time (min) profile for TA formulations

*TA-SOL significantly > TA-NLC, CH-TA-NLC, TMC-TA-NLC

**TMC-TA-NLC significantly > TA-SOL

Table 14. Non-compartmental analysis of tear fluid concentrations post dosing of TA-NLC, TMC-TA NLC, CH-TA NLC and TA-SOL using software PK Solver 2.0

Formulations	$AUC_{0-\infty}$ (μg/mL*min)	$t_{1/2}$ (min)	C_{max} (μg/mL)	Cl (mL/min)	MRT (min)
TA-NLC	23001.28	43.72	1660.87	0.0043	30.45
CH-TA-NLC	24220.04	67.67	1211.79	0.0021	32.19
TMC-TA-NLC	39466.58	32.59	1635.50	0.0013	49.50
TA-SOL	22763.02	2.93	2821.33	0.0022	1.08

***In vivo* bioavailability**

Male NZW rabbits were dosed consecutively with 50 μg of TA formulations; TA-NLC, TMC-TA-NLC, CH-TA-NLC and TA-SOL. The tissues analyzed were Cor, AH, VH, IC, RC and SC. Looking at Figure.26., TA-SOL was not retained in the pre-corneal area and depicted lower concentrations (289 ± 99.6 ng/ g of tissue) in the Cor. This result is consistent with the ocular pharmacokinetics (Figure.8.), with high levels of TA-SOL detected on the 0-time point and quick drainage from the precorneal region post dosing. The concentrations in the Cor further impacts the distribution of TA in the ocular tissues and we observe 242 ± 17.5 ng/ mL in the AH, 22.7 ± 7.39 ng/ g of tissue in the IC and 53.4 ± 20.3 ng/ g of tissue in the SC.

With TA-NLC and CH-TA-NLC (Figure.26.), we observe comparable levels of TA, i.e. 533 ± 175 ng/ g of tissue weight and 524 ± 211 ng/ g of tissue weight in the Cor respectively. For TMC-TA-NLC, TA concentrations were lower than that of CH-TA-NLC and TA-NLC (454 ± 163 ng/ g of tissue weight). As TA permeates further into the tissues, we observe greater levels of TA delivered

to the AH via CH-TA-NLC (493 ± 144 ng/ g of tissue weight) in comparison to TA-NLC (377 ± 32.6 ng/ g of tissue weight), indicating that CH enhances permeation of TA across the cornea. Previous reports of multiple dosing of 0.2% TA liposome formulation demonstrated levels of TA permeating into the VH and retina 12 h after topical administration. Considering the multiple dosing regimen and formulation concentration, there was 50-fold difference in the dosing reported in comparison to our data. Possible reasons for improved penetration could be the presence of formulation components such as permeability enhancers, which could be another possible approach employed for increasing TA bioavailability. [172]

Looking at the tissue concentrations, we can speculate that the drug permeates the tissues via two routes, the corneal route into the AH and IC and from the back of the eye, through the SC. A similar trend as in the AH is observed with the IC, CH-TA-NLC delivers higher levels of TA (146 ± 77.1 ng/ g of tissue weight) than TA-NLC (36.4 ± 5.44 ng/ g of tissue weight). We also observe that the formulations facilitate permeation through non-corneal routes with drug concentrations detected in the SC; 66 ± 25.6 ng/ g of tissue weight from CH-TA-NLC, 52 ± 9.43 ng/ g of tissue weight from TA-NLC, 53.4 ± 20.3 ng/ g of tissue weight for TA-SOL and 38.3 ± 7.91 ng/ g of tissue weight for TMC-TA-NLC. However, TA does not permeate significantly from the SC into the posterior tissues from any of the formulations.

Comparing the ocular bioavailability to the pre-corneal pharmacokinetic parameters (Table 14.), we observe that the NLCs reside in the pre-corneal area for a longer duration in comparison to TA-SOL. This further translates into higher TA concentrations in the anterior segment for the NLCs in comparison to the SOL. By looking at the overall ocular tissue disposition for TA we can state that residence time is not the only factor that would govern the ocular bioavailability of a lipophilic API, inherent molecule characteristics would play a vital role in determining the ADME

characteristics of the molecule. TA is a lipophilic molecule, and entrapment of TA in lipid based nanocarriers results into slow release of TA into the hydrophilic tissue microenvironment which further hindering the overall ocular bioavailability of the molecule.

Reportedly, CH and TMC increase the drug bioavailability by two mechanisms; by increasing the precorneal residence time and increasing the paracellular transport of the molecule [161]. CH and its derivatives work as permeation enhancers because of an interaction between the positively charged amino groups on the C-2 position of chitosan with negatively charged sites on the cell membranes and tight junctions. This alters the integrity of the tight junctions, increasing the overall paracellular transport of the molecule. [69] TA, being a molecule with some degree of lipophilicity, would adopt a transcellular pathway for permeation, rather than a paracellular pathway. The lack in elevation of overall ocular bioavailability could possibly be attributed to the mechanism of permeation enhancement of TMC, which might not be suitable for a lipophilic molecule such as TA. Another factor to be taken into consideration is the total positive charge at the site of action, along with the molecular weight and the DQ which affects the interaction of TMC with the mucin layer. [173] As inferred from the *in vitro* mucoadhesion study, CH and TMC do interact with the mucin elements, however, due to the aforementioned reasons, the increase in pre-corneal retention might not increase the overall permeation profile of the molecule [76]. Reportedly, CH also increases permeation of molecules by endocytosis and transcytosis along with affecting the paracellular transport, which could be an explanation for increase in bioavailability of TA by surface modification using CH but not by TMC. [174-175]

Another possible explanation could be the drug load of the optimized NLCs, a 0.1% W/V drug load is not high enough a drug load to create a significant concentration gradient for diffusion of the molecule from the lipophilic carrier into the tissue micro-environment. Increasing the TA load

could possibly intensify the differences between the groups enough to make conceivable conclusions.

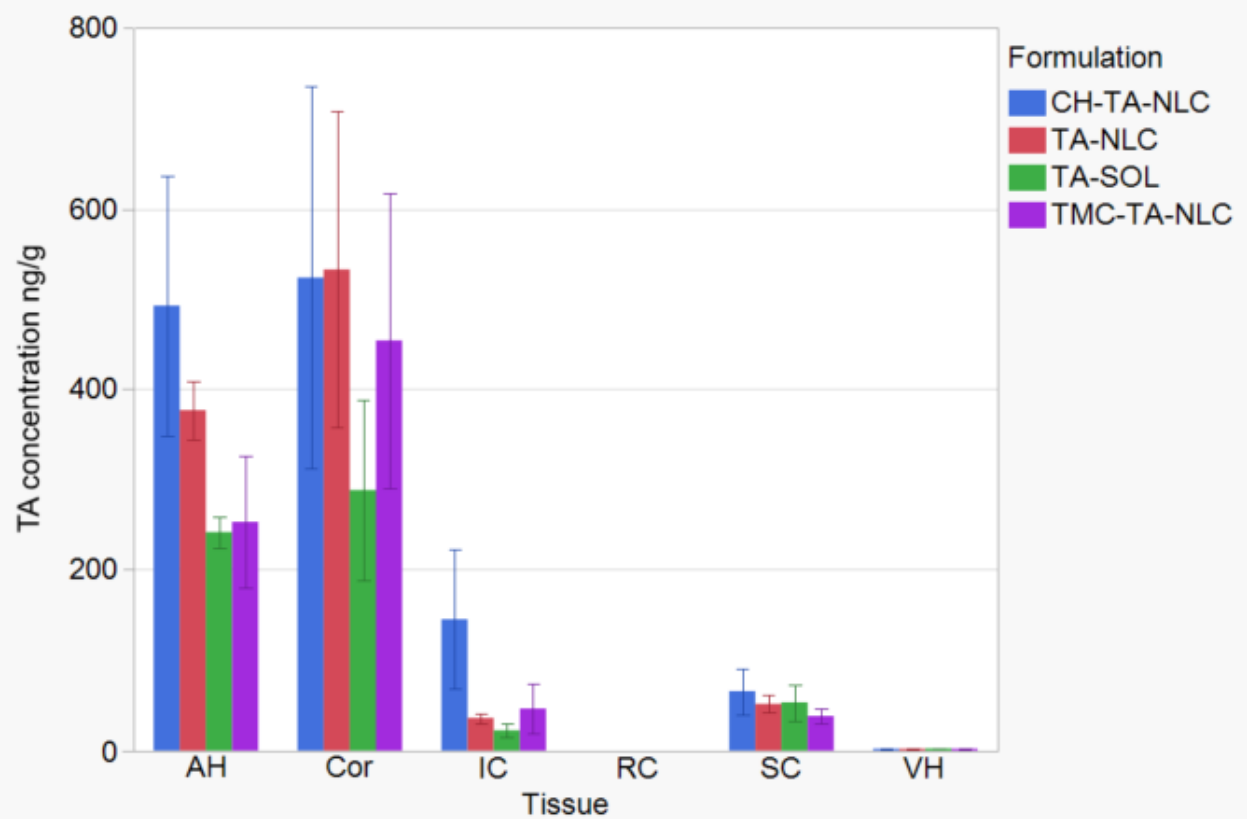

Figure.26. Tissue concentrations three hours post dosing of TA formulations (Dose: 100 µg TA) + TA-NLC, TMC-TA-NLC, CH-TA-NLC and TA-SOL in New Zealand White rabbits (n=3)

Conclusion

Topical administration is the preferred route for ophthalmic drug delivery, however anatomical barriers and precorneal factors affect the bioavailability of the formulation. The ocular bioavailability of any lipophilic molecule post topical dosing is controlled by its solubility in the hydrophilic tissue environment. Formulation approaches can enhance delivery of the molecule to the site of application. Lipid based nanoparticles have been previously reported to sustain the

release of the entrapped moiety by slowly releasing it over a prolonged period. This work attempted in developing a lipid based nanoparticulate system, NLCs to improve drug load, prolong the release and reduce dosing frequency of the molecule. Currently, TA is available as an intravitreal injection and development of a topical route is a desirable alternative. The optimized TA-NLCs with a 0.1% W/V drug load enhanced the ocular bioavailability of TA in comparison to a cyclodextrin solution. Furthermore, increasing the drug load would help in delivering sustained amounts of TA to the site of action. Surface modification of TA-NLCs with TMC increased the residence time of the formulation, however did not affect the overall ocular bioavailability. CH-TA-NLCs on the other hand were able to deliver higher concentrations of TA across the Cor. Investigations explaining mechanisms of CH on permeation enhancement by non-paracellular routes would help understand the role of CH and CH derivatives in permeation enhancement for lipophilic molecules.

Supplementary Data

Table 15. Tear concentration (ng/mg tear weight) post dosing of TA formulations (Dose: 50 µg) in male New Zealand White rabbits for time points up to 2 hours post dosing (n=3)

TA concentrations (ng/mg tear weight)			
Formulation	**Time point (min)**	**Mean**	**Std Err**
CH-TA-NLC	0	1211.79	138.99
	15	357.17	255.77
	30	142.31	90.41
	60	58.65	30.24
	90	14.98	4.65
	120	39.13	11.11
TA-NLC	0	1660.87	116.05
	15	158.88	130.06
	30	99.26	24.38
	60	76.33	4.19
	90	61.97	14.22
	120	21.48	12.75
TA-SOL	0	2821.33	78.31

	15	105.03	37.71
	30	2.34	2.34
	60	0.00	0.00
	90	0.00	0.00
	120	0.00	0.00
TMC-TA-NLC	0	1635.50	222.47
	15	828.99	282.90
	30	264.12	59.74
	60	147.75	82.28
	90	63.95	18.71
	120	12.38	7.30

Table 16. Tissue concentration (ng/g tissue weight) post dosing of TA formulations (Dose: 100 µg TA) TA-NLC, TMC-TA-NLC, CH-TA-NLC and TA-SOL in New Zealand White rabbits (n=3)

TA concentration ng/g			
Formulation	**Tissue**	**Mean**	**Std Err**
CH-TA-NLC	AH	493	144
	Cor	524	211
	IC	146	77.1
	RC	0	0
	SC	66	25.6
	VH	2.09	0.2
TA-NLC	AH	377	32.6
	Cor	533	175
	IC	36.4	5.44
	RC	0	0
	SC	52	9.43
	VH	2.36	0.34
TA-SOL	AH	242	17.5
	Cor	289	99.6
	IC	22.7	7.39
	RC	0	0
	SC	53.4	20.3
	VH	2.63	0.21
TMC-TA-NLC	AH	253	73.3
	Cor	454	163
	IC	46.7	28
	RC	0	0
	SC	38.3	7.91
	VH	2.24	0.38

CHAPTER 5

ANTI-FUNGAL & ANTI-BACTERIAL PEGYLATED-NLCS FOR OCULAR APPLICATIONS: FORMULATION DEVELOPMENT, CHARACTERIZATION AND IN VITRO EFFICACY TESTING

Introduction

Keratitis or corneal inflammation is commonly associated with bacterial or viral microorganisms resulting in corneal scarring and even permanent vision loss.[176-177] Fungal keratitis is widespread in tropical and developing countries with an occurrence of over 50%.[178] Fungal keratitis is more challenging to treat and can be more virulent and damaging than bacterial origin. Primarily an infection of the corneal epithelium, fungal keratitis (keratomycosis) may also affect the stroma and in more severe cases, the endothelium and the anterior chamber.[179] While spreading through the cornea, into the anterior chamber, fungal organisms often penetrate through the corneal stroma without rupturing the cornea.[179] A molecular target controlling fungal keratitis should penetrate across the cornea further into the stroma and other sites of infection. The aim of treating a patient with fungal keratitis is to conserve vision, which can be achieved by a timely diagnosis and antifungal therapy. Currently, the groups of antifungal agents used for the treatment of fungal keratitis are polyenes (natamycin, amphotericin B), azoles (voriconazole, posaconazole, econazole, fluconazole) and echinocandins (caspofungin).[178] A 5% Natamycin suspension is available commercially as a topical ophthalmic preparation, however it is used for superficial

infections due poor bioavailability on topical application.[177-178] Voriconazole (VRC), a second generation triazole derivative of fluconazole, has emerged as a promising candidate for the treatment of fungal keratitis because of its wide therapeutic window and high potency.[180] VRC inhibits synthesis of ergosterol in the fungal membranes by binding to the active site of P450-dependent enzyme lanosterol 14-demethylase, resulting in depletion of ergosterol, thus affecting the overall integrity and function of the fungal membrane. VRC has been approved by the US Food and Drug Administration for the treatment of systemic fungal infections. It is also commercially available for oral and parenteral use against fungal keratitis.[178-180] Studies indicate that VRC is more potent than amphotericin B against filamentous fungi such as *Aspergillus* and *Pseudallescheriaboydii.*[180-182] It is also effective against common pathogens such as *C. albicans, C. parapsilosis, C. tropicalis, A. fumigatus*, *Aspergillus flavus*, and *Fusarium solani*. The drawback with using VRC orally for treatment of fungal keratitis is associated side effects and possible drug interactions.[183] An efficient strategy would be delivering VRC locally; minimizing the drug interactions and side effects. Development of a dosage form of VRC having topical utility, and enabling VRC to permeate through the ocular tissues, to the desired site of action is necessary.

Developing a topical formulation for VRC would involve overcoming the anatomical and physiological barriers such as blinking, high tear turnover and drainage and tissue barriers such as cornea, conjunctiva, blood aqueous barrier, blood-retinal barrier.[184] Only about 3-5% of a topically dosed formulation penetrates into the deeper tissues after crossing the aforementioned barrier system, which makes development of a topical formulation challenging. VRC, being a lipophilic molecule unstable in an aqueous environment, needs a carrier system that would provide it with stability in-solution, along with sustained release by increasing the pre-corneal residence time.

Antifungal drugs such as VRC have been reported to have a synergistic effect with fluoroquinolones such as Ciprofloxacin (CIP) via binding to fungal topoisomerase II and inhibiting DNA replication.[185] CIP in itself is devoid of anti-fungal activity, but may demonstrate synergistic interactions with antifungals such as amphotericin B, voriconazole and caspofungin.[185-186] Reportedly, CIP enhances the action of azoles by increasing intracellular concentrations of the anti-fungal agents due to an overlap of substrate specificity of ATP binding cassette multidrug transporters.[187]

Different ocular delivery systems attempting to increase residence time of the formulation in the *cul-de-sac* have been investigated.[127, 132, 188] NLCs are colloidal nano-carriers synthesized by blending a mixture of solid and liquid lipids. The resulting formulation is a suspension, particles which have a melting point lower than that of their counterpart, SLNs but still solid at body temperature.[189] The imperfections in the matrix caused due to the presence of the liquid lipid result in accommodation of the API and a higher drug load (DL).[189-190] NLCs enhance trans-corneal drug delivery and increase precorneal retention time, thus a favorable system for ocular drug delivery.[132, 191]

In these set of studies VRC loaded NLCs were optimized, with the goal of achieving a stable formulation with an optimum DL which can be delivered topically for the treatment of fungal keratitis. CIP was loaded along with VRC in this nano-carrier to evaluate the synergism between anti-bacterial and anti-fungal agents. For efficient excipient selection and methodical formulation optimization, a statistical DOE methodology was employed. Being an optimization study, we wanted to look at the curvature in the model and thus a central composite design (CCD), response surface methodology (RSM) was employed to develop VRC and CIP loaded PEGylated nanostructured lipid carrier (PEG-NLC) system (VRC-CIP-PEG-NLC). The optimized

formulation was characterized in an *in vitro* setup for particle size (d. nm), DL, EE. Also, the permeation efficacy of the optimized formulation was evaluated across isolated rabbit corneas.

Materials and Methods

Materials

The active molecules, VRC and CIP were purchased from Acros Organics (NJ, USA) along with glycerin, castor oil and Tween® 80. Pluronic® F68 (Poloxamer 188) was purchased from Spectrum Pharmaceuticals (Henderson, NV). Lipids, Compritol® 888 ATO, Precirol® 888 ATO (glyceryl behenate), Geleol Mono and Diglycerides NF and Gelucire 50/13 were obtained as a gift sample from Gattefossé (Paramus, NJ, USA), mPEG-2K-DSPE sodium salt (PEG) was purchased from Lipoid®. HPLC - grade solvents, and other chemicals (analytical grade) were obtained from Fisher Scientific (Hampton, NH, USA). Amicon® Ultra centrifugal filter devices, regenerated cellulose membrane (MWCO 100 kDa) were purchased from EMD Millipore (Billerica, MA). VRC for injection, Vfend® and Ciprofloxacin Hydrochloride Ophthalmic Solution 0.3% was obtained from The University of Mississippi, Health Center. Male albino New Zealand rabbits were procured from Harlan Labs (Indianapolis, IN, USA).

Formulation optimization for NLCs

Excipient selection

NLCs are lipid-based carriers constituted with both solid and liquid lipids. As a pre-formulation screening, both solid and liquid lipids were evaluated for solubility of both the APIs. Lipids demonstrating maximum solubility were further optimized to an optimum binary mixture. Solid lipids (Compritol® 888 ATO, Precirol® 888 ATO, Stearic Acid, Geleol Mono and Diglycerides NF) and liquid lipids (castor oil, Oleic acid and Miglyol) were screened to maximize loading of both VRC and CIP. Primarily, the lipids were heated/melted by maintaining the temperature of the water bath to 80°C. After attaining the temperature, 100 mg of VRC and CIP were added

individually to the heated lipids (100 mg) under constant magnetic stirring at 2000 rpm. The API was allowed to dissolve (in case of VRC) and disperse (in case of CIP) under magnetic stirring for 2-5 minutes. The CIP-lipid and VRC-lipid mixtures were then cooled and evaluated for precipitation of the API. The basis of lipid selection in this study was optimum solubility and compatibility with CIP and VRC.

Selection of a binary lipid phase

Presence of a liquid lipid in a lipid based nano-carrier allows for imperfections and accommodation of a higher load of API. To determine the best solubilizing potential of the solid-lipid-liquid-lipid mixture, an optimum ratio of the solid and liquid lipid was determined. 100 mg of individual molecules, CIP and VRC were admixed with the lipids demonstrating maximum solubility in the excipient selection in three different ratios, i.e.; 2:3, 1:1, 3:2. The API addition took place under constant magnetic stirring over a period of 30 minutes, with the lipids heated to a temperature of 80°C. The binary lipid phase was then spread on a glass slide and was inspected for bleeding of the oil from the solid lipid.

Experimental design

After excipient selection, the next step was to optimize the levels of individual ingredients using a statistical experimental design. A mathematical optimization technique known as RSM was involved in modeling of the response variables in the dataset. This technique was used in order to make statistical predictions by fitting a polynomial equation to the set of experimental data. RSM is generally employed to a multivariate design wherein change in individual independent variables affects a response or a set of responses.

Keeping in mind the number of trials, the optimization procedure designed experiments with different levels of the independent variables generating multiple responses. On analysis, these

responses can be used to determine main effects and the predictions of these responses would help us design the appropriate formulation with target goals. A CCD of the RSM was employed wherein the amount of PEG and 1:1 Castor oil and Precirol® 888 ATO each coded as Factors B and C respectively, was varied at different levels of VRC and CIP loading (Factors A and D respectively). Each of the factors was studied at 5 levels, the end limits of which were determined based on screening trials conducted before the optimization study (Table 17.).

Table 17. Independent factors at their five coded levels from the Central Composite Design: Response Surface Methodology (The amounts (in mg) are per 10 ml of the formulation)

	Levels				
Independent Factors	-α	-1	0	+1	+α
A: Voriconazole (mg)	0	15	30	45	60
B: mPEG-2K-DSPE sodium salt (mg)	0	75	150	225	300
C: 1:1 Castor oil and Precirol® 888 ATO (Lipid ratio)	360	450	540	630	720
D: Ciprofloxacin	0	15	30	45	60

Once the limits of the input variables were established, a response surface optimization study was conducted using Design-Expert® software (Version 8.0.7.1, Stat-Ease Inc., MN). The CCD involved placement of center points (0), factorial points (+1, -1) and augmented axial points (+α, - α), with the value of α being 1.682, allowing estimation of curvature and to maintain rotatability. A 30-run design was generated using the software; runs are depicted in Table 18. This design placed fewer runs on the extremes and focused on the center of the design space, making it

a robust predictor design. The dependent variables or the responses evaluated to obtain the optimal formulations were mean particle size of VRC-CIP-PEG-NLC (d. nm), polydispersity index of the same (PDI), drug EE and DL for each of VRC and CIP.

Table 18. Runs designed by the Central Composite Design for the optimization study

Run	A: Voriconazole	B: DSPE PEG	C: Lipid Ratio	D: Ciprofloxacin
1	30	150	540	0
2	15	75	630	45
3	45	75	450	45
4	15	225	450	45
5	30	300	540	30
6	15	225	630	45
7	30	150	540	30
8	15	225	630	15
9	45	225	630	45
10	15	75	630	15
11	30	0	540	30
12	60	150	540	30
13	45	75	630	15
14	15	75	450	15
15	30	150	540	30
16	45	225	450	45
17	15	225	450	15
18	30	150	540	30
19	30	150	360	30
20	45	75	630	45
21	45	225	630	15
22	30	150	540	30
23	30	150	720	30
24	0	150	540	30
25	15	75	450	45
26	45	225	450	15
27	45	75	450	15
28	30	150	540	60
29	30	150	540	30
30	30	150	540	30

Preparation of VRC-CIP-PEG-NLC

The VRC and CIP loaded PEG-NLCs were prepared by an ultra-sonication- cold homogenization technique. APIs 0.15% VRC and 0.3 % CIP were dispersed in the lipid system and heated at 80°C. The lipid phase consisted of both the APIs, Precirol® 888 ATO, castor oil and PEG. The aqueous phase comprised of Poloxamer 188 (0.25% w/v), Tween 80 (0.75% w/v) and Glycerin (2.25% w/v) was and simultaneously heated in de-ionized water. The hot aqueous phase was added dropwise to the melted lipid phase to form a premix under constant magnetic stirring at 2000 rpm for 5 minutes. Further, the premix was homogenized for particle size reduction resulting in the formation of a pre-emulsion, using T 25 digital Ultra-Turrax™ at 11,000 rpm for 10 min by a cold homogenization method. The temperature through the second step was maintained at 35 ± 2°C. The particle size of the pre-emulsion was further reduced using a Vibra-Cell™ Ultrasonic Liquid Processor, at an amplitude of 40%. A pulse cycle was opted for this step, based on optimizations cycles run previously, and a 10 sec on and 15 seconds off pulse rate was set for a time duration of 10 minutes. The final formulation obtained post this step was further characterized morphologically and for its permeation characteristics.

Formulation Characterization

Assay and Entrapment

For the extraction of VRC and CIP, a 1:1 mixture of 0.025M O-Phosphoric acid and acetonitrile was used. Primarily, a volume of 10 µL was aliquoted from the formulation into centrifuge tubes. VRC and CIP was extracted from this aliquot using 990 µL of the aforementioned extracting solvent. This mixture was then sonicated at 30°C in a bath sonicator for 15 minutes to lyse the nanoparticles and extract both VRC and CIP. Post extraction, the tubes were centrifuged 13,000 rpm for 15 min and the supernatant was analyzed for VRC and CIP content using a HPLC-UV method.

The formulations were analyzed for the %EE for VRC and CIP. Five hundred µL of the formulation was aliquoted in a 100 kDa centrifugal unit made of regenerated cellulose membrane (Amicon Ultra). This sample was centrifuged at 13,000 rpm, for 20 mins, following which the filtrate was analyzed for unentrapped VRC and CIP content. Percentage EE was calculated using the formula,

% EE = ((Total drug content-Amount of free drug in aqueous phase) *100)/ (Total drug content)

The DL on the other hand was calculated using the following formula,

% DL = (Amount of drug entrapped / Total lipid content) * 100

Chromatography

In vitro quantification took place by using a HPLC-UV method for simultaneously analyzing both VRC and CIP. The HPLC-UV system comprised of a Waters 717 plus Autosampler, Waters 600E pump controller, Waters 2487 dual λ Absorbance detector and an Agilent 3395 integrator. A mobile phase consisting of 65: 35 of 0.025M O-Phosphoric acid and acetonitrile was used on a Phenomenex® C18 (4.6 x 250 mm) column at a flow rate of 1 mL/min. The stock solution of VRC was prepared in acetonitrile and that for CIP was prepared in 0.025 M O-Phosphoric acid. A standard curve ranging from 1 to 100 µg/ml of both VRC and CIP was prepared by spiking required concentrations from the individual stock solutions, whereas the dilutions were prepared using the mobile phase. Detection was carried out at 254 nm.

Dynamic light scattering (DLS)

Photon correlation spectroscopy was one of the methods used to determine the particle size and polydispersity index of the formulations. A Zetasizer Nano ZS Zen3600 (Malvern Instruments, Inc.) was used to make all the DLS measurements at 25°C and with 173° backscatter detection in

disposable folded capillary clear cells. A 100 times sample dilution was performed using bidistilled water filtered using 0.2 µ syringe filters for all the measurements.

Scanning transmission electron microscopy

Morphological characterization of VRC-CIP-PEG-NLC was carried out using STEM analysis. This study helped in particle visualization and comparison of the morphology and particle size to measurements made by DLS. The NLCs were stained using 1% uranyl acetate, using a negative staining procedure. A 40-dual beam scanning transmission electron microscope by Zeiss Auriga® was used to characterize the nanoparticles. The sample volume used for the study was 20 µL, which was placed on a piece of parafilm. A 200-mesh glow discharged copper grid coated with a thin carbon film was floated on top of the sample for about 30 secs, with the film facing the sample. The grid was then removed, and the excess sample blotted off using a filter paper. This step was followed by washing, the grid was placed on a drop of the ultrapure water and excess water was blotted out. The grid was placed on a drop of 1% uranyl acetate for 1 minute with the sample facing the stain. After the staining step, the excess stain was then removed, and the sample was dried completely. After sample preparation, imaging took place using a Zeiss Libra operating at 30 kV in STEM mode. (The STEM studies were performed at University of Tennessee, Knoxville).

***In-vitro* trans-corneal permeation**

Transmembrane permeability of VRC and CIP from the VRC-CIP-PEG-NLC formulation was evaluated across isolated rabbit corneas using PermeGear® vertical diffusion apparatus. To establish the effect of dual drug loading, PEG-NLCs with each of the individual APIs, CIP-PEG-NLC & VRC-PEG-NLC were also evaluated for their transcorneal permeability. Bearing in mind the clinical implications of the optimized formulation, its permeability was compared to marketed formulations; Ciprofloxacin Hydrochloride Ophthalmic Solution (0.3% as base) and Lyophilized Voriconazole for Injection (200mg/vial, dose normalized using Dulbecco's phosphate-buffered saline (DPBS) to 0.1% VRC). Five percent RMβCD in DPBS (5ml) was used in the receiver

compartment. Aliquots (0.6 ml) were withdrawn from the receiver chamber at predetermined time-points up to 3 hours and replaced with an equal volume of 5% w/v RMβCD in DPBS. The concentration of VRC and CIP in the receiver medium was determined using an established HPLC-UV method. At the end of 3 hours, the corneas were evaluated for the retention of API.

Results and Discussion

Excipient selection

Based on the excipient solubility screening studies, the lipids that demonstrated the maximum solubility for both VRC and CIP were selected. Precirol® 888 ATO was chosen as the solid lipid and castor oil as the liquid lipid.

Selection of a binary lipid phase

With each of the different ratios, we observed CIP finely dispersed and VRC completely solubilized. However, with higher level of a liquid lipid we observed bleeding of the castor oil from the Precirol® 888 ATO and API melt. A 1:1 ratio of solid lipid-liquid lipid was chosen to formulate the NLCs.

Formulation optimization of VRC-CIP-PEG-NLC using RSM-CCD statistical design

Changing parameters or independent variables is the basis of determining the optimum conditions or a level to a stable and effective formulation. This can be done by using the "one-factor-at-a-time" technique, which involves running trials by individually changing singular independent variables. However, this technique fails to take into consideration complex excipient interactions. The presence of multiple components in a final formulation leads to the development of a complex interactive concoction, and in this scenario, it is important to evaluate the independent and interactive effects of all these variables. Table 19 lists the independent variables that were evaluated in this design along with the different levels at which they were evaluated. The DOE in

this case was used for excipient selection and enhancement of the drug loading of CIP and VRC. The dependent variables, based on which the 30 formulation runs were evaluated were% Assay, % DL, % EE, particle size (d. nm) and PDI. The run schedule at the different levels of independent variables is listed in Table 18. Based on the design, 5 levels of each of the independent variables was selected, with points concentrated around the center of the design, being a response surface methodology.

Table.19. Effects of Independent Factors on the Response Variables, regression analysis performed using Design-Expert® software

Response variable	**Model**	**Model F-value**	**Degree of freedom**	**R^2 values**	
				R^2	**Adjusted R^2**
%EE (VRC)	Linear	14.35	1	0.338	0.315
%EE (CIP)	Quadratic	1.95	14	0.66	0.321
PDI	Quadratic	2.87	5	0.374	0.243
% DL (VRC)	Quadratic	10.18	9	0.997	0.996
% DL (CIP)	2FI	858.52	7	0.996	0.995
%Assay (VRC)	Linear	17.77	4	0.747	0.705

Table 20. Statistical significance using One-way ANOVA for individual response variables

Response variables	**Independent factors that affect the response variable significantly**	**p-value**	**Model equation**
%EE (VRC)	A	0.0007	EE (VRC) = +81.24 +10.18 A
%EE (CIP)	D	<0.0001	EE (CIP) = +90.96 + 12.99 D -9.54 D^2
	D^2	<0.0001	
PDI	A^2	0.0057	PDI = +0.4073 -0.0163 A +0.0107 B +0.0171 C -0.0584 BC - 0.0664 A^2
	BC	0.0582	
%DL (VRC)	A	<0.0001	DL (VRC) = +3.31 +1.84 A -0.3630 B -0.4632 C -0.2111 AB - 0.268 AC +0.0938 BC +0.0893 A^2 +0.0636 B^2 +0.0828 C^2
	B	<0.0001	
	C	<0.0001	
	AB	<0.0001	
	AC	<0.0001	

Response variables	Independent factors that affect the response variable significantly	p-value	Model equation
	BC	0.0029	
	A^2	0.0004	
	B^2	0.0066	
	C^2	0.0008	
%DL (CIP)	A	0.00234	DL (CIP) = +3.62 -0.0641 A -0.3753 B -0.4463 C +1.94 D +0.0852 BC -0.1970 BD -0.2398 CD
	B	<0.0001	
	C	<0.0001	
	D	<0.0001	
	BC	0.0149	
	BD	<0.0001	
	CD	<0.0001	
%Assay (VRC)	A	<0.0001	Assay (VRC) = 64.56 -16.02 A + 2.75 B + 1.72 C - 3.06 D

The optimum formulation should aim for a maximum DL for both, VRC and CIP without affecting the overall formulation stability, maintaining particle size and PDI at the minimum. Figure 27. is a 3D graph representing the effect of PEG and lipid ratio on particle size of the formulation. The regression analysis for this response variable did not determine any model fitting the data with a significant p-value (<0.05), however the 3D surface graph enables us to visualize the trend in the data. We observe a particle size increase at increasing levels of PEG (Figure.27. A), from 195 mg and above and with an increase with the total lipid concentration. A quadratic model best fit the PDI data (Table 19.); the variables that significantly affected the PDI values as per the model equation in Table 20. are VRC concentration (A) and an interaction term (BC), between the PEG and lipid ratio. Looking at Figure 27.B. which depicts the change in PDI, a similar trend is followed as the particle size, with higher PDI at high levels of PEG and lipid content. However, at high levels of both lipid and PEG we observe a drop in the PDI, which explains the negative sign on the significant BC interaction (Table 20.). Reportedly, PEG forms a

layer on top of the solidified lipids, stabilizing the colloidal system[192]. High levels of PEG, with low lipid content could lead to self-association of the PEG and further aggregation, as seen with the slight increase in PDI in Figure.27.B. Increasing the overall solid bulk reflects with an increase in the particle size and for maintaining a particle size of about 200 d. nm, a total lipid ratio below 570 mg and PEG concentration below 195 mg would be desirable.

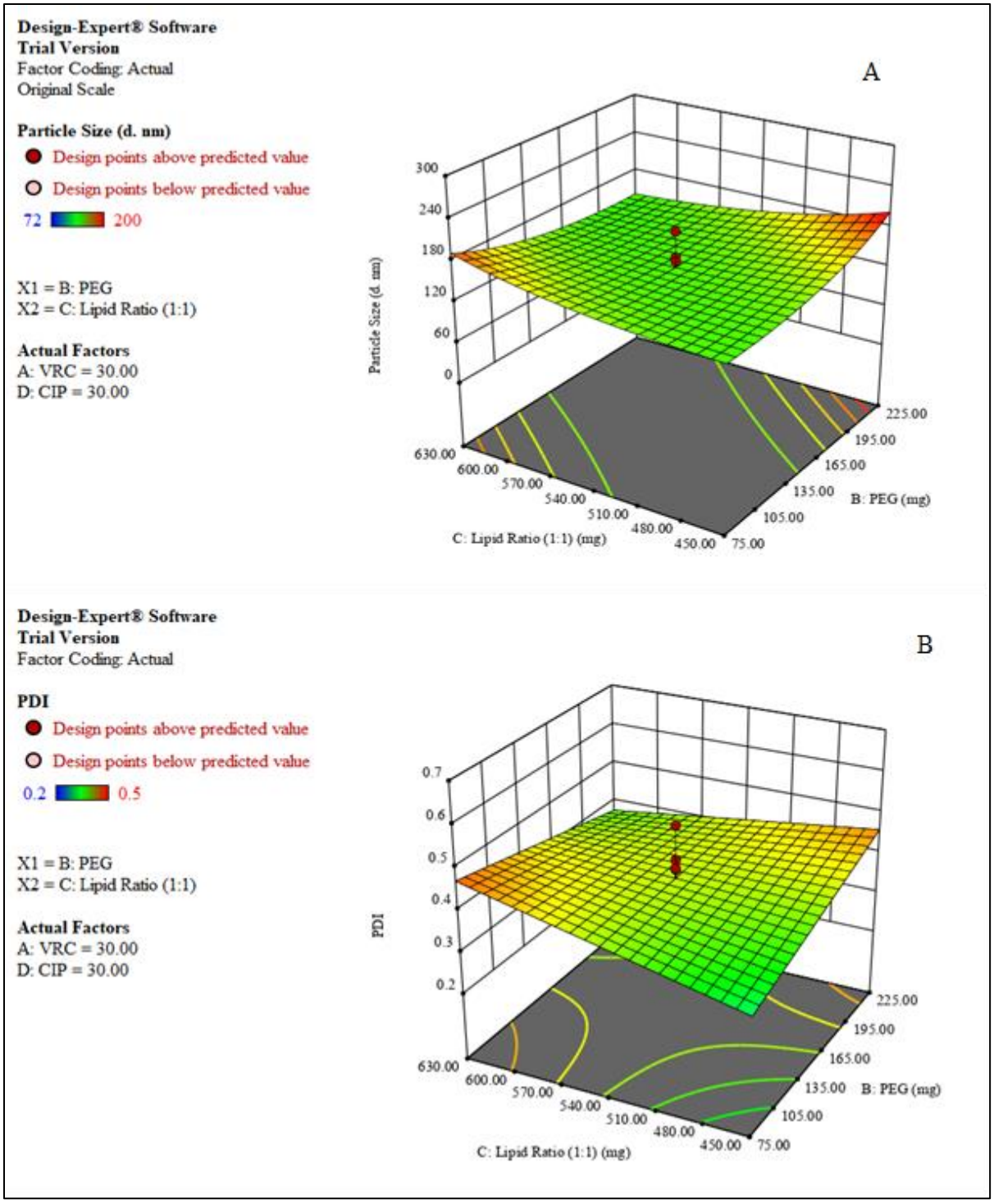

Figure.27. 3D Surface plots showing the effect of PEG and 1:1 castor oil and Precirol® 888 ATO on the Particle Size (d. nm) (A) and PDI (B)

Figure.28. depicts the effect of PEG and Lipid Ratio on the %DL of VRC. Increasing PEG concentration resulted in lowering of the %DL of VRC at both low (450 mg) and high (630 mg) of total lipid content. However, at a lower lipid ratio, the decrease in drug loading on increasing the PEG was higher than at a higher lipid ratio. From this observation, we can deduce that presence of PEG affects the loading of VRC; possible reasons for the decrease in DL could be the time of addition of PEG into the lipid melt during the initial mixing step, which would be a critical parameter in this situation, allowing VRC to partition into the lipid phase. Presence of high levels of PEG could possibly hinder the partitioning of VRC into the lipids by displacing the same.

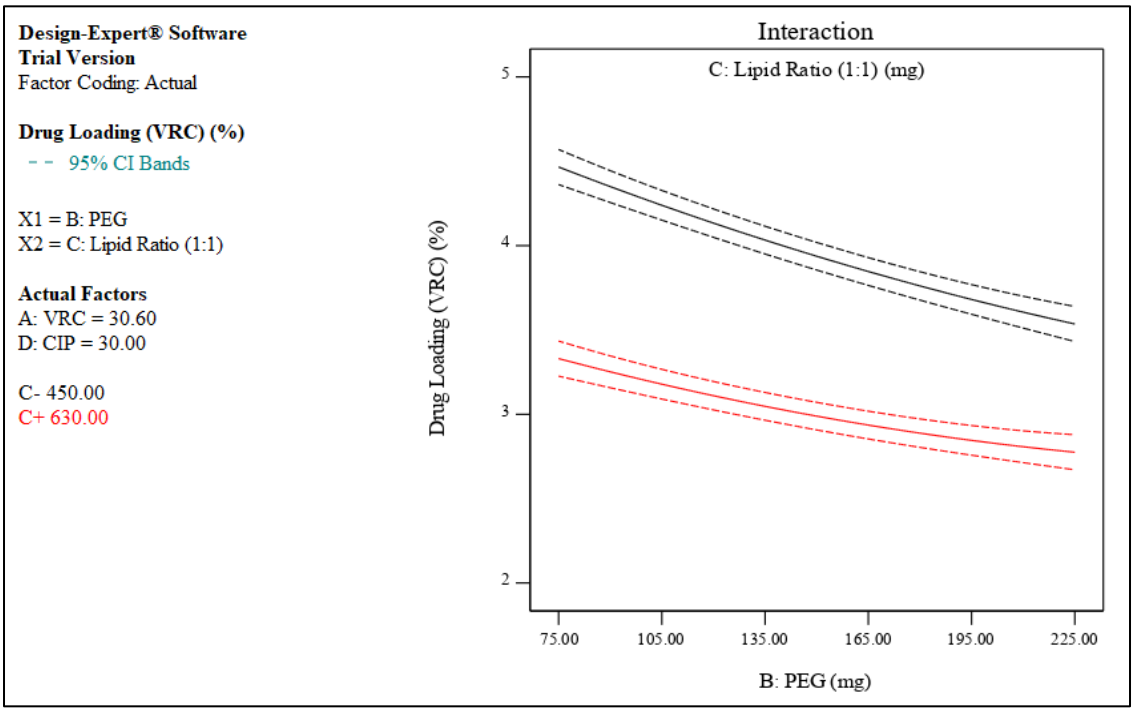

Figure.28. Interaction plots depicting the effect of PEG and 1:1 castor oil and Precirol® 888 ATO on the % Drug Loading of VRC

Looking at the equation for %Assay of VRC (Table 20.), both VRC and CIP have a negative impact on the drug content of VRC, as denoted by the negative signs. From Figure.29. A, we can see that increasing CIP content in the formulation has a negative effect on the %Assay of VRC. We also observe an effect of total lipid content on % Assay of VRC; at lower loading levels of CIP, a high lipid content improves the % Assay. Distribution of CIP in the lipids may saturate their solubilizing potential for VRC, possibly resulting in leaching of the drug outside the lipid matrix, or lower amount of drug being encapsulated in the first place. Overall, on increasing the PEG and total lipid content, the % Assay of VRC increases (Figure.29. B.), indicating that PEG and the lipids encase the drug and stabilize it, protecting it from degradation.

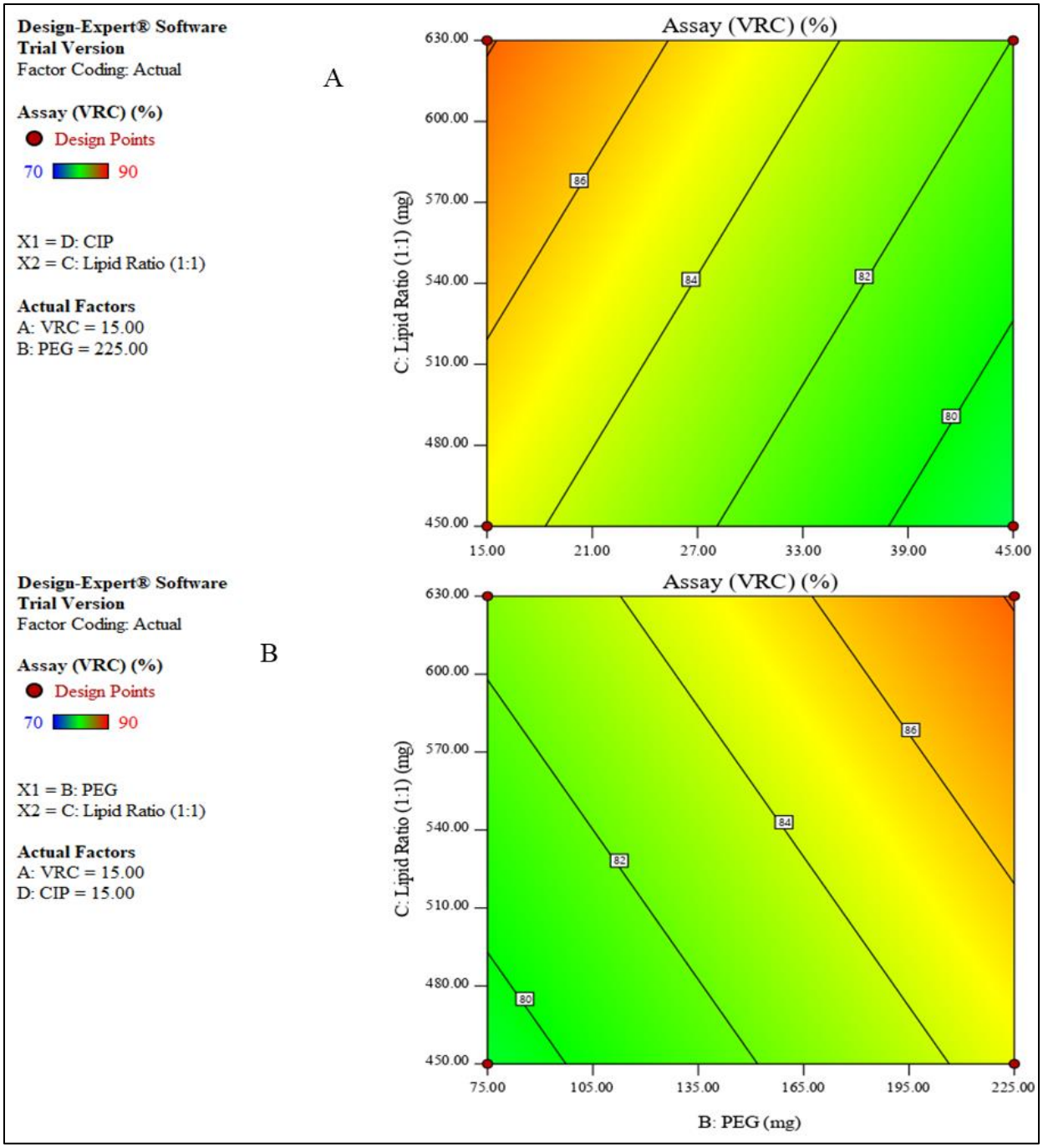

Figure.29. Contour plot describing the effect of (A) CIP loading amount and (B) PEG and 1:1 castor oil and Precirol® 888 ATO on the % Assay of VRC.

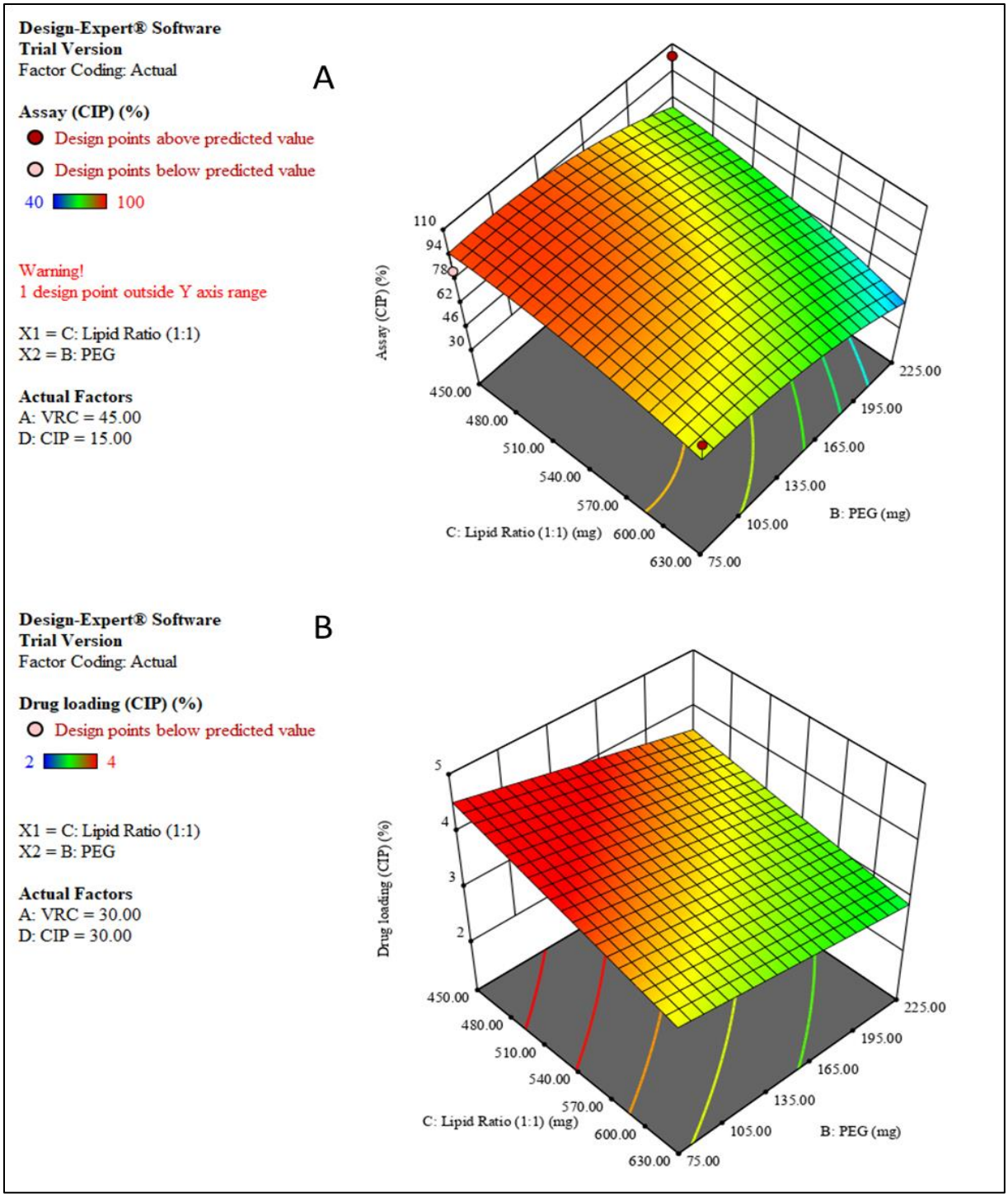

Figure.30. 3D Surface plots showing the effect of PEG and 1:1 castor oil and Precirol® 888 ATO on the (A) % Assay and (B) % Drug Loading of CIP

For % Assay of CIP, on the other hand (Figure.30. A), increasing the total lipid content above 600 mg at lower levels of PEG (75-165 mg) results in a lower % Assay of CIP. A high PEG content is not favorable for increasing CIP content in the formulation. This observation agrees with the % DL for CIP, a lower total lipid content and a lower PEG content is favorable for CIP content.

Based on the models generated for the response variables with the 30 runs, a composite function was developed by Design-Expert® Software to compute the desirability of a factor combination. The desirability of a composition can be calculated by incorporating factor constraints and modifying the factor selection criteria. The aim was to minimize the particle size and the PDI and maximize the % DL and % EE. Table 21. depicts the composition of the optimized formulation with a desirability of 0.768. Comparing the model predicted values to the actual values of the formulated suspension, the values of most responses are close to the predicted values, indicating that the model is a good predictor for the current formulation (Table 21.). The particle size of the optimized VRC-CIP-PEG-NLC formulation was 240.67 ± 2.4 d. nm with a PDI of 0.19 ± 0.02 and zeta potential of -49 ± 1.28 mV. The drug content was 92.63 ± 0.91 % for VRC and 101.93 ± 0.41 for CIP with an entrapment efficiency of 73.98 ± 1.71 for VRC and 98.86 ± 0.49 for CIP. The formulation was stable for 1 month at both storage conditions of 25°C/75% RH and 4°C (Figure.31.); we observe that the particle size and PDI of the formulation is maintained around 230-240 d. nm and 0.1-0.2 respectively. We do not observe a significant drop in the % Assay and % EE for both VRC and CIP, pointing towards a stable formulation.

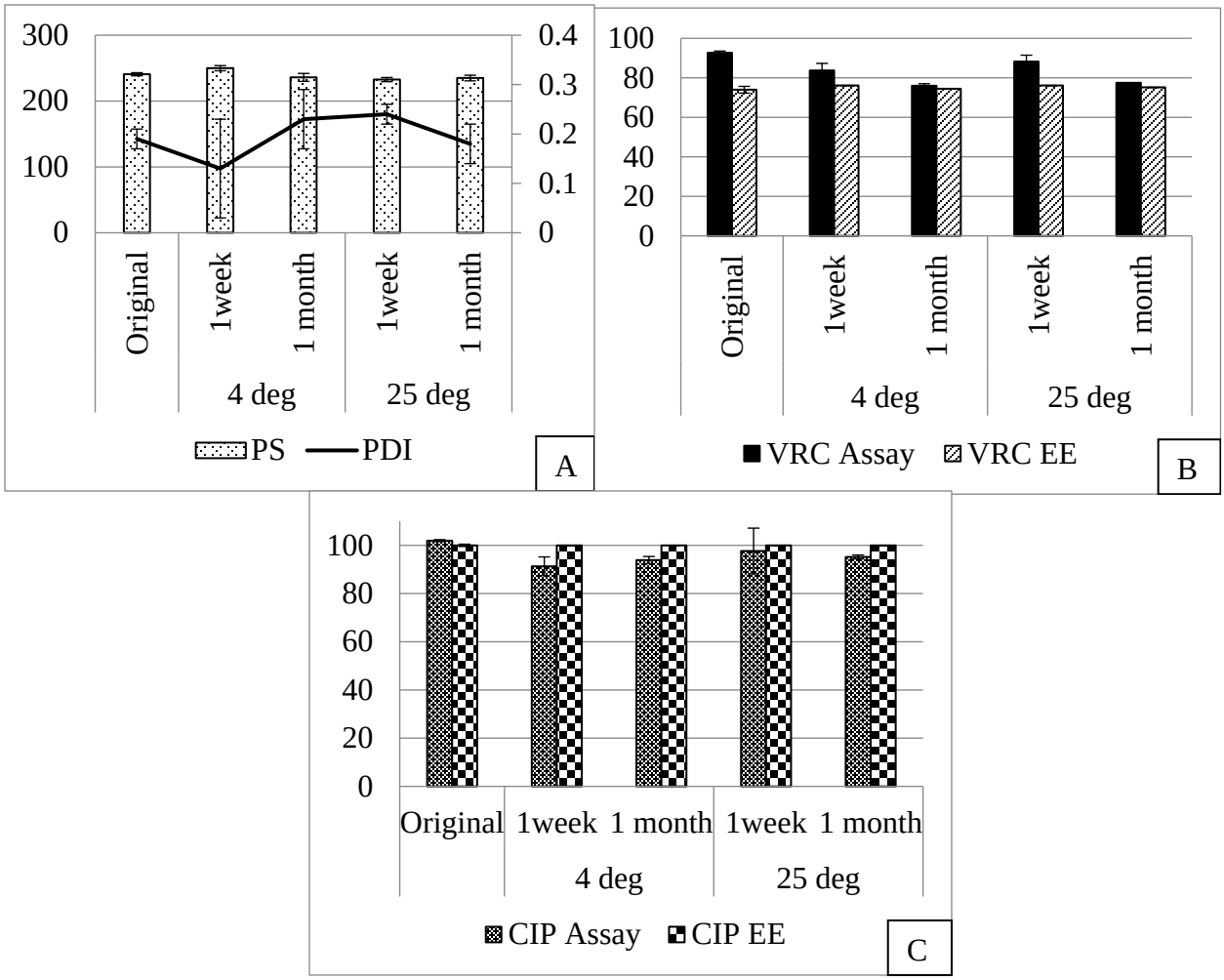

Figure.31. Changes in (A) Particle size and PDI, (B) % Assay, %EE for VRC in VRC-CIP-PEG-NLC, (C) % Assay, %EE for CIP in VRC-CIP-PEG-NLC stored 4°C and 25°C/75% RH over a period of 1 month

Table 21. Composition of the Most Desirable Formulation Obtained by Design-Expert® Software with Predicted and Experimental Values

Formulation composition		Predicted values	Experimental values
VRC (15 mg)	%DL (VRC)	2.09	2.38
CIP (30 mg)	%EE (VRC)	71.35	73.98

PEG (100 mg)	%DL (CIP)	4.44	6.06
Lipid Ratio (450 mg)	% EE (CIP)	90.96	100
	% Assay (VRC)	76.59	92.63
	PDI	0.29	0.19

Morphological characterization

Figure.32. depicts the morphology of the VRC-CIP-PEG-NLC formulation. The morphology of a nanoparticulate system is significantly governed by the processing conditions used. A cold homogenization-ultrasonication method was used for the formulation of the NLCs. During formulation development attempts, we observed that VRC, at higher processing temperatures, migrated outside the oily lipid phase and precipitated in the form of shiny crystals. In order to prevent migration of VRC outside the lipid, during the first processing step, i.e. magnetic stirring, a high temperature of 80°C was employed, but, post this step, the temperature of the entire process was maintained below the melting temperature of the lipid mixture. The cold homogenization-ultrasonication that followed, was more a fragmentation process to reduce the particle size, which can be seen in the STEM images in Figure.32. The NLCs have a well-defined periphery, but in comparison to the well-rounded NLCs as synthesized by a hot homogenization or a high pressure homogenization process, [192] the spherical particles so formed have an un-even rounded structure. However, the morphology does not affect the stability of the NLCs; presence of a stable surfactant system and PEG help in stabilizing this nano-colloidal system. The particle size observed in Figure.32. is in close agreement with the particle size measurements from DLS as mentioned previously.

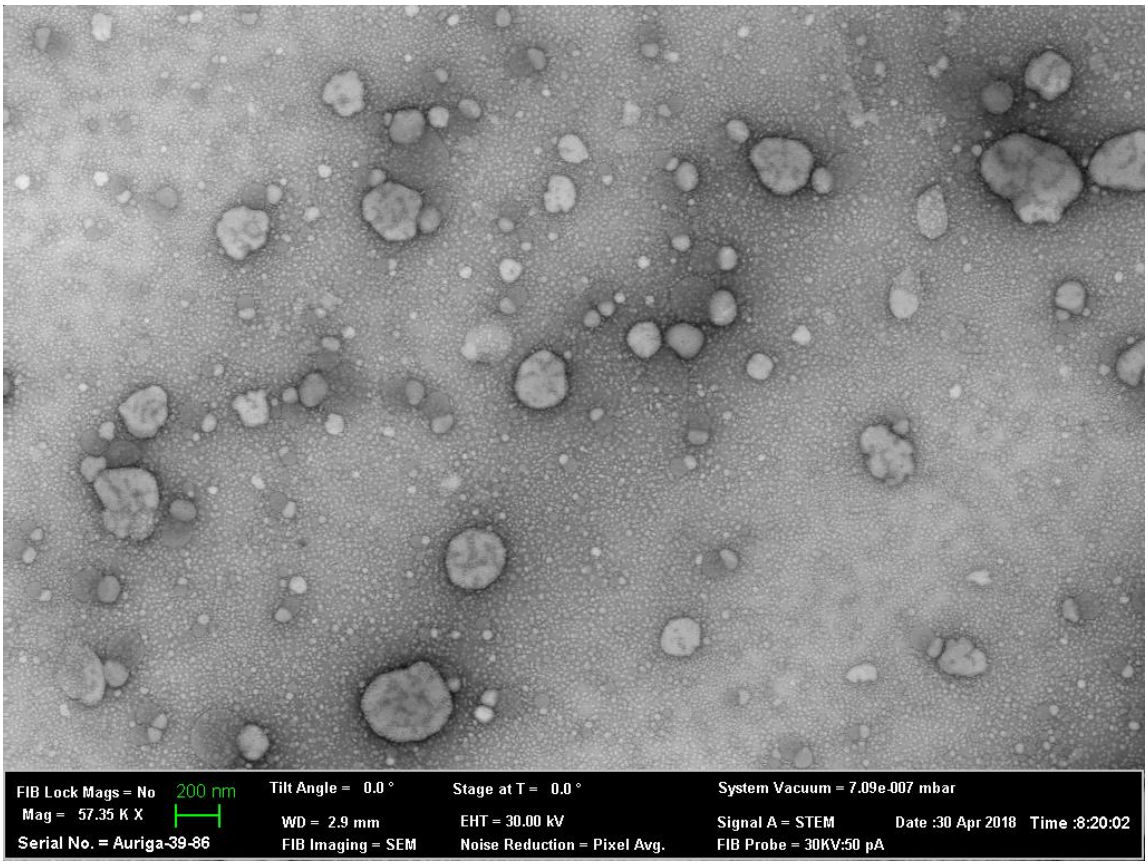

Figure.32. STEM images for the optimized VRC-CIP-PEG-NLC formulation

In-vitro trans-corneal permeation

Permeation of the VRC-CIP-PEG-NLC formulation across isolated rabbit corneas was observed (Figure.33.); VRC-CIP-PEG-NLCs, being targeted as an antifungal formulation, the major sites of action for this formulation would be the cornea and the anterior chamber. To establish effective comparators, the transcorneal permeation of marketed Ciprofloxacin Hydrochloride Ophthalmic Solution and Lyophilized Voriconazole for Injection was also evaluated. To establish the effect of a dual-drug loaded formulation on the *in-vitro* transcorneal permeation, if any, individual drugs loaded in the same base formulation were also evaluated in a similar setup.

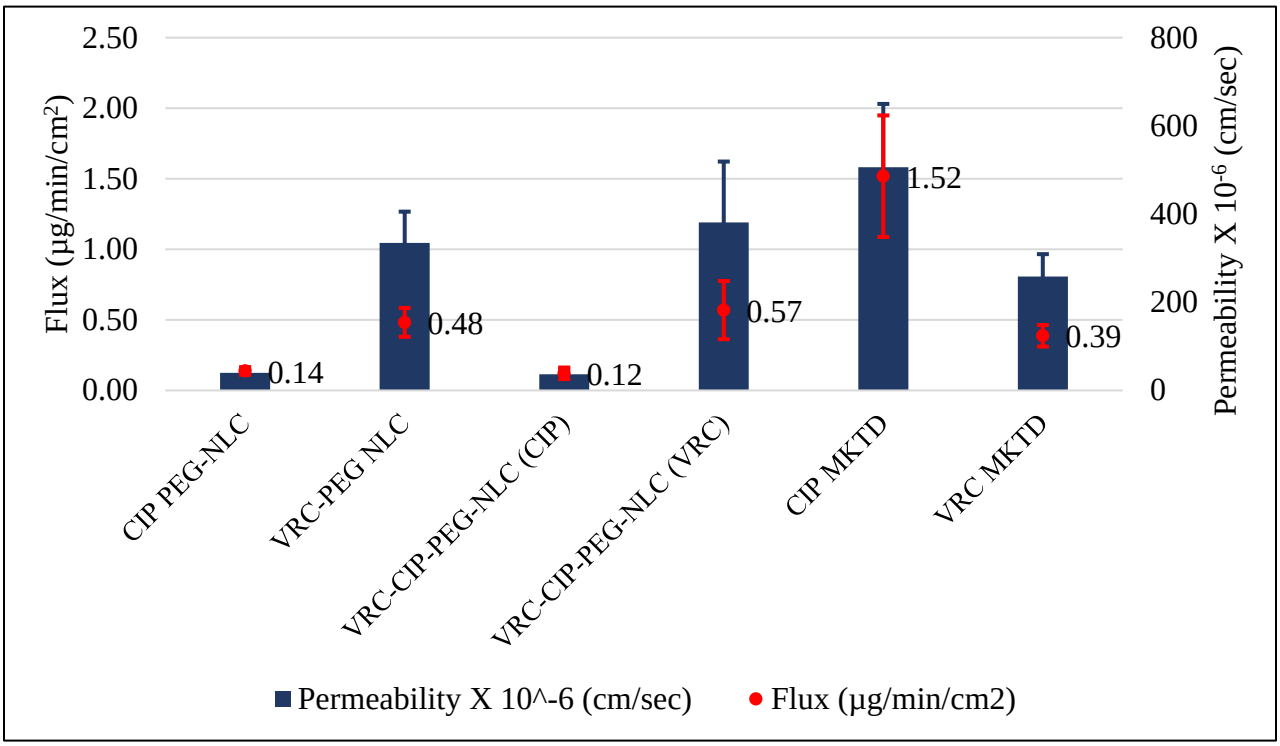

Figure.33. Graphical representation of the Permeability (cm/sec) and Flux (µg/min/cm^2) across isolated rabbit corneas of VRC and CIP from CIP-PEG-NLC, VRC-PEG-NLC, VRC-CIP-PEG-NLC and CIP and VRC marketed formulations (n=3) over a period of 3 hours

Table 22. Significant p-values enlisted post one-way ANOVA analysis for the ordered between group differences for CIP-PEG-NLC, VRC-PEG-NLC, VRC-CIP-PEG-NLC and CIP and VRC marketed formulations (n=3). A p value < 0.05 was significant.

Parameter	Formulations		p-value
Flux (µg/min/cm^2)	CIP MKTD	VRC-CIP-PEG-NLC (CIP)	0.0034
	CIP MKTD	CIP-PEG-NLC	0.0036
Permeability (cm/sec)	CIP MKTD	VRC-CIP-PEG-NLC (CIP)	0.0032
	CIP MKTD	CIP-PEG-NLC	0.0034

Corneal concentrations (µg/ml)	VRC-CIP-PEG-NLC (VRC)	VRC-MKTD	0.0005
	VRC-PEG-NLC	VRC-MKTD	0.0084
	VRC-CIP-PEG-NLC (VRC)	VRC-PEG-NLC	0.0326

The transcorneal flux for CIP from the marketed Ciprofloxacin Hydrochloride Ophthalmic Solution (0.3% as base) was greater than 10 times (1.52 ± 0.43 µg/min/cm^2) that from CIP-PEG-NLC (0.14 ± 0.03 µg/min/cm^2) and the VRC-CIP-PEG-NLC (0.12 ± 0.04 µg/min/cm^2) (Figure.33.). Table 22. enlists these differences as statistically significant. The transcorneal permeability of CIP was 506.06 ± 143.65 cm/sec for the marketed Ciprofloxacin Hydrochloride Ophthalmic Solution, significantly greater than the permeability of CIP from both CIP-PEG-NLC (39.96 ± 8.02 cm/sec) and VRC-CIP-PEG-NLC (36.77 ± 12.39 cm/sec) (Figure 33., Table 22.). The concentrations of CIP retained on the isolated corneas post the study were 40.46 ± 2.78 µg/ml, 4.85 ± 1.58 µg/ml, 3.97 ± 0.46 µg/ml for the CIP-MKTD, VRC-CIP-PEG-NLC (CIP) and CIP-PEG-NLC formulations respectively (Figure.34.). CIP MKTD being a Ciprofloxacin Hydrochloride (salt -form) has a high solubility in the pre-corneal area. The formulation is in a solution form resulting in high transcorneal permeation and corneal retention. CIP being entrapped in a lipid-based system demonstrates a controlled release and permeation.

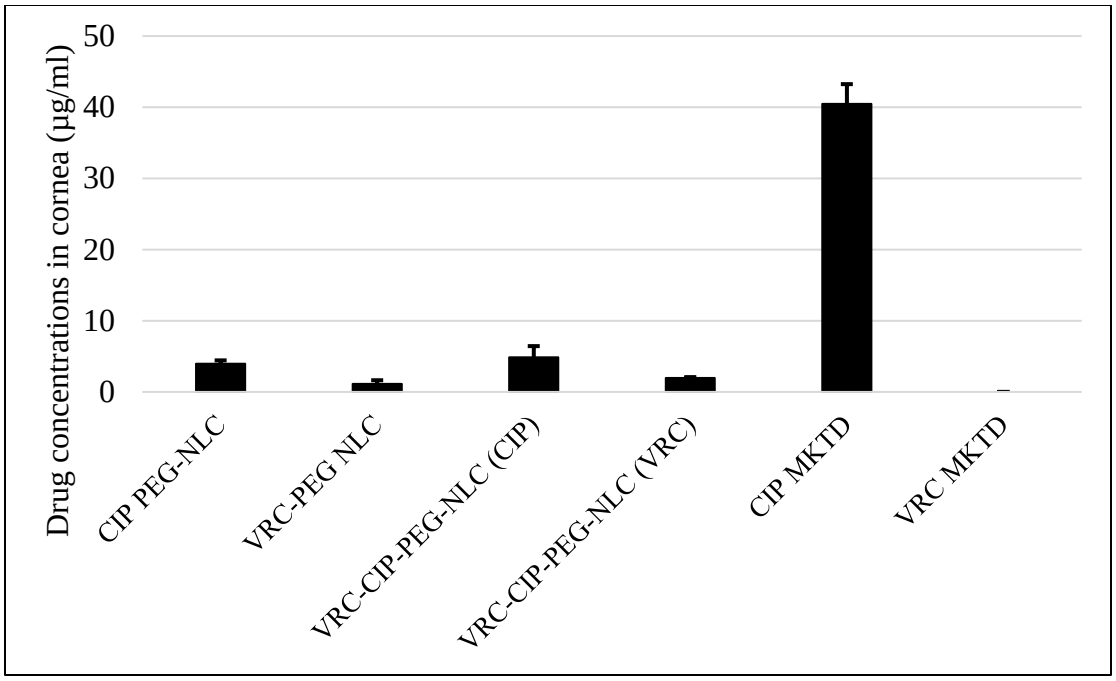

Figure.34. Graphical representation of the concentrations (µg/ml) of CIP and VRC retained in isolated rabbit corneas 3 hours post dosing of CIP-PEG-NLC, VRC-PEG-NLC, VRC-CIP-PEG-NLC and CIP and VRC marketed formulations (n=3) in an in-vitro transcorneal permeation setup.

The transmembrane permeation of VRC from the PEG-NLCs was better than the marketed Lyophilized Voriconazole for Injection. The flux for VRC from the marketed formulation was 0.39 ± 0.08 µg/min/cm^2 whereas from the VRC-PEG-NLC was 0.48 ± 0.1 µg/min/cm^2 and that from VRC-CIP-PEG-NLC was 0.57 ± 0.21 µg/min/cm^2. The permeability of VRC from the VRC-PEG-NLC and VRC-CIP-PEG-NLC was 334.46 ± 71.01 cm/sec and 381 ± 138.04 cm/sec and that from the marketed formulation was 258.25 ± 50.82 cm/sec. The corneal tissue concentrations were 1.14 ± 0.51 µg/ml from VRC-PEG-NLC and 1.97 ± 0.11 µg/ml from the VRC-CIP-PEG-NLC, whereas no VRC was detected in the corneas treated with the VRC MKTD formulation. Higher permeation of VRC across the corneas from the lipid based nano-systems could be as a result of

interaction of this colloidal system with the cornea and possible internalization of the same [193]. However, vehicle-related permeation enhancement of a molecule is also a function of the inherent molecule properties and the permeation pathway best-fitting the molecule. Lipophilic VRC entrapped in a PEGylated NLC system demonstrated enhanced permeation, whereas for a highly water-soluble molecule like CIP, when entrapped in a lipid based nanocarrier failed to demonstrate a similar effect. From Figure 34. we observe higher amounts of CIP retained in the cornea, but not permeating across. CIP being a hydrophilic moiety, may be entrapped in the hydrophilic stromal layers, whereas VRC could be permeating by a different (transcellular) pathway altogether. We should also keep in mind that the loading of the two APIs is at two different levels, with a 0.15% w/v load for VRC and a 0.3% w/v loading for CIP, despite which the lipid-based carrier system enhances the permeation of VRC in comparison to both the VRC-MKTD and the CIP formulations.

Conclusion

These set of studies successfully used a DOE method to optimize a dual drug loaded PEGylated lipid nanocarrier. An RSM-CCD was utilized for excipient level optimization, furthermore, a cold-homogenization- probe sonication process was optimized for the development of the formulation. The optimized formulation was nano-sized and stable over a period of 1 month at both 4°C and 25°C/75% RH over a period of 1 month.

The VRC-CIP-PEG-NLC have a comparable permeability and flux to the individual drug loaded formulations, indicating that each of the APIs are compatible and permeate freely across isolated corneas. The marketed CIP solution, being in the salt form depicts high transcorneal flux and permeability as well as high corneal retention. In terms of VRC, however, the PEGylated NLCs demonstrate a slightly better permeation profile than the marketed formulation and

improved corneal retention. Thus, a PEGylated nanocarrier system increased the penetration of VRC across the cornea and controlled the release and permeation of CIP. Further studies investigating the efficacy of the formulation as an antifungal preparation and exploring the synergism between CIP and VRC would be a great asset for utilizing this dual drug loaded formulation as an alternative to conventional therapy.

CHAPTER 6

OPTIMIZATION OF CAPPING PARAMETERS FOR LOW TEMPERATURE STORAGE OF A PLASTIC VIAL-RUBBER STOPPER COMBINATION

Introduction

Most of vaccines and biologic drug products (DP) being thermosensitive, are stored at 2-8°C, ensuring product quality and potency. However, for some products like Zostavax®, which is an attenuated varicella virus, a frozen storage state (-80°C) is preferred to ensure sufficient stability for the required shelf life.[194-195] Such products are often shipped in a frozen state using dry ice, subjecting the product to temperatures lower than -50°C.

Container closure systems (CCS) for drug products usually comprise of a glass vial, elastomeric stopper and an aluminum crimp cap. The glass transition temperature, (T_g') of most rubber stoppers is in the range of –50 to – 65 °C. Aforementioned low storage temperatures might lead to shrinkage of the rubber and loss of elastomeric properties. In addition, storage temperatures of -80°C can cause condensation of air in the vial headspace resulting in a low-pressure environment. Loss of stopper elasticity coupled with under pressure in the vial headspace can end up with ingress of cold dense gas from the immediate environment, implying a potential container closure integrity (CCI) compromise.[196] [197] While shipping the DP on dry ice, this CCI breach can lead to carbon dioxide (CO_2) ingress, which may further cause a pH drop affecting DP stability.

Methods such as dye ingress, vacuum decay and microbial ingress can be used to study CCI at ambient conditions. However, evaluation of CCI of frozen drug products is a relatively new area and not much has been spoken about it. In a frozen state, investigative techniques such as Helium (He) leak detection test and nondestructive gas headspace analysis can be employed.

CCI can be enhanced by selecting CCS components with good compatibility i.e. marriage of the elastomer and the vial and implementing a tightly sealed vial at all storage conditions. Residual Seal Force (RSF (Lbs)) is the force exerted by the compressed rubber stopper on the vial-sealing surface and is a measure of the seal tightness or the seal integrity. A quality seal requires optimal amount of force in the capping process, which is reflected by a high RSF (Lbs). This can be measured by the RSF tester, an instrument calculating RSF by a compression stress/distance plot as it applies a known force over a distance on a capped vial. In addition, visual acceptability is an important factor to take into consideration in the capping process; the capping parameters have to be modified to prevent defects such as wrinkling of cap skirt and dimpling rubber stoppers. It is important to consider visual inspection of crimped vials as a part of any optimization process. [194]

This project focuses on enhancing CCI of a particular vial stopper combination by maximizing the RSF during the capping process whilst generating a visually acceptable seal. We also attempt to standardize the crimping process across single-station cappers by using RSF as the output variable. A systematic approach was employed for optimizing the crimping parameters using DOE for a selected container closure combination (CZ® vial and chlorobutyl rubber stopper) for -80 °C storage. Two single-station cappers were studied, both the cappers use different techniques to crimp the vial. The Integra West Capper® uses a spinning roller technique for crimping a stoppered vial using an aluminum crimp cap. The spinning rollers tuck the skirt of the cap under the vial

flange to attain a visually acceptable seal. The Bausch and Strobel® capper on the other hand features a capping station with a plunger and stationary roller blades and a rotating vial holder.

Each capping instrument has a set of input variables (factors) that affect the seal quality. RSM - CCD was used to generate a design space for crimping for the Integra West Capper®. Due to the multiple instrument parameters on the Bausch and Strobel® capper, a D-optimal design was initially employed to determine the main effects for the design. The D-optimal design was then augmented into an I-optimal design for capping process optimization on the Bausch and Strobel® capper. RSF was modelled as the response variable along and the vials were verified for visual acceptability.

Materials and Methods

Materials

Daikyo (Tokyo, Japan) Crystal Zenith (CZ®) vials with a 20mm vial neck diameter were stoppered using FluroTec® barrier coated 20mm chlorobutyl rubber stoppers by West (Exton, PA, USA). All vials were sealed using 20mm aluminum crimp cap by West (Exton, PA, USA) with a flip-off seal.

Equipment

Vials were sealed using two single-station cappers, (a) Integra West Capper® (Genesis Packaging Technologies, Exton, PA, USA) and (b) Bausch and Strobel® capping equipment HVM4610 (Ilshofen, Germany).

RSF Measurements

All RSF measurements were conducted using the RSF tester by Genesis Packaging Technologies, Exton, PA, USA.

Statistical Experimental Design

Capping Process Optimization: Integra West Capper®

The Integra West Capper® is a single station capping machine used on a laboratory scale and has two modifiable capping process parameters affecting the final seal quality, namely, Pre-compression force (Lbs) and Pressure Block Reference Height (thousands of an inch). Pre-compression force is the force applied by the plunger on the aluminum seal with the flip-off cap (Figure 35. A), whereas Pressure Block Reference Height is the distance between the plunger and the capping plate (Figure 35. B).

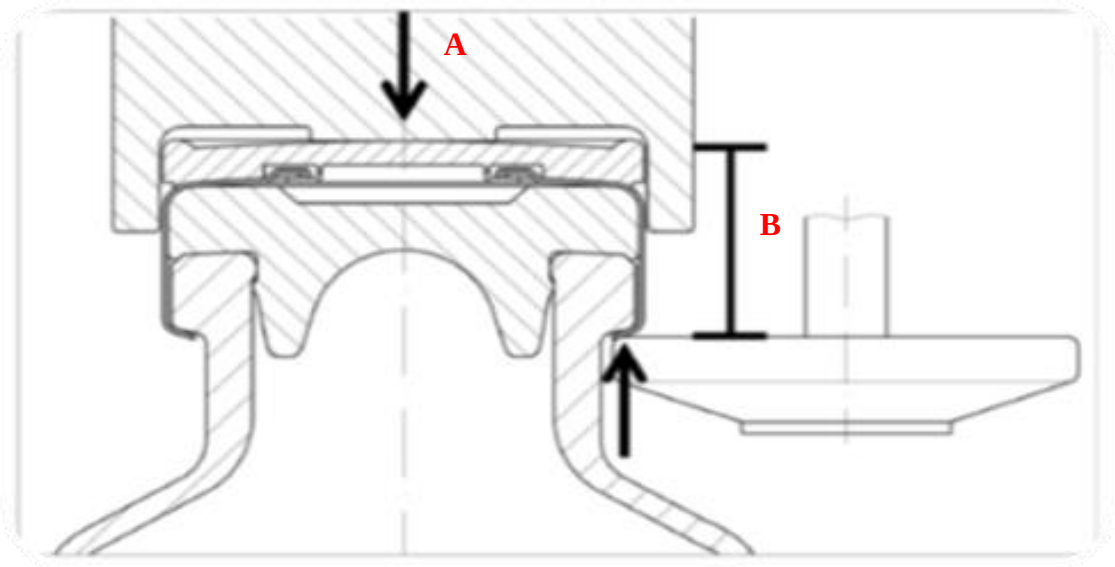

*Mathaes, R., Impact of Vial Capping on Residual Seal Force and Container Closure Integrity, PDA (copyright pending)

Figure 35. Vial crimping for the Integra West Capper®

A CCD was employed in the capping process optimization experimental design using JMP® 12 statistical software (SAS Institute, NC, USA) with the independent variables being (A) Pre-compression force and (B) Pressure Block Reference Height whereas RSF was considered as the response variable (dependent variable). A CCD uses RSM suitable for investigating the quadratic response surface and for constructing a second order polynomial model. The limits of the independent parameters were determined on the basis of random trials conducted before the

optimization study. In the given study, the above-mentioned two factors were coded as A and B respectively, each, studied at five levels, A as -α: 10, -1: 13.98, 0: 35, +1: 56.02, +α: 60 and B as -α: 100, -1: 103.2, 0: 120, +1: 136.8, +α: 140 in 9 different combinations: (0, +α), (-1, +1), (+1, +1), (-α, 0), (0, 0), (0, +α), (-1,-1), (+1, -1), (0, -α), each combination repeated five times. Table 23. provides the details on the experimental design employed in this study.

Table 23. Design space for the CCD for the vial crimping process on the Integra West Capper®

Run number	Pre-compression Force (Lbs)	Pressure Block Reference Height (inch*10^{-3})
1	13.98	103.2
2	35.00	120.0
3	10.00	120.0
4	10.00	120.0
5	13.98	136.8
6	56.02	103.2
7	35.00	120.0
8	56.02	103.2
9	35.00	120.0
10	35.00	100.0
11	13.98	103.2
12	60.00	120.0
13	35.00	140.0
14	13.98	103.2
15	56.02	136.8
16	60.00	120.0
17	13.98	136.8
18	56.02	103.2
19	60.00	120.0
20	35.00	120.0
21	35.00	100.0
22	13.98	103.2
23	10.00	120.0
24	60.00	120.0
25	56.02	103.2

26	35.00	100.0
27	56.02	136.8
28	56.02	136.8
29	35.00	120.0
30	56.02	103.2
31	10.00	120.0
32	13.98	103.2
33	35.00	140.0
34	13.98	136.8
35	13.98	136.8
36	35.00	100.0
37	60.00	120.0
38	10.00	120.0
39	35.00	140.0
40	13.98	136.8
41	35.00	140.0
42	56.02	136.8
43	35.00	100.0
44	56.02	136.8
45	35.00	140.0

The general form of the model generated from the design is given below,

$$Y = \beta_0 + \beta_1 A + \beta_2 B + \beta_3 AB + \beta_4 A^2 + \beta_5 B^2 + \varepsilon$$

Where Y is the measured value of the response variable and β_0, the intercept, is the arithmetic average of all quantitative outcomes of 45 experimental runs, β_1-β_5 are the coefficients computed from the observed experimental values of Y, and A and B are the coded levels of the independent factors. The A and B terms indicate the average result of changing one factor at a time from its low to high value. The interaction term, AB suggests the response changes when these two factors are changed simultaneously whereas the terms A^2 and B^2 depict the quadratic terms. The equation aids in understanding the effect of the independent factor/s on the response variables after considering the intensity of coefficient and the mathematical sign it carries, that is, positive or negative. A positive sign indicates additive effect. Statistical validity was established based on

ANOVA provided in the JMP® 12 statistical software (SAS Institute, NC, USA), with level of significance considered at $p < 0.05$.

The model thus generated was then validated by testing multiple points on the design space and comparing the generated actual results to the values predicted by the model.

Capping Process Optimization: Bausch and Strobel® capper

The Bausch and Strobel® Capper is a single station, hand sensor activated capping machine with in-built settings allowing to modify the capping recipe. This machine has a greater number of modifiable crimping parameters in comparison to the Integra West Capper®, namely, Lower position of crimping tool (in mm) (X_1), Crimping tool lift (in mm) (X_2), Crimping tool swivel movement pre--crimping position (in °) (X_3), Crimping tool swivel movement crimping position (in °) (X_4), Container rotation revolutions (X_5). However, the parameters X_3 and X_4 denoting position of the crimping disc before and at the end of the crimping process had to be constant for a single vial-capper combination in accordance to the manufacturer recommendation.

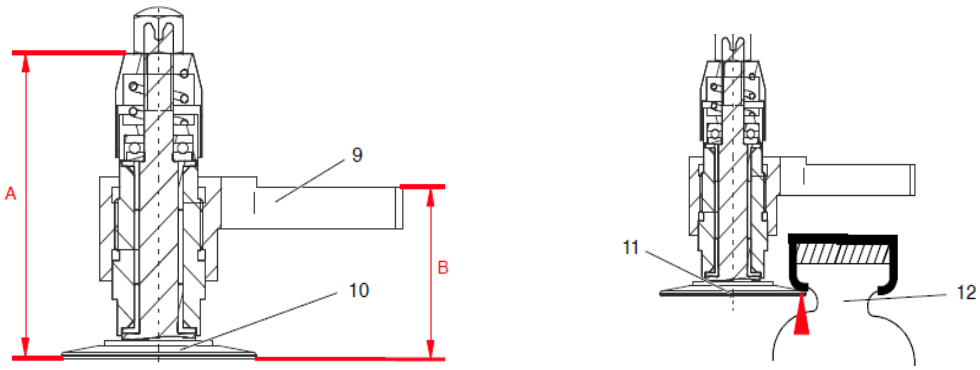

Figure 36. Capping parameters on the Bausch and Strobel® capper

The distance (A) in Figure 36. was preset whereas distance (B) corresponding to the factor X_1 and had to be modified physically and measured with the help of Vernier calipers. This value determined how hard the crimping disc (11) pressed against the container neck (12) from below. The three major factors or input variable identified that affect the seal quality were Distance B (mm) X_1, Tool lift (mm) X_2 and number of rotations X_5. A D-optimal design space was generated to screen the modifications of these parameters. The number of rotations (X_5) were studied as a categorical variable at three levels i.e. 4, 7 and 10. The crimp quality was measured in terms of the response variable, RSF. D-optimal experimental design was used for creating the experimental design attesting statistical significance using ANOVA and empirical modelling. This method has some advantages compared to other designs resulting in smaller number of runs and the ability to include categorical factors in the DOE. This optimization strategy can be employed to evaluate the relationship between multiple independent variables and determination the optimum conditions required to produce a specific desired response. [198]

The first step of generating the design space was to estimate the machine as well as acceptability limits of the input variables, i.e. create the edges of the design space. This was done by conducting random trials individually modifying the input variables (data not shown). Once the limits of the input variables were established, a D-optimal screening study was conducted using JMP® 12 statistical software (SAS Institute, NC, USA). A 50-run design was generated using the software; runs are depicted in Table 24.

Table. 24 Design space for the D-optimal design on the Bausch and Strobel® capper

Run number	X1: Distance B (mm)	X2: Tool Lift (mm)	X5: (Categorical variable) Number of rotations
1	34	20	10
2	35.5	2	7
3	34	2	4
4	34	2	4
5	35.5	2	10
6	34	20	10
7	34	20	10
8	34	20	10
9	34	20	7
10	34	20	10
11	34.75	11	7
12	34	2	10
13	34	2	10
14	34	2	10
15	35.5	2	10
16	35.5	2	10
17	34	2	4
18	35.5	2	4
19	34.75	11	7
20	35.5	2	4
21	35.5	20	10
22	34	20	4
23	34	20	4
24	35.5	20	10
25	35.5	20	4
26	35.5	20	10
27	35.5	2	4
28	34	2	10
29	34.75	11	7
30	34	2	10
31	35.5	2	4
32	35.5	2	10
33	34	2	4
34	35.5	20	4
35	34	2	4
36	34	2	4

37	34	20	4
38	35.5	2	10
39	35.5	20	7
40	34	2	7
41	35.5	20	4
42	34	20	4
43	35.5	20	10
44	35.5	20	10
45	35.5	20	4
46	35.5	2	4
47	34	20	4
48	35.5	20	4
49	35.5	2	7
50	34	20	4

The general form of the model generated from the design is given below,

$$Y = \beta_0 + \beta_1 X_1 + \beta_2 X_2 + \beta_3 X_3 + \beta_1 \beta_2 X_1 X_2 + \beta_1 \beta_3 X_1 X_3 + \beta_2 \beta_3 X_2 X_3 + \beta_1 \beta_2 \beta_3 X_1 X_2 X_3 + \varepsilon$$

D-Optimal designs are appropriate for screening experiments because the optimality criterion focuses on precise estimates of the coefficients. This design focuses more on the extremities of the design than in the center and is efficient for determining the extent of a design space. D-optimal designs, however, are not appropriate for experiments where the primary goal is prediction. On the other hand, an I-optimal design places fewer runs on the extremes and focuses on the center of the design space, making them robust predictor designs. Based on the data generated by the D-optimal design, a response surface screening study was conducted (I-optimal design). Zones of interest were identified from the D-optimal design, factor constraints and variable limits were defined accordingly. The I-optimal study allowed us to focus on the optimization area of interest by tailoring the limits of the design space. (Height B: 34-34.8 mm; Tool Lift: 12-20 mm; Rotations: 7, 10) The design was augmented with an additional 50 runs as shown in Table 25.

Table 25. Design space for the I-optimal design on the Bausch and Strobel® capper

Run number	X1: Distance B (mm)	X2: Tool Lift (mm)	X5: (Categorical variable) Number of rotations
51	34	12.4	7
52	34	12.4	7
53	34.6	20	7
54	34.6	20	7
55	34	12.4	7
56	34	12.4	7
57	34	12.4	7
58	34.6	20	7
59	34	12.4	7
60	34.6	20	7
61	34.7	12.4	7
62	34	12.4	7
63	34	20	10
64	34	12.4	7
65	34	12.4	7
66	34	20	10
67	34.7	12	7
68	34.7	12	10
69	34.6	20	7
70	34.6	20	7
71	34.7	12	10
72	34.6	20	7
73	34.7	12	10
74	34	20	10
75	34	12.4	7
76	34.7	12	10
77	34.6	20	7
78	34.6	20	7
79	34.7	12	7
80	34.6	20	7
81	34.7	12	7
82	34.7	12	10
83	34.7	12	7
84	34	20	10
85	34.6	20	7

86	34.7	12	10
87	34	12.8	7
88	34.7	12	7
89	34.7	12	10
90	34.7	12.4	7
91	34.7	12.4	7
92	34.7	12	10
93	34.6	20	7
94	34.7	12	10
95	34.7	12	10
96	34	12.4	7
97	34.6	20	7
98	34.7	12	10
99	34.6	20	7
100	34.7	12	10

Statistical validity was established based on ANOVA provided in the JMP® 12 statistical software (SAS Institute, NC, USA), with level of significance considered at $p < 0.05$.

The model thus generated was then validated by testing multiple points on the design space and comparing the generated actual results to the values predicted by the model.

Results and Discussion

Capping Process Optimization: Integra West Capper®

Table 26 summarizes the regression analyses evaluating effects of factors on the response variable (RSF). On the basis of lack-of-fit p-value (0.762) and sequential p-value (<0.0001), a quadratic model was chosen with a Power $(y + k)^{\lambda}$ transformation as suggested by the Box-Cox diagnostics. The positive unstandardized coefficients (β) represent an increase in response variable with a unit increase in the predictor. The reverse applies to coefficients with negative values (7). The extent of the effect of the independent factors on RSF was determined using the regression analyses and plots that provided RSM analyses. Table 27 lists the factors that significantly affect RSF and also the predictive equation for the quadratic model. It is observed that both factors A and B, which are

the Pre-compression force (Lbs) and Pressure block reference height (inch*10^{-3}) significantly affect RSF and they also have a quadratic effect which is evident by the curvature in the Figures 37.A, and 37.B. As the Pressure block reference height is increased up to 120-125 inch*10^{-3} (Fig.37.A) at a constant Pre-compression force, the RSF value increases.

Table 26. Regression analyses for evaluating the effects of independent factors on the response variable

Capper	**Model**	**Model F-value**	**Degree of freedom**	**R^2 values**	
				R^2	**Adjusted R^2**
Integra West Capper®	Quadratic	107.67	5	0.932	0.924
Bausch and Strobel® (D-optimal)	2FI	36.104	4	0.762	0.741
Bausch and Strobel® (I-optimal)	Quadratic	53.895	5	0.741	0.728

Table 27. One-way ANOVA analysis for Quadratic Model on the Integra West Capper®

Response variables	**Independent factors that affect the response variable significantly**	**p-value**	**Model equation**
RSF (Lbs)	A	<0.0001	RSF = -5.71 + 0.25 A + 0.132 B + 0.011 AB + 0.006 A^2 -0.028 B^2
	B	<0.0001	
	AB	<0.0001	
	A^2	0.0001	
	B^2	<0.0001	

On further increasing the Pressure block reference height, there is an extreme drop in the RSF. This observation can be explained as Pressure Block reference height determines the length of the aluminum skirt tucked under the vial flange. As this height is increased, the capping plate to plunger distance reduces causing the aluminum skirt of the cap to deform and resulting in low RSF values. However, looking at the effect of the other factor, RSF increases with an increase in the Pre-compression force at constant Pressure block reference height of 120 inch*10^{-3}. (Fig.37.B)

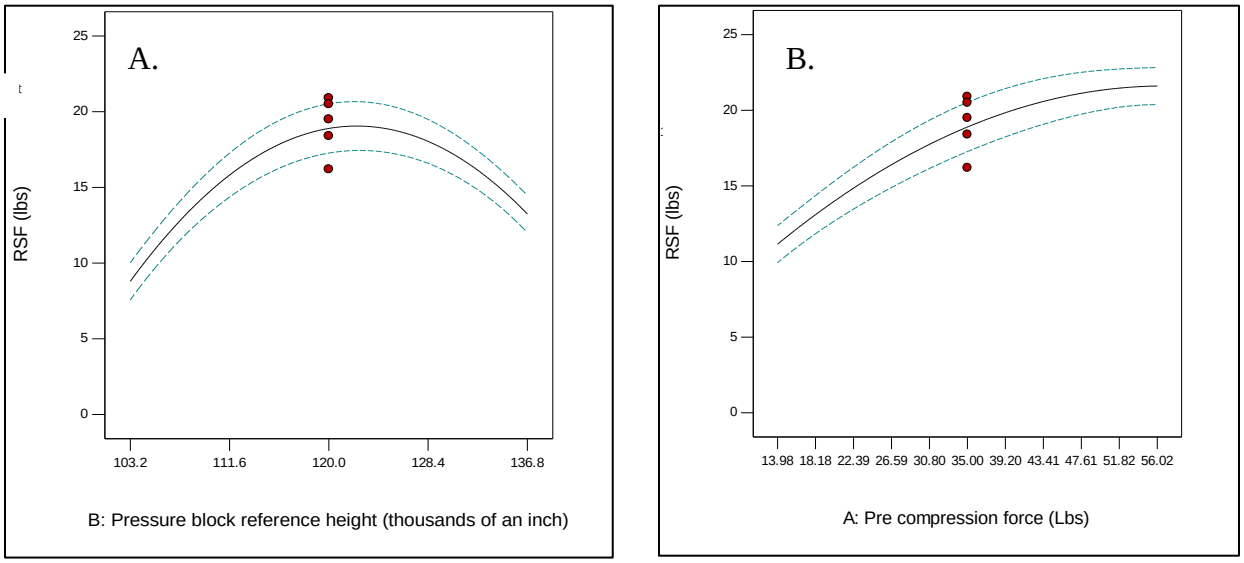

Figure 37. A. RSF at increasing values of Pressure block reference height when Pre-compression force is at a constant of 35 Lbs; **B.** RSF at increasing values of Pre-compression force when Pressure block reference height is at a constant of 120 inch*10^{-3}.

The model also presents with a significant AB interaction (Table 27.) represented graphically in Figure 38. The increase in RSF with Pressure Block reference height is significantly dependent on the level of Pre-compression force. At a lower level of Pre-compression force (103.2 inch*10^{-3}), increase in the Pressure-block reference height does not lead to a significant change in

the RSF, however at a higher level of Pre-compression force (136.8 inch*10^{-3}), there is a significant increase in RSF with an increase in Pressure Block reference height.

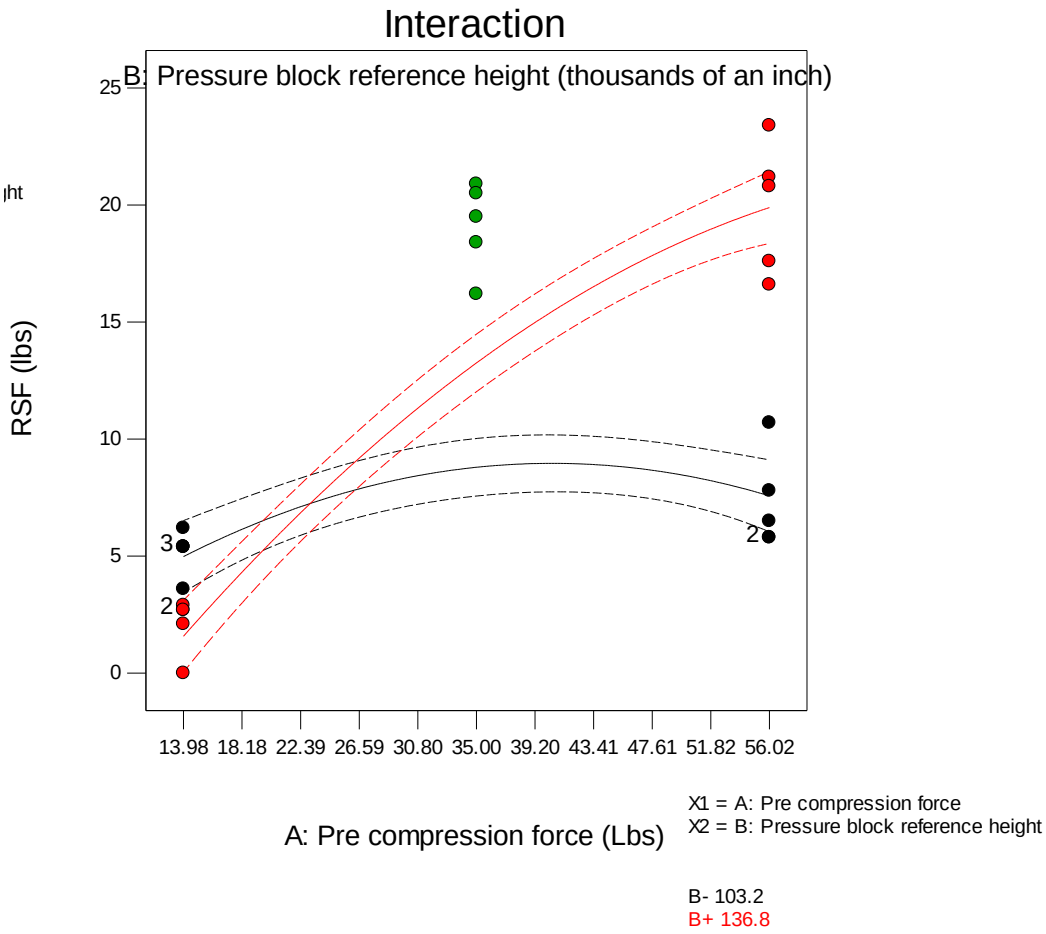

Figure 38. Significant interaction between Precompression force and pressure block reference height for the Quadratic model on the Integra West Capper®

Figure 39. Illustrates a 3D surface profiler, the X1 axis representing increasing levels of Pressure block reference height whereas the X2 axis portraying increasing levels of Pre-compression force, with a single output (response) variable on the Y axis, RSF (Lbs). Increasing the Pre-compression force at lower levels of Pressure Block reference height does not significantly

affect RSF values. However, at Pressure block reference height 120-130 inch*10^{-3} the predicted RSF values are above 20 Lbs, making it the optimum working range for this process. The orange-red region in the 3D graph are the model predicted zones for process parameters leading to maximum RSF values.

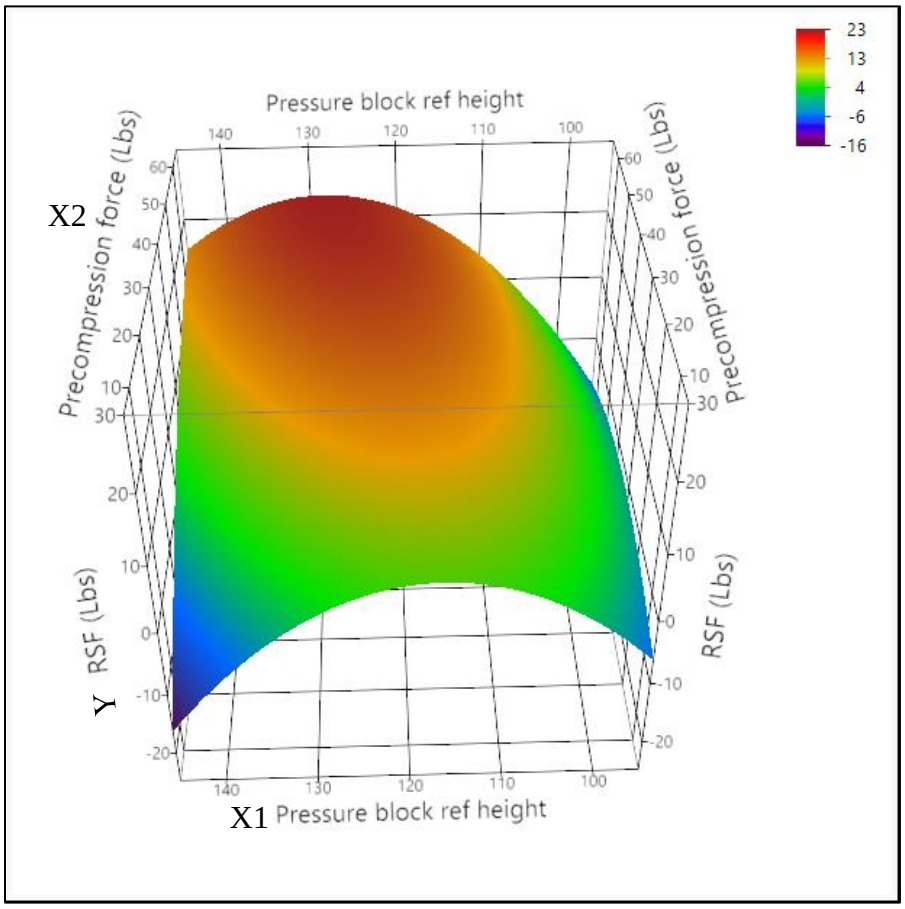

Figure 39. RSM generated 3D Surface Profiler for Integra West Capper® depicting RSF (Lbs) at different levels of Independent variables

The robustness of model predictions was verified by crimping vials at different factor combinations and comparing the actual RSF to the model predicted RSF. Table 28 represents the factor combinations chosen for the validation study. (n=10) Figure 40. illustrates the results of this

validation. Mean RSF (Lbs.) (red bar) and Mean RSF predicted (blue bar) are plotted on the Y-axis against increasing levels of Pressure Block reference height divided by Pre-compression force on the Y2-axis. There is no statistically significant difference amongst the actual vs the predicted RSF values at any level of Pre-compression force or Pressure Block reference height.

Table 28. Model Validation parameters for Integra West Capper®

Pre-compression Force (Lbs)	Pressure Block Reference Height (inch*10^{-3})	Predicted RSF (Lbs)
25	125	15.2
32	128	17.1
37	128	18.8
40	130	19.1
60	110	14.7

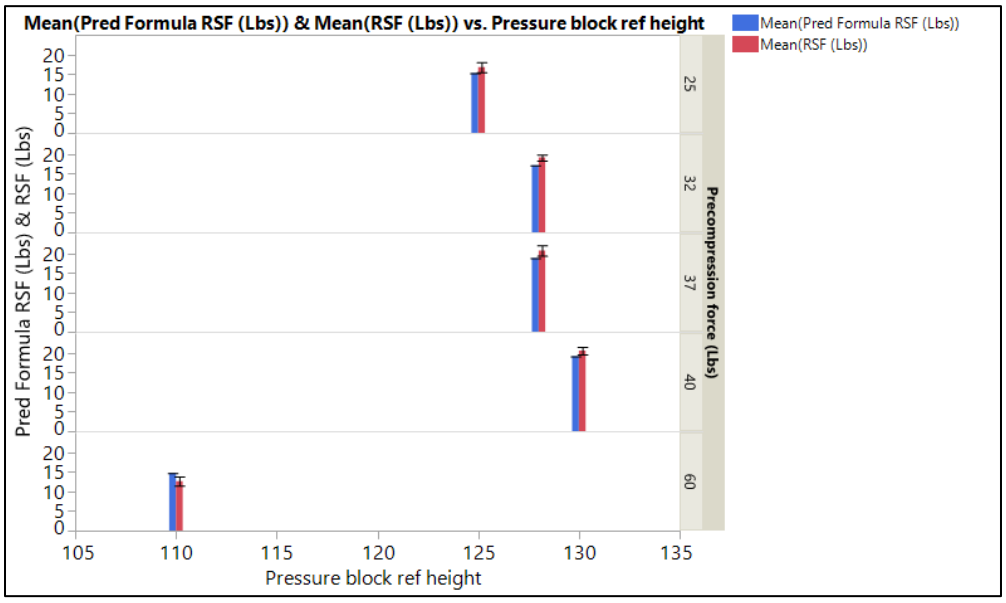

Figure 40. Design validation, Actual vs Predicted RSF (LBS) varying Pre-compression force and pressure block reference height.

Capping Process Optimization: Bausch and Strobel® Capper

The Bausch and Strobel® capper had a greater number of factors affecting the RSF in comparison to the Integra West Capper® including a categorical variable. A D-optimal design was chosen as a screening study to initially study the design space and observe the effect of single factors/ interactions on the response variable. Table 29. summarizes the regression analyses evaluating effects of factors on the response variable (RSF). A 2FI (2 Factor Interaction) model was selected for this analyses on the basis of favorable R- Squared value (0.762) and the Lack of Fit test p-value (0.915). Table 29 lists the factors that significantly affect RSF and the predictive equation for the 2FI model. According to this model, factors Distance B (mm), Tool lift (mm) and Number of rotations significantly affect RSF of the final crimp.

Table 29. ANOVA for 2FI model and Quadratic model for D-optimal and I-optimal design respectively

Experimental design	**Independent factors that affect the response variable significantly**	**p-value**	**Model equation in terms of Coded Factors**
D-optimal design (Screening)	X_1	<0.0001	RSF = 9.29 -5.24 * X_1 + 3.40* X_2 + 1.72 * X_5 [1] -0.12* X_5 [2] -4.46 * X_1X_2
	X_2	<0.0001	
	X_5	0.0161	
	X_1X_2	<0.0001	
I-optimal design (Optimization)	X_1	<0.0001	RSF = 16.82+ -2.756 * X1 + 2.39* X2 + 1.298 * X5 + {X1 X2* -1.021} + {X12* -0.763}
	X_2	<0.0001	
	X_5	0.0161	
	X_1X_2	<0.0001	
	X_1^2	0.0026	

We also observe a significant two factor interaction between Distance B and the Tool lift (Figure 41.). From Figure 41 we can conclude that RSF is not significantly dependent on the Distance B

at low levels of the Tool lift (2mm), however, at a higher level of Tool lift (20 mm), RSF decreases with an increase in Distance B.

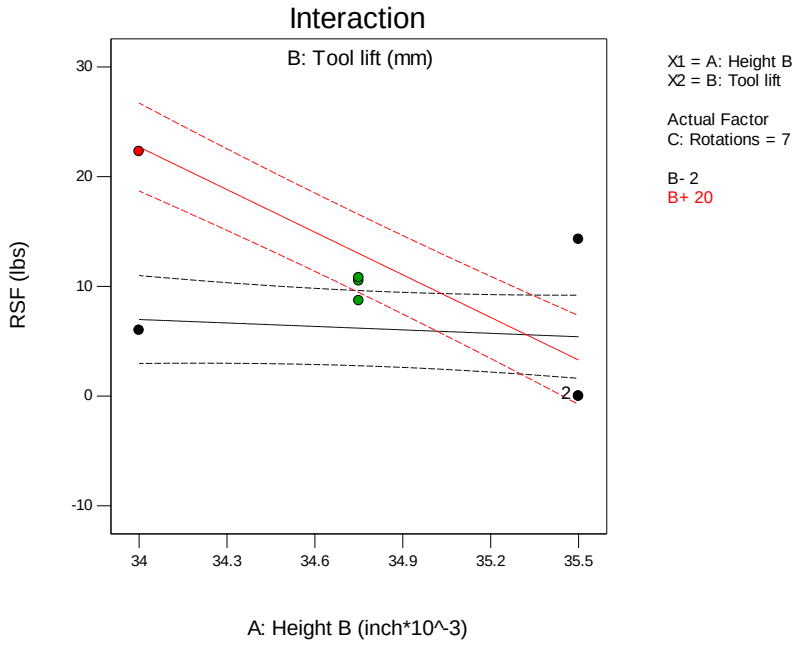

Figure 41. 2FI for the D-optimal screening design, Factors Distance B and Tool lift.

Distance B corresponds to the height of the container with a loosely positioned cap and lesser this distance, snugger is the fit of the cap. The crimping tool protrudes (lifts) during the time of crimping. Tool lift is the lift of the crimping tool during the crimping process, and thus at higher value of tool lift the vial is sealed more tightly and corresponds to high RSF value. The D-optimal screening study provides us with a general idea about the acceptable factor limits for the model. Figure 42. depicts the prediction profiler for the D-optimal design helping us determine factor constraints for further augmenting this design. It is not desirable (desirability factor below 0.5) to increase the distance B above 34.8 mm or to reduce the Tool lift below 12 mm. Taking into consideration the data from both of the output variables, the factors were further tailored for the

augmentation, Distance B was studied from 34-34.8 mm, Tool lift was studied from 12-20 mm and number of rotations were restricted to 7 and 10.

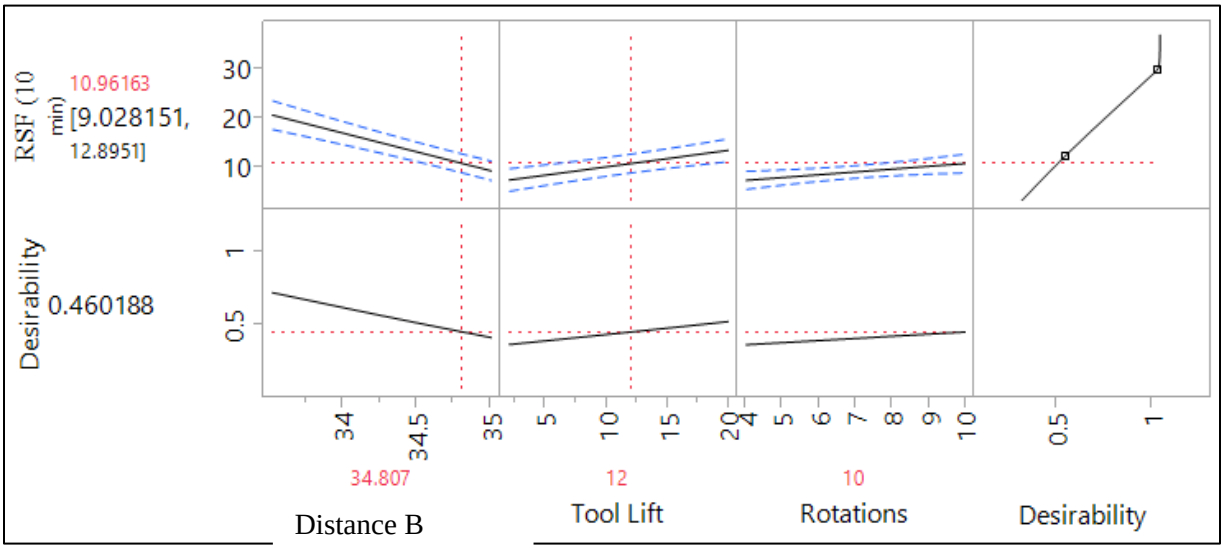

Figure 42. Prediction profiler for the D-optimal screening design: Output variable RSF, Input variables: Distance B, Tool lift and Number of rotations and the predicted Desirability

Table 29 enlists the significance testing for the I-optimal design; a quadratic model was chosen for this data based on the model R- Squared value and the Lack of Fit (p-value 0.9926) (Table 26.). The individual factors that significantly affect RSF include all the three independent variables; Distance B (mm), Tool lift (mm) and number of rotations. Also, Distance B has a slight quadratic effect on the observed RSF values, observed in Figure 43. Figure 43 is the 3D surface profiler for the I-optimal design and it plots Tool Lift and Distance B on the X1 and X2 axes respectively, while RSF as the response on the Y axis. According to the model predictions, the red zone as shown in Figure 43 are the areas of maximum RSF predicted. To achieve values of RSF 20 Lbs

and above, it is advisable to operate with Tool lift maintained above 15mm and Distance B maintained below 34.4mm. The rotations have been maintained at number 10, however there is no major difference in RSF by changing the number of rotations from 7 to 10.

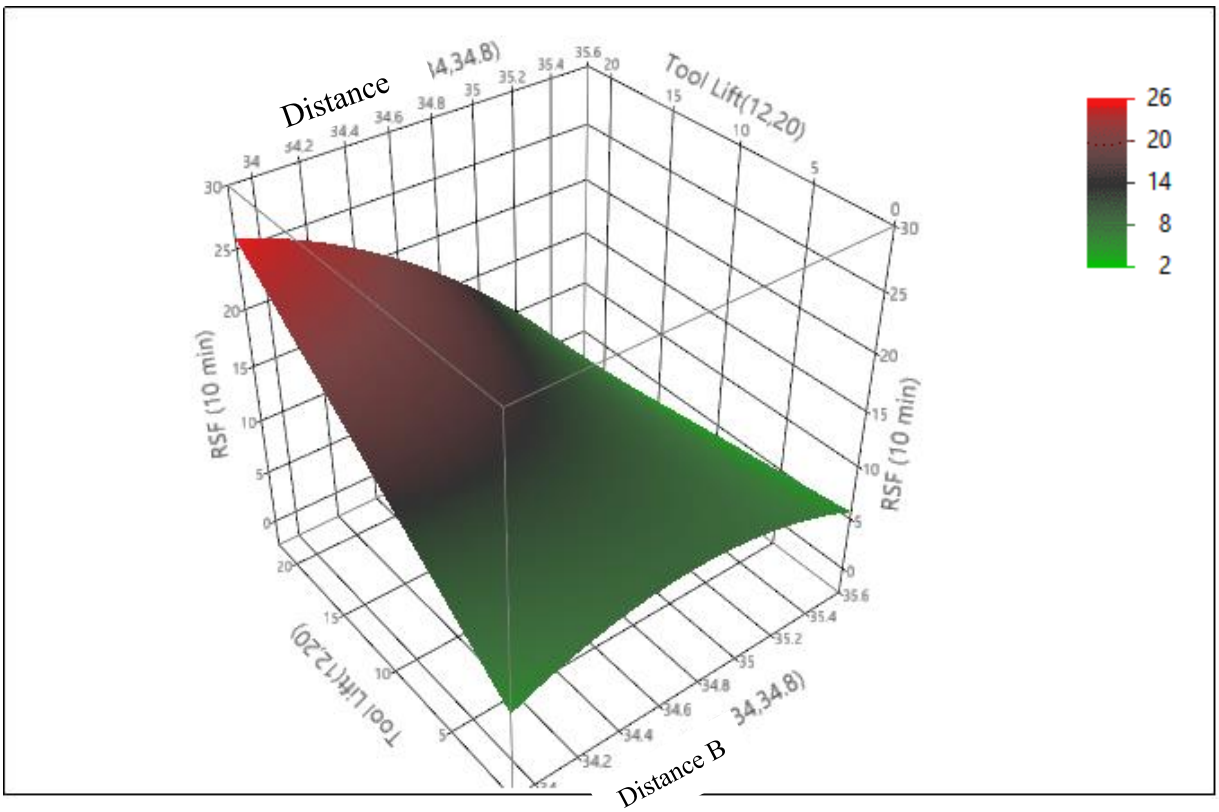

Figure 43. Surface profiler for the I-optimal screening design: Output variable RSF, Input variables: Height C, Tool lift Number of Rotations set at 10

The robustness of the I-optimal design model was verified by crimping vials at different factor combinations and comparing the actual RSF to the model predicted RSF. Table 30 represents the factor combinations chosen for the validation study. (n=10) In terms of percentage, there is about 4%, 22%, 8%, 6%, 4% for factor combinations 1, 2, 3, 4, 5 (Sr.no.) respectively. The model has

very good predictability with % error less than 10% for all combinations except Sr.no 2, which has a 21.8% deviation from the predicted value. This explains that the model has good predictability for factors near the center of the model, but its prediction efficacy reduces at the edges of the design.

Table 30. Design validation, Actual vs Predicted RSF (LBS) varying factors Distance B, Tool Lift and Number of rotations

Sr. no.	Distance B mm	Tool Lift mm	Number of rotations	Predicted RSF (Lbs)	Actual RSF (Lbs)
1	34.4	12	7	14.83	14.2 ± 1.2
2	35.2	12	10	8.7	6.8 ± 1.3
3	34.6	22	7	18.29	16.8 ± 1.0
4	34	20	7	22.84	21.4 ± 1.5
5	34	22	10	25.21	26.4 ± 1.9

Conclusion

Using a statistical Design of Experiment technique, capping parameters were optimized for single station cappers, Integra West Capper® and Bausch and Strobel® capper to increase CCI of crimped vials in all storage and transport conditions. On the basis of these generated models CCI can be studied as a function of unit processes, such as capping. This study also helped us co-relate the crimping mechanisms for lab-scale single station cappers in turn helping us standardize the capping process for a vial-stopper combination across lab-scale equipment. For the Integra West Capper®, in order to maintain CCI and obtain a high RSF value, Pre-compression force of 35 Lbs and above and Pressure Block reference height of 120 to 130 inch*10^{-3} are instrumental. For the Bausch and Strobel® capper, lower position of crimping

tool (Distance B) of 34-34.4 mm and Tool lift of 15mm and above are important. Increasing the number of rotations during crimping from 7 to 10 did not play a significant role in optimizing the RSF values.

BIBLIOGRAPHY

1. Walters, W. P., Going further than Lipinski's rule in drug design. *Expert Opinion on Drug Discovery* **2012,** *7* (2), 99-107.

2. Lipinski, C. A., Lead- and drug-like compounds: the rule-of-five revolution. *Drug Discovery Today: Technologies* **2004,** *1* (4), 337-341.

3. Choy, Y. B.; Prausnitz, M. R., The Rule of Five for Non-Oral Routes of Drug Delivery: Ophthalmic, Inhalation and Transdermal. *Pharmaceutical Research* **2011,** *28* (5), 943-948.

4. Lee, V., Mechanisms and facilitation of corneal drug penetration. *J Control Release* **1990,** *11* (1–3), 79–90.

5. Hussain, A.; Truelove, J. E., Prodrug approaches to enhancement of physicochemical properties of drugs IV: novel epinephrine prodrug. *Journal of Pharmaceutical Sciences* **1976,** *65* (10), 1510-1512.

6. Hussain, A.; Truelove, J. E., Prodrug approaches to enhancement of physicochemical properties of drugs IV: novel epinephrine prodrug. *J Pharm Sci* **1976,** *65* (10), 1510-1512.

7. Attar, M.; Schiffman, R.; Borbridge, L.; Farnes, Q.; Welty, D., Ocular pharmacokinetics of 0.45% ketorolac tromethamine. *Clin Ophthalmol* **2010,** *4*, 1403-1408.

8. Rácz, P.; Ruzsonyi, M. R.; Nagy, Z. T.; Bito, L. Z., Maintained intraocular pressure reduction with once-a-day application of a new prostaglandin F2 alpha analogue (PhXA41). An in-hospital, placebo-controlled study. *Arch. Ophthalmol.* **1993,** *111* (5), 657-661.

9. Gerald, W. B.; Carl, B. C., Commercially available prostaglandin analogs for the reduction of intraocular pressure: similarities and differences. *Survey of Ophthalmology* **2008,** *53* (6).

10. Kikuchi, H.; Carlsson, A.; Yachi, K.; Hirota, S., Possibility of heat sterilization of liposomes. *Chem Pharm Bull (Tokyo)* **1991,** *39* (4), 1018-1022.

11. Sharma, A.; Sharma, U. S., Liposomes in drug delivery: progress and limitations. *International Journal of Pharmaceutics* **1997,** *154* (2), 123-140.

12. Puglia, C.; Offerta, A.; Carbone, C.; Bonina, F.; Pignatello, R.; Puglisi, G., Lipid nanocarriers (LNC) and their applications in ocular drug delivery. *Curr. Med. Chem.* **2015,** *22* (13), 1589-1602.

13. Hippalgaonkar, K.; Adelli, G. R.; Hippalgaonkar, K.; Repka, M. A.; Majumdar, S., Indomethacin-loaded solid lipid nanoparticles for ocular delivery: development, characterization, and in vitro evaluation. *J Ocul Pharmacol Ther* **2013,** *29* (2), 216-228.

14. Urtti, A., Challenges and obstacles of ocular pharmacokinetics and drug delivery. *Adv Drug Deliv Rev* **2006,** *58* (11), 1131–1135.

15. Lee, V. H.; Robinson, J. R., Topical ocular drug delivery: recent developments and future challenges. *Journal of ocular pharmacology* **1986,** *2* (1), 67-108.

16. Achouri, D.; Alhanout, K.; Piccerelle, P.; Andrieu, V., Recent advances in ocular drug delivery. *Drug Dev Ind Pharm* **2013,** *39* (11), 1599-1617.

17. Maurice, D. M.; Mishima, S., Ocular Pharmacokinetics. In *Pharmacology of the Eye*, Sears, M. L., Ed. Springer: Berlin Heidelberg, 1984; pp 19-116.

18. Khurana, *Ophthalmology*. New Age International: New Delhi, 2003; p 576.

19. Fangueiro, J. F.; Veiga, F.; Silva, A. M.; Souto, E. B., Ocular drug delivery - new strategies for targeting anterior and posterior segments of the eye. *Current pharmaceutical design* **2015,** *22* (9), 1135-46.

20. Goel, M.; Picciani, R. G.; Lee, R. K.; Bhattacharya, S. K., Aqueous Humor Dynamics: A Review. *Open Ophthalmol J* **2010,** *4*, 52-9.

21. Järvinen, K.; Järvinen, T.; Urtti, A., Ocular absorption following topical delivery. *Adv Drug Deliv Rev* **1995,** *16* (1), 3-19.

22. Becker, B., Chemical composition of human aqueous humor: effects of acetazoleamide. *AMA Arch Ophthalmol* **1957,** *57* (6), 793-800.

23. Lee, V. H.; Li, V. H., Prodrugs for improved ocular drug delivery. *Adv Drug Deliv Rev* **1989,** *3* (1), 1-38.

24. Lund-Andersen, H.; Sebag, J.; Sander, B.; La Cour, M., The vitreous. *Adv Organ Biol* **2005,** *10*, 181–194.

25. Lee, V. H.-L.; Robinson, J. R., Mechanistic and quantitative evaluation of precorneal pilocarpine disposition in albino rabbits. *J. Pharm. Sci.* **1979,** *68* (6), 673-684.

26. Dartt, D.; Hodges, R.; Zoukhri, D., Tears and their secretion. *Adv Organ Biol* **2005,** *10*, 21–82.

27. Cunha-Vaz, J., The blood-ocular barriers. *Survey of Ophthalmology* **1979,** *23* (5), 279-296.

28. Barar, J.; Javadzadeh, A. R.; Omidi, Y., Ocular novel drug delivery: impacts of membranes and barriers. *Expert Opin Drug Deliv* **2008,** *5* (5), 567-581.

29. Komarova, Y.; Malik, A. B., Regulation of endothelial permeability via paracellular and transcellular transport pathways. *Annu Rev Physiol* **2010,** *72* (1), 463-493.

30. Klyce, S. D.; Crosson, C. E., Transport processes across the rabbit corneal epithelium: a review. *Curr Eye Res* **1985,** *4* (4), 323-331.

31. Ehlers, N.; Hjortdal, J., The cornea: epithelium and stroma. *Adv Organ Biol* **2005,** *10*, 83–111.

32. Wang, W.; Sasaki, H.; Chien, D. S.; Lee, V. H., Lipophilicity influence on conjunctival drug penetration in the pigmented rabbit: a comparison with corneal penetration. *Curr Eye Res* **1991,** *10* (6), 571-9.

33. Ahmed, I.; Gokhale, R. D.; Shah, M. V.; Patton, T. F., Physicochemical determinants of drug diffusion across the conjunctiva, sclera, and cornea. *J. Pharm. Sci.* **1987,** *76* (8), 583-6.

34. Huang, H.-S.; Schoenwald, R. D.; Lach, J. L., Corneal penetration behavior of β-blocking agents II: assessment of barrier contributions. *J. Pharm. Sci.* **1983,** *72* (11), 1272-1279.

35. Saha, P.; Yang, J. J.; Lee, V. H., Existence of a p-glycoprotein drug efflux pump in cultured rabbit conjunctival epithelial cells. *Investigative ophthalmology & visual science* **1998,** *39* (7), 1221-6.

36. Mannermaa, E.; Vellonen, K.-S.; Urtti, A., Drug transport in corneal epithelium and blood–retina barrier: emerging role of transporters in ocular pharmacokinetics. *Adv Drug Deliv Rev* **2006,** *58* (11), 1136-1163.

37. Rautio, J., *Prodrugs and Targeted Delivery: Towards Better ADME Properties*. John Wiley & Sons: Weinheim, Germany, 2011; p 523.

38. Hosoya, K.-i.; Tomi, M., Advances in the cell biology of transport *via* the inner blood-retinal barrier: establishment of cell lines and transport functions. *Biol Pharm Bull* **2005,** *28* (1), 1-8.

39. Ahmed, T.; Patton, I., Importance of the noncorneal absorption route in topical ophthalmic drug delivery. *Investigative ophthalmology & visual science* **1985**, 584-7.

40. Rizzolo, L. J., Polarity and the development of the outer blood-retinal barrier. *Histology and histopathology* **1997,** *12* (4), 1057-67.

41. Ban, Y.; Rizzolo, L. J., Differential regulation of tight junction permeability during development of the retinal pigment epithelium. *American journal of physiology. Cell physiology* **2000,** *279* (3), C744-50.

42. Bauer, H. C.; Krizbai, I. A.; Bauer, H.; Traweger, A., "You Shall Not Pass"—tight junctions of the blood brain barrier. *Front Neurosci* **2014,** *8*, 392.

43. Stella, V.; Borchardt, R.; Hageman, M.; Oliyai, R.; Maag, H.; Tilley, J., *Prodrugs: Challenges and Rewards*. Springer Science + Business Media: New York, NY, 2007.

44. Tężyk, M.; Jakubowska, E.; Milanowski, B.; Lulek, J., Implementation of quality by design approach in manufacturing process optimization of dry granulated, immediate release, coated tablets – a case study. *Drug Development and Industrial Pharmacy* **2017,** *43* (10), 1626-1636.

45. Huerva, V.; #xed; Ascaso, F. J.; Grzybowski, A., Ocular Inflammation. *Mediators of Inflammation* **2015,** *2015*, 2.

46. Cheung, N.; Mitchell, P.; Wong, T. Y., Diabetic retinopathy. *The Lancet* **2010,** *376* (9735), 124-136.

47. Bourne, R. R. A.; Stevens, G. A.; White, R. A.; Smith, J. L.; Flaxman, S. R.; Price, H.; Jonas, J. B.; Keeffe, J.; Leasher, J.; Naidoo, K.; Pesudovs, K.; Resnikoff, S.; Taylor, H. R., Causes of vision loss worldwide, 1990–2010: a systematic analysis. *The Lancet Global Health* **2013,** *1* (6), e339-e349.

48. Yau, J. W. Y.; Rogers, S. L.; Kawasaki, R.; Lamoureux, E. L.; Kowalski, J. W.; Bek, T.; Chen, S.-J.; Dekker, J. M.; Fletcher, A.; Grauslund, J.; Haffner, S.; Hamman, R. F.; Ikram, M. K.; Kayama, T.; Klein, B. E. K.; Klein, R.; Krishnaiah, S.; Mayurasakorn, K.; O'Hare, J. P.; Orchard, T. J.; Porta, M.; Rema, M.; Roy, M. S.; Sharma, T.; Shaw, J.; Taylor, H.; Tielsch, J. M.; Varma, R.; Wang, J. J.; Wang, N.; West, S.; Xu, L.; Yasuda, M.; Zhang, X.; Mitchell, P.; Wong, T. Y.,

Global Prevalence and Major Risk Factors of Diabetic Retinopathy. *Diabetes Care* **2012,** *35* (3), 556.

49. Neely, K. A.; Gardner, T. W., Ocular Neovascularization : Clarifying Complex Interactions. *The American Journal of Pathology* **1998,** *153* (3), 665-670.

50. El-Remessy, A. B.; Al-Shabrawey, M.; Khalifa, Y.; Tsai, N.-T.; Caldwell, R. B.; Liou, G. I., Neuroprotective and Blood-Retinal Barrier-Preserving Effects of Cannabidiol in Experimental Diabetes. *The American Journal of Pathology* **2006,** *168* (1), 235-244.

51. El-Remessy, A. B.; Behzadian, M. A.; Abou-Mohamed, G.; Franklin, T.; Caldwell, R. W.; Caldwell, R. B., Experimental Diabetes Causes Breakdown of the Blood-Retina Barrier by a Mechanism Involving Tyrosine Nitration and Increases in Expression of Vascular Endothelial Growth Factor and Urokinase Plasminogen Activator Receptor. *The American Journal of Pathology* **2003,** *162* (6), 1995-2004.

52. Qaum, T.; Xu, Q.; Joussen, A. M.; Clemens, M. W.; Qin, W.; Miyamoto, K.; Hassessian, H.; Wiegand, S. J.; Rudge, J.; Yancopoulos, G. D.; Adamis, A. P., VEGF-initiated Blood–Retinal Barrier Breakdown in Early Diabetes. *Investigative ophthalmology & visual science* **2001,** *42* (10), 2408-2413.

53. JOUSSEN, A. M.; POULAKI, V.; MITSIADES, N.; KIRCHHOF, B.; KOIZUMI, K.; DÖHMEN, S.; ADAMIS, A. P., Nonsteroidal anti-inflammatory drugs prevent early diabetic retinopathy via TNF-α suppression. *The FASEB Journal* **2002,** *16* (3), 438-440.

54. Nakagami, H.; Morishita, R.; Yamamoto, K.; Yoshimura, S.-i.; Taniyama, Y.; Aoki, M.; Matsubara, H.; Kim, S.; Kaneda, Y.; Ogihara, T., Phosphorylation of p38 Mitogen-Activated Protein Kinase Downstream of Bax-Caspase-3 Pathway Leads to Cell Death Induced by High

d-Glucose in Human Endothelial Cells. *Diabetes* **2001,** *50* (6), 1472.

55. Liou, G. I.; El-Remessy, A. B.; Ibrahim, A. S.; Caldwell, R. B.; Khalifa, Y. M.; Gunes, A.; Nussbaum, J. J., Cannabidiol As a Putative Novel Therapy for Diabetic Retinopathy: A Postulated Mechanism of Action as an Entry Point for Biomarker-Guided Clinical Development. *Current pharmacogenomics and personalized medicine* **2009,** *7* (3), 215-222.

56. Butcher, J. M.; Austin, M.; McGalliard, J.; Bourke, R. D., Bilateral cataracts and glaucoma induced by long term use of steroid eye drops. *BMJ : British Medical Journal* **1994,** *309* (6946), 43-43.

57. Buchman, A. L., Side Effects of Corticosteroid Therapy. *Journal of Clinical Gastroenterology* **2001,** *33* (4), 289-294.

58. Richard H. Roe, M. M.; H. Richard McDonald, M. D., Complications of Vitreoretinal Surgery. *Review of Ophthalmology* **2008**.

59. M, T. D.; Cairns Elizabeth, A.; Szczesniak, A.-M.; Toguri James, T.; Caldwell Meggie, D.; Kelly Melanie, E., The Cannabinoids Δ8THC, CBD, and HU-308 Act via Distinct Receptors to Reduce Corneal Pain and Inflammation. *https://home.liebertpub.com/can* **2018**.

60. Toguri, J. T.; Caldwell, M.; Kelly, M. E. M., Turning Down the Thermostat: Modulating the Endocannabinoid System in Ocular Inflammation and Pain. *Frontiers in Pharmacology* **2016,** *7* (304).

61. Pertwee, R. G., The diverse CB1 and CB2 receptor pharmacology of three plant cannabinoids: Δ9-tetrahydrocannabinol, cannabidiol and Δ9-tetrahydrocannabivarin. *British Journal of Pharmacology* **2009,** *153* (2), 199-215.

62. Porcella, A.; Casellas, P.; Gessa, G. L.; Pani, L., Cannabinoid receptor CB1 mRNA is highly expressed in the rat ciliary body: implications for the antiglaucoma properties of marihuana. *Brain Res Mol Brain Res* **1998,** *58* (1-2), 240-5.

63. Porcella, A.; Maxia, C.; Gessa, G. L.; Pani, L., The human eye expresses high levels of CB1 cannabinoid receptor mRNA and protein. *The European journal of neuroscience* **2000,** *12* (3), 1123-7.

64. Hall, W.; Solowij, N., Adverse effects of cannabis. *The Lancet* **1998,** *352* (9140), 1611-1616.

65. Straiker, A. J.; Maguire, G.; Mackie, K.; Lindsey, J., Localization of cannabinoid CB1 receptors in the human anterior eye and retina. *Investigative ophthalmology & visual science* **1999,** *40* (10), 2442-8.

66. Gérard, C. M.; Mollereau, C.; Vassart, G.; Parmentier, M., Molecular cloning of a human cannabinoid receptor which is also expressed in testis. *Biochemical Journal* **1991,** *279* (Pt 1), 129-134.

67. Reggio, P. H., Endocannabinoid Binding to the Cannabinoid Receptors: What Is Known and What Remains Unknown. *Current medicinal chemistry* **2010,** *17* (14), 1468-1486.

68. Grotenhermen, F.; Müller-Vahl, K., The Therapeutic Potential of Cannabis and Cannabinoids. *Dtsch Arztebl Int* **2012,** *109* (29-30), 495-501.

69. Kowapradit, J.; Opanasopit, P.; Ngawhiranpat, T.; Apirakaramwong, A.; Rojanarata, T.; Ruktanonchai, U.; Sajomsang, W., Methylated N-(4-N,N-Dimethylaminobenzyl) Chitosan, a Novel Chitosan Derivative, Enhances Paracellular Permeability Across Intestinal Epithelial Cells (Caco-2). *AAPS PharmSciTech* **2008,** *9* (4), 1143-1152.

70. Liou, G. I.; Auchampach, J. A.; Hillard, C. J.; Zhu, G.; Yousufzai, B.; Mian, S.; Khan, S.; Khalifa, Y., Mediation of cannabidiol anti-inflammation in the retina by equilibrative nucleoside transporter and A2A adenosine receptor. *Investigative ophthalmology & visual science* **2008,** *49* (12), 5526-31.

71. Cunha-Vaz, J., The blood-ocular barriers. *Survey of Ophthalmology* **1979,** *23* (5), 279-296.

72. Han, H. K.; Oh, D. M.; Amidon, G. L., Cellular uptake mechanism of amino acid ester prodrugs in Caco-2/hPEPT1 cells overexpressing a human peptide transporter. *Pharm Res* **1998,** *15* (9), 1382-6.

73. Nelson, W. L.; Walker, R. B., The structure of propranolol hemisuccinate. *Research communications in chemical pathology and pharmacology* **1978,** *22* (3), 435-45.

74. Ambrose, P. J., Clinical pharmacokinetics of chloramphenicol and chloramphenicol succinate. *Clinical pharmacokinetics* **1984,** *9* (3), 222-38.

75. Zhang, X.; Mehvar, R., Dextran-methylprednisolone succinate as a prodrug of methylprednisolone: dose-dependent pharmacokinetics in rats. *Int J Pharm* **2001,** *229* (1-2), 173-82.

76. Taskar, P.; Tatke, A.; Majumdar, S., Advances in the use of prodrugs for drug delivery to the eye. *Expert Opinion on Drug Delivery* **2017,** *14* (1), 49-63.

77. Mississippi, M. A. E.; Soumyajit, M.; Waseem, G.; Mohammad Khalid, A.; Kenneth Joseph, S.; Hannah Marie, H.; University, O., Biologically active cannabidiol analogs. **2017**.

78. Bradford, M. M., A rapid and sensitive method for the quantitation of microgram quantities of protein utilizing the principle of protein-dye binding. *Analytical biochemistry* **1976,** *72*, 248-54.

79. *Design of Amino Acid Prodrugs of Acyclovir for Improved Bioavailability and Therapeutic Activity: Utility in Treating Ocular, Oral and Genital Herpes Infections*. ProQuest: 2007; p 182.

80. Atluri, H.; Anand, B. S.; Patel, J.; Mitra, A. K., Mechanism of a model dipeptide transport across blood-ocular barriers following systemic administration. *Exp. Eye Res.* **2004,** *78* (4), 815-822.

81. Beauchamp, L. M.; Orr, G. F.; de Miranda, d. P.; Bumette, T.; Krenitsky, T. A., Amino acid ester prodrugs of acyclovir. *Antiviral Chemistry and Chemotherapy* **1992,** *3* (3), 157-164.

82. Vig, B. S.; Huttunen, K. M.; Laine, K.; Rautio, J., Amino acids as promoieties in prodrug design and development. *Advanced Drug Delivery Reviews* **2013,** *65* (10), 1370-1385.

83. Quigley, H. A.; Addicks, E. M.; Green, W.; Maumenee, A. E., Optic nerve damage in human glaucoma: Ii. the site of injury and susceptibility to damage. *Archives of Ophthalmology* **1981,** *99* (4), 635-649.

84. Abe, R. Y.; Diniz-Filho, A.; Costa, V. P.; Gracitelli, C. P. B.; Baig, S.; Medeiros, F. A., The Impact of Location of Progressive Visual Field Loss on Longitudinal Changes in Quality of Life of Patients with Glaucoma. *Ophthalmology* **2016,** *123* (3), 552-557.

85. Cook, C.; Foster, P., Epidemiology of glaucoma: what's new? *Canadian journal of ophthalmology. Journal canadien d'ophtalmologie* **2012,** *47* (3), 223-6.

86. Adelli, G. R.; Bhagav, P.; Taskar, P.; Hingorani, T.; Pettaway, S.; Gul, W.; ElSohly, M. A.; Repka, M. A.; Majumdar, S., Development of a Delta9-Tetrahydrocannabinol Amino Acid-Dicarboxylate Prodrug With Improved Ocular Bioavailability. *Investigative ophthalmology & visual science* **2017,** *58* (4), 2167-2179.

87. Quigley, H. A.; Broman, A. T., The number of people with glaucoma worldwide in 2010 and 2020. *The British Journal of Ophthalmology* **2006,** *90* (3), 262-267.

88. (NEI), N. E. I. Glaucoma, Open-angle https://nei.nih.gov/eyedata/glaucoma.

89. Grüb, M.; Mielke, J., [Aqueous humor dynamics]. *Ophthalmologe* **2004,** *101* (4), 357-365.

90. Macri, F. J.; Cevario, S. J., The formation and inhibition of aqueous humor production: A proposed mechanism of action. *Archives of Ophthalmology* **1978,** *96* (9), 1664-1667.

91. Brubaker, R. F., Goldmann's equation and clinical measures of aqueous dynamics. *Exp. Eye Res.* **2004,** *78* (3), 633-637.

92. Goel, M.; Picciani, R. G.; Lee, R. K.; Bhattacharya, S. K., Aqueous Humor Dynamics: A Review. *The Open Ophthalmology Journal* **2010,** *4*, 52-59.

93. Gabelt, B. A. T.; Kaufman, P. L., Changes in aqueous humor dynamics with age and glaucoma. *Progress in Retinal and Eye Research* **2005,** *24* (5), 612-637.

94. Yablonski, M. E.; Zimmerman, T. J.; Waltman, S. R.; Becker, B., A fluorophotometric study of the effect of topical timolol on aqueous humor dynamics. *Exp. Eye Res.* **1978,** *27* (2), 135-142.

95. Tătaru, C. P.; Purcărea, V. L., Antiglaucoma pharmacotherapy. *Journal of Medicine and Life* **2012,** *5* (3), 247-251.

96. Toris, C. B., Pharmacology of Aqueous Humor Formation A2 - Dartt, Darlene A. In *Encyclopedia of the Eye*, Academic Press: Oxford, 2010; pp 312-315.

97. Patil, A.; Singh, S.; Opere, C.; Dash, A., Sustained-Release Delivery System of a Slow Hydrogen Sulfide Donor, GYY 4137, for Potential Application in Glaucoma. *AAPS PharmSciTech* **2017,** *18* (6), 2291-2302.

98. New Medical Therapies for Glaucoma. https://www.glaucoma.org/treatment/new-medical-therapies-for-glaucoma.php.

99. Schehlein, E. M.; Novack, G.; Robin, A. L., New pharmacotherapy for the treatment of glaucoma. *Expert Opinion on Pharmacotherapy* **2017,** *18* (18), 1939-1946.

100. Twitchell, W.; Brown, S.; Mackie, K., Cannabinoids Inhibit N- and P/Q-Type Calcium Channels in Cultured Rat Hippocampal Neurons. *Journal of Neurophysiology* **1997,** *78* (1), 43-50.

101. Malinowska, B.; Godlewski, G.; Bucher, B.; Schlicker, E., Cannabinoid CB1 receptor-mediated inhibition of the neurogenic vasopressor response in the pithed rat. *Naunyn-Schmiedeberg's Archives of Pharmacology* **1997,** *356* (2), 197-202.

102. Sugrue, M. F., New Approaches to Antiglaucoma Therapy. *Journal of Medicinal Chemistry* **1997,** *40* (18), 2793-2809.

103. Allingham, R. R.; de Kater, A. W.; Ethier, R. C., Schlemm 's Canal and Primary Open Angle Glaucoma: Correlation Between Schlemm 's Canal Dimensions and Outflow Facility. *Exp. Eye Res.* **1996,** *62* (1), 101-110.

104. Tomida, I.; Pertwee, R. G.; Azuara-Blanco, A., Cannabinoids and glaucoma. *The British Journal of Ophthalmology* **2004,** *88* (5), 708-713.

105. Panahi, Y.; Manayi, A.; Nikan, M.; Vazirian, M., The arguments for and against cannabinoids application in glaucomatous retinopathy. *Biomedicine & pharmacotherapy = Biomedecine & pharmacotherapie* **2016,** *86*, 620-627.

106. Porcella, A.; Maxia, C.; Gessa, G. L.; Pani, L., The synthetic cannabinoid WIN55212-2 decreases the intraocular pressure in human glaucoma resistant to conventional therapies. *The European journal of neuroscience* **2001,** *13* (2), 409-12.

107. Morgan-Davies, J.; Taylor, N.; Hill, A. R.; Aspinall, P.; O'Brien, C. J.; Azuara-Blanco, A., Three dimensional analysis of the lamina cribrosa in glaucoma. *The British Journal of Ophthalmology* **2004,** *88* (10), 1299-1304.

108. Agarwal, R.; Gupta, S. K.; Agarwal, P.; Saxena, R.; Agrawal, S. S., Current concepts in the pathophysiology of glaucoma. *Indian Journal of Ophthalmology* **2009,** *57* (4), 257-266.

109. Abe, R. Y.; Gracitelli, C. P. B.; Diniz-Filho, A.; Tatham, A. J.; Medeiros, F. A., Lamina Cribrosa in Glaucoma: Diagnosis and Monitoring. *Current ophthalmology reports* **2015,** *3* (2), 74-84.

110. Almasieh, M.; Wilson, A. M.; Morquette, B.; Cueva Vargas, J. L.; Di Polo, A., The molecular basis of retinal ganglion cell death in glaucoma. *Progress in Retinal and Eye Research* **2012,** *31* (2), 152-181.

111. El-Remessy, A. B.; Khalil, I. E.; Matragoon, S.; Abou-Mohamed, G.; Tsai, N. J.; Roon, P.; Caldwell, R. B.; Caldwell, R. W.; Green, K.; Liou, G. I., Neuroprotective Effect of(−)Δ9-Tetrahydrocannabinol and Cannabidiol in N-Methyl-d-Aspartate-Induced Retinal Neurotoxicity : Involvement of Peroxynitrite. In *Am J Pathol*, 2003; Vol. 163, pp 1997-2008.

112. Ko, M. L.; Hu, D. N.; Ritch, R.; Sharma, S. C., The Combined Effect of Brain-Derived Neurotrophic Factor and a Free Radical Scavenger in Experimental Glaucoma. *Investigative ophthalmology & visual science* **2000,** *41* (10), 2967-2971.

113. Naveh, N.; Weissman, C.; Muchtar, S.; Benita, S.; Mechoulam, R., A submicron emulsion of HU-211, a synthetic cannabinoid, reduces intraocular pressure in rabbits. *Graefe's archive for clinical and experimental ophthalmology = Albrecht von Graefes Archiv fur klinische und experimentelle Ophthalmologie* **2000,** *238* (4), 334-8.

114. Shohami, E.; Gallily, R.; Mechoulam, R.; Bass, R.; Ben-Hur, T., Cytokine production in the brain following closed head injury: dexanabinol (HU-211) is a novel TNF-α inhibitor and an effective neuroprotectant. *Journal of Neuroimmunology* **1997,** *72* (2), 169-177.

115. Crandall, J.; Matragoon, S.; Khalifa, Y. M.; Borlongan, C.; Tsai, N. T.; Caldwell, R. B.; Liou, G. I., Neuroprotective and Intraocular Pressure-Lowering Effects of (–)Δ⁹-Tetrahydrocannabinol in a Rat Model of Glaucoma. *Ophthalmic Research* **2007,** *39* (2), 69-75.

116. Crandall, J.; Matragoon, S.; Khalifa, Y. M.; Borlongan, C.; Tsai, N. T.; Caldwell, R. B.; Liou, G. I., Neuroprotective and intraocular pressure-lowering effects of (-)Delta9-tetrahydrocannabinol in a rat model of glaucoma. *Ophthalmic Res* **2007,** *39* (2), 69-75.

117. Grotenhermen, F.; Russo, E., *Cannabis and Cannabinoids: Pharmacology, Toxicology, and Therapeutic Potential*. Haworth Integrative Healing Press: 2002.

118. Hepler, R. S.; Frank, I. R., Marihuana smoking and intraocular pressure. *Jama* **1971,** *217* (10), 1392.

119. Green, K., Marijuana smoking vs cannabinoids for glaucoma therapy. *Archives of Ophthalmology* **1998,** *116* (11), 1433-1437.

120. Crawford, W. J.; Merritt, J. C., Effects of tetrahydrocannabinol on arterial and intraocular hypertension. *International journal of clinical pharmacology and biopharmacy* **1979,** *17* (5), 191-6.

121. Merritt, J. C.; Perry, D. D.; Russell, D. N.; Jones, B. F., Topical Δ9-Tetrahydrocannabinol and Aqueous Dynamics in Glaucoma. *The Journal of Clinical Pharmacology* **1981,** *21* (S1), 467S-471S.

122. Elsohly, M. A.; Harland, E.; Murphy, J. C.; Wirth, P.; Waller, C. W., Cannabinoids in Glaucoma: A Primary Screening Procedure. *The Journal of Clinical Pharmacology* **1981,** *21* (S1), 472S-478S.

123. Jay, W. M.; Green, K., Multiple-drop study of topically applied 1% δ9-tetrahydrocannabinol in human eyes. *Arch Ophthalmol* **1983,** *101* (4), 591-593.

124. Muchtar, S.; Almog, S.; Torracca, M. T.; Saettone, M. F.; Benita, S., A Submicron Emulsion as Ocular Vehicle for Delta-8-Tetrahydrocannabinol: Effect on Intraocular Pressure in Rabbits. *Ophthalmic Research* **1992,** *24* (3), 142-149.

125. Song, Z.-H.; Slowey, C.-A., Involvement of Cannabinoid Receptors in the Intraocular Pressure-Lowering Effects of WIN55212-2. *Journal of Pharmacology and Experimental Therapeutics* **2000,** *292* (1), 136-139.

126. Elsohly, M. A.; Gul, W.; Repka, M. A.; Majumdar, S., Compositions containing delta-9-thc-amino acid esters and process of preparation. Google Patents.

127. Punyamurthula, N. S.; Adelli, G. R.; Gul, W.; Repka, M. A.; ElSohly, M. A.; Majumdar, S., Ocular Disposition of 8-Tetrahydrocannabinol from Various Topical Ophthalmic Formulations. *AAPS PharmSciTech* **2016,** *18* (6), 1936-1945.

128. Elsohly, M. A.; Gul, W.; Repka, M. A.; Majumdar, S., Compositions containing delta-9-thc-amino acid esters and process of preparation. Google Patents: 2011.

129. Schubert, M. A.; Müller-Goymann, C. C., Characterisation of surface-modified solid lipid nanoparticles (SLN): Influence of lecithin and nonionic emulsifier. *European Journal of Pharmaceutics and Biopharmaceutics* **2005,** *61* (1), 77-86.

130. Green, K.; Bigger, J. F.; Kim, K.; Bowman, K., Cannabinoid penetration and chronic effects in the eye. *Exp. Eye Res.* **1977,** *24* (2), 197-205.

131. Hingorani, T.; Adelli, G. R.; Punyamurthula, N.; Gul, W.; ElSohly, M. A.; Repka, M. A.; Majumdar, S., Ocular Disposition of the Hemiglutarate Ester Prodrug of Δ9-Tetrahydrocannabinol from Various Ophthalmic Formulations. *Pharm Res* **2013,** *30* (8).

132. Balguri, S. P.; Adelli, G. R.; Majumdar, S., Topical ophthalmic lipid nanoparticle formulations (SLN, NLC) of indomethacin for delivery to the posterior segment ocular tissues. *European Journal of Pharmaceutics and Biopharmaceutics* **2016,** *109* (Supplement C), 224-235.

133. Hingorani, T.; Gul, W.; Elsohly, M.; Repka, M. A.; Majumdar, S., Effect of ion pairing on in vitro transcorneal permeability of a Delta(9) -tetrahydrocannabinol prodrug: potential in glaucoma therapy. *J. Pharm. Sci.* **2011,** *101* (2), 616-26.

134. Thumma, S.; Majumdar, S.; ElSohly, M. A.; Gul, W.; Repka, M. A., Preformulation Studies of a Prodrug of Δ9-Tetrahydrocannabinol. In *AAPS PharmSciTech*, 2008; Vol. 9, pp 982-90.

135. Duvvuri, S.; Majumdar, S.; Mitra, A. K., Drug delivery to the retina: challenges and opportunities. *Expert Opinion on Biological Therapy* **2003,** *3* (1), 45-56.

136. Kaur, I. P.; Kakkar, S., Nanotherapy for posterior eye diseases. *Journal of Controlled Release* **2014,** *193* (Supplement C), 100-112.

137. Patil, A.; Lakhani, P.; Taskar, P.; Wu, K.-W.; Sweeney, C.; Avula, B.; Wang, Y.-H.; Khan, I. A.; Majumdar, S., Formulation Development, Optimization, and In-Vitro Characterization of Natamycin-Loaded PEGylated Nano-Lipid Carriers for Ocular Applications. *Journal of Pharmaceutical Sciences* **2018,** *107* (8), 2160-2171.

138. Lakhani, P.; Patil, A.; Taskar, P.; Ashour, E.; Majumdar, S., Curcumin-loaded Nanostructured Lipid Carriers for ocular drug delivery: Design optimization and characterization. *Journal of Drug Delivery Science and Technology* **2018,** *47*, 159-166.

139. Thumma, S.; ElSohly, M. A.; Zhang, S. Q.; Gul, W.; Repka, M. A., Influence of plasticizers on the stability and release of a prodrug of Delta(9)-tetrahydrocannabinol incorporated in poly (ethylene oxide) matrices. *European journal of pharmaceutics and biopharmaceutics : official journal of Arbeitsgemeinschaft fur Pharmazeutische Verfahrenstechnik e.V* **2008,** *70* (2), 605-14.

140. Munjal, M.; ElSohly, M. A.; Repka, M. A., Chemical stabilization of a Delta9-tetrahydrocannabinol prodrug in polymeric matrix systems produced by a hot-melt method: Role of microenvironment pH. *AAPS PharmSciTech* **2006,** *7* (3), E114-e125.

141. Munjal, M.; Elsohly, M. A.; Repka, M. A., Polymeric Systems for Amorphous Δ9-Tetrahydrocannabinol Produced by a Hot-Melt Method. Part II: Effect of Oxidation Mechanisms and Chemical Interactions on Stability. *J. Pharm. Sci.* **2006,** *95* (11), 2473-85.

142. Punyamurthula, N. S.; Hingorani, T.; Adelli, G.; Gul, W.; ElSohly, M. A.; Repka, M. A.; Majumdar, S., Controlled release tablet formulation containing natural Delta(9)-tetrahydrocannabinol. *Drug Dev Ind Pharm* **2015,** *42* (7), 1158-64.

143. Lizunova, A. A.; Loshkarev, A. A.; Tokunov, Y. M.; Ivanov, V. V., Comparison of the Results of Measurements of the Sizes of Nanoparticles in Stable Colloidal Solutions by the Methods of Acoustic Spectroscopy, Dynamic Light Scattering, and Transmission Electron Microscopy. *Measurement Techniques* **2017,** *59* (11), 1151-1155.

144. Anderson, W.; Kozak, D.; Coleman, V. A.; Jämting, Å. K.; Trau, M., A comparative study of submicron particle sizing platforms: Accuracy, precision and resolution analysis of polydisperse particle size distributions. *Journal of Colloid and Interface Science* **2013,** *405* (Supplement C), 322-330.

145. Freitas, C.; Müller, R. H., Effect of light and temperature on zeta potential and physical stability in solid lipid nanoparticle (SLN™) dispersions. *International Journal of Pharmaceutics* **1998,** *168* (2), 221-229.

146. Goldman, J. N.; Kuwabara, T., Histopathology of corneal edema. *International ophthalmology clinics* **1968,** *8* (3), 561-79.

147. Wang, J.; Xia, Q., Alpha-lipoic acid-loaded nanostructured lipid carrier: sustained release and biocompatibility to HaCaT cells in vitro. *Drug Delivery* **2014,** *21* (5), 328-341.

148. Montenegro, L.; Parenti, C.; Turnaturi, R.; Pasquinucci, L., Resveratrol-Loaded Lipid Nanocarriers: Correlation between In Vitro Occlusion Factor and In Vivo Skin Hydrating Effect. *Pharmaceutics* **2017,** *9* (4).

149. Wang, J.; Zhao, F.; Liu, R.; Chen, J.; Zhang, Q.; Lao, R.; Wang, Z.; Jin, X.; Liu, C., Novel cationic lipid nanoparticles as an ophthalmic delivery system for multicomponent drugs: development, characterization, in vitro permeation, in vivo pharmacokinetic, and molecular dynamics studies. *International Journal of Nanomedicine* **2017,** *12*, 8115-8127.

150. Sarpotdar, P. p.; Zatz, J. L., Percutaneous Absorption Enhancement by Nonionic Surfactants. *Drug Development and Industrial Pharmacy* **1986,** *12* (11-13), 1625-1647.

151. Araújo, J.; Gonzalez-Mira, E.; Egea, M. A.; Garcia, M. L.; Souto, E. B., Optimization and physicochemical characterization of a triamcinolone acetonide-loaded NLC for ocular antiangiogenic applications. *International Journal of Pharmaceutics* **2010,** *393* (1), 168-176.

152. Jermak, C. M.; Tulane University Health Sciences Center, N. O. L.; Retina Consultants of Western New York, B. N. Y. U. S. A.; Dellacroce, J. T.; Tulane University Health Sciences Center, N. O. L.; Heffez, J.; Tulane University Health Sciences Center, N. O. L.; Peyman, G. A.; Tulane University Health Sciences Center, N. O. L., Triamcinolone Acetonide in Ocular Therapeutics. *Survey of Ophthalmology* **2007,** *52* (5), 503-522.

153. Chen, H.; Sun, S.; Li, J.; Du, W.; Zhao, C.; Hou, J.; Xu, Y.; Cheng, L., Different Intravitreal Properties of Three Triamcinolone Formulations and Their Possible Impact on Retina Practice. *Investigative ophthalmology & visual science* **2013,** *54* (3), 2178-2185.

154. Erkiliç, A. Ö.; aozkiris@erciyes.edu.tr; Kuddusi, Complications of intravitreal injection of triamcinolone acetonide. *Canadian Journal of Ophthalmology* **2005,** *40* (1), 63-68.

155. Reichel, C. A. P.; Pravin, U. D.; Scott, W. C.; Kirk, H. P.; Alexander, M. E.; Richard, K. P.; Szilárd, K.; Elias, Improving Outcomes for Patients With Diabetic Macular Edema. *Ophthalmic Surgery, Lasers and Imaging Retina* **2015,** *46* (10).

156. Gaudana, R.; Ananthula, H. K.; Parenky, A.; Mitra, A. K., Ocular drug delivery. *AAPS J* **2010,** *12* (3), 348-60.

157. Morrison, P. W.; Khutoryanskiy, V. V., Advances in ophthalmic drug delivery. *Ther Deliv* **2014,** *5* (12), 1297-315.

158. Sultana, Y.; Jain, R.; Aqil, M.; Ali, A., Review of ocular drug delivery. *Curr Drug Deliv* **2006,** *3* (2), 207-17.

159. Hippalgaonkar, K.; Adelli, G. R.; Hippalgaonkar, K.; Repka, M. A.; Majumdar, S., Indomethacin-loaded solid lipid nanoparticles for ocular delivery: development, characterization, and in vitro evaluation. *J Ocul Pharmacol Ther* **2013,** *29* (2), 216-228.

160. Bonferoni, M. C.; Sandri, G.; Rossi, S.; Ferrari, F.; Caramella, C., Chitosan and its salts for mucosal and transmucosal delivery. *Expert Opin Drug Deliv* **2009,** *6* (9), 923-39.

161. Caramella, C.; Ferrari, F.; Bonferoni, M. C.; Rossi, S.; Sandri, G., Chitosan and its derivatives as drug penetration enhancers. *Journal of Drug Delivery Science and Technology* **2010,** *20* (1), 5-13.

162. Liu, D.; Li, J.; Pan, H.; He, F.; Liu, Z.; Wu, Q.; Bai, C.; Yu, S.; Yang, X., Potential advantages of a novel chitosan-N-acetylcysteine surface modified nanostructured lipid carrier on the performance of ophthalmic delivery of curcumin. *Sci Rep* **2016,** *6*, 28796.

163. da Silva, S. B.; Ferreira, D.; Pintado, M.; Sarmento, B., Chitosan-based nanoparticles for rosmarinic acid ocular delivery—In vitro tests. *International Journal of Biological Macromolecules* **2016,** *84*, 112-120.

164. Mourya, V. K.; Inamdar, N. N., Trimethyl chitosan and its applications in drug delivery. *Journal of materials science. Materials in medicine* **2008,** *20* (5), 1057-79.

165. Ranaldi, G.; Marigliano, I.; Vespignani, I.; Perozzi, G.; Sambuy, Y., The effect of chitosan and other polycations on tight junction permeability in the human intestinal Caco-2 cell line(1). *J Nutr Biochem* **2002,** *13* (3), 157-167.

166. Murugan, K.; Choonara, Y. E.; Kumar, P.; Bijukumar, D.; du Toit, L. C.; Pillay, V., Parameters and characteristics governing cellular internalization and trans-barrier trafficking of nanostructures. *Int J Nanomedicine* **2015,** *10*, 2191-206.

167. M. N. V. Ravi Kumar; R. A. A. Muzzarelli; C. Muzzarelli; H. Sashiwa, a.; Domb‖, A. J., Chitosan Chemistry and Pharmaceutical Perspectives. **2004**.

168. van der Merwe, S. M.; Verhoef, J. C.; Kotzé, A. F.; Junginger, H. E., N-Trimethyl chitosan chloride as absorption enhancer in oral peptide drug delivery. Development and characterization of minitablet and granule formulations. *European Journal of Pharmaceutics and Biopharmaceutics* **2004,** *57* (1), 85-91.

169. Sieval, A. B.; Thanou, M.; Kotze´, A. F.; Verhoef, J. C.; Brussee, J.; Junginger, H. E., Preparation and NMR characterization of highly substitutedN-trimethyl chitosan chloride. *Carbohydrate Polymers* **1998,** *36* (2), 157-165.

170. Davidson, H. J.; Kuonen, V. J., The tear film and ocular mucins. *Veterinary Ophthalmology* **2004,** *7* (2), 71-77.

171. Adelli, G. R.; Balguri, S. P.; Majumdar, S., Effect of Cyclodextrins on Morphology and Barrier Characteristics of Isolated Rabbit Corneas. *AAPS PharmSciTech* **2015,** *16* (5), 1220-1226.

172. C., A.-V. J.; Jose, N.-P.; Alejandro, G.-D. l. R.; H., H. J.; S., O.-G. J.; C., G.-V. A.; C., K. B.; Lourdes, B.-L.; Arturo, S., Characterization and Pharmacokinetics of Triamcinolone Acetonide-Loaded Liposomes Topical Formulations for Vitreoretinal Drug Delivery. *Journal of Ocular Pharmacology and Therapeutics* **2018,** *34* (5), 416-425.

173. Sadeghi, A. M. M.; Dorkoosh, F. A.; Avadi, M. R.; Weinhold, M.; Bayat, A.; Delie, F.; Gurny, R.; Larijani, B.; Rafiee-Tehrani, M.; Junginger, H. E., Permeation enhancer effect of chitosan and chitosan derivatives: Comparison of formulations as soluble polymers and nanoparticulate systems on insulin absorption in Caco-2 cells. *European Journal of Pharmaceutics and Biopharmaceutics* **2008,** *70* (1), 270-278.

174. Sandri, G.; Bonferoni, M. C.; Rossi, S.; Ferrari, F.; Boselli, C.; Caramella, C., Insulin-Loaded Nanoparticles Based on N-Trimethyl Chitosan: In Vitro (Caco-2 Model) and Ex Vivo (Excised Rat Jejunum, Duodenum, and Ileum) Evaluation of Penetration Enhancement Properties. *AAPS PharmSciTech* **2010,** *11* (1), 362-371.

175. Rosenthal, R.; Günzel, D.; Finger, C.; Krug, S. M.; Richter, J. F.; Schulzke, J.-D.; Fromm, M.; Amasheh, S., The effect of chitosan on transcellular and paracellular mechanisms in the intestinal epithelial barrier. *Biomaterials* **2012,** *33* (9), 2791-2800.

176. McClintic, S. M.; Srinivasan, M.; Mascarenhas, J.; Greninger, D. A.; Acharya, N. R.; Lietman, T. M.; Keenan, J. D., Improvement in corneal scarring following bacterial keratitis. *Eye* **2012,** *27*, 443.

177. Ansari, Z.; Miller, D.; Galor, A., Current Thoughts in Fungal Keratitis: Diagnosis and Treatment. *Current fungal infection reports* **2013,** *7* (3), 209-218.

178. Al-Badriyeh, D.; Neoh, C. F.; Stewart, K.; Kong, D. C. M., Clinical utility of voriconazole eye drops in ophthalmic fungal keratitis. *Clinical Ophthalmology (Auckland, N.Z.)* **2010,** *4*, 391-405.

179. Tuli, S. S., Fungal keratitis. *Clinical Ophthalmology (Auckland, N.Z.)* **2011,** *5*, 275-279.

180. Gao, H.; Pennesi, M. E.; Shah, K.; et al., Intravitreal voriconazole: An electroretinographic and histopathologic study. *Archives of Ophthalmology* **2004,** *122* (11), 1687-1692.

181. Maesaki, S.; Iwakawa, J.; Higashiyama, Y.; Miyazaki, Y.; Yanagihara, K.; Tomono, K.; Tashiro, T.; Kohno, S., Antifungal activity of a new triazole, voriconazole (UK-109496), against clinical isolates of Aspergillus spp. *Journal of Infection and Chemotherapy* **2000,** *6* (2), 101-103.

182. Espinel-Ingroff, A.; Boyle, K.; Sheehan, D. J., In vitro antifungal activities of voriconazole and reference agents as determined by NCCLS methods: Review of the literature. *Mycopathologia* **2001,** *150* (3), 101-115.

183. Jurkunas, U. V.; Langston, D. P.; Colby, K., Use of Voriconazole in the Treatment of Fungal Keratitis. *International ophthalmology clinics* **2007,** *47* (2), 47-59.

184. Sánchez-López, E.; Espina, M.; Doktorovova, S.; Souto, E. B.; García, M. L., Lipid nanoparticles (SLN, NLC): Overcoming the anatomical and physiological barriers of the eye – Part I – Barriers and determining factors in ocular delivery. *European Journal of Pharmaceutics and Biopharmaceutics* **2017,** *110*, 70-75.

185. Stergiopoulou, T.; Meletiadis, J.; Sein, T.; Papaioannidou, P.; Tsiouris, I.; Roilides, E.; Walsh, T. J., Isobolographic Analysis of Pharmacodynamic Interactions between Antifungal Agents and Ciprofloxacin against Candida albicans and Aspergillus fumigatus. *Antimicrobial Agents and Chemotherapy* **2008,** *52* (6), 2196-2204.

186. Brilhante, R. S. N.; Caetano, E. P.; Sidrim, J. J. C.; Cordeiro, R. A.; Camargo, Z. P.; Fechine, M. A. B.; Lima, R. A. C.; Castelo Branco, D. S. C. M.; Marques, F. J. F.; Mesquita, J. R. L.; Lima, D. T.; Monteiro, A. J.; Rocha, M. F. G., Ciprofloxacin shows synergism with classical antifungals against Histoplasma capsulatum var. capsulatum and Coccidioides posadasii. *Mycoses* **2013,** *56* (3), 397-401.

187. White, T. C.; Marr, K. A.; Bowden, R. A., Clinical, Cellular, and Molecular Factors That Contribute to Antifungal Drug Resistance. *Clinical Microbiology Reviews* **1998,** *11* (2), 382-402.

188. Adelli, G. R.; Hingorani, T.; Punyamurthula, N.; Balguri, S. P.; Majumdar, S., Evaluation of topical hesperetin matrix film for back-of-the-eye delivery. *European Journal of Pharmaceutics and Biopharmaceutics* **2015,** *92*, 74-82.

189. Müller, R. H.; Radtke, M.; Wissing, S. A., Solid lipid nanoparticles (SLN) and nanostructured lipid carriers (NLC) in cosmetic and dermatological preparations. *Advanced Drug Delivery Reviews* **2002,** *54*, S131-S155.

190. Müller, R. H.; Petersen, R. D.; Hommoss, A.; Pardeike, J., Nanostructured lipid carriers (NLC) in cosmetic dermal products. *Advanced Drug Delivery Reviews* **2007,** *59* (6), 522-530.

191. Mo, Z.; Ban, J.; Zhang, Y.; Du, Y.; Wen, Y.; Huang, X.; Xie, Q.; Shen, L.; Zhang, S.; Deng, H.; Hou, D.; Chen, Y.; Lu, Z., Nanostructured lipid carriers-based thermosensitive eye drops for enhanced, sustained delivery of dexamethasone. *Nanomedicine* **2018,** *13* (11), 1239-1253.

192. Patil, A.; Lakhani, P.; Taskar, P.; Wu, K.-W.; Sweeney, C.; Avula, B.; Wang, Y.-H.; Khan, I. A.; Majumdar, S., Formulation Development, Optimization, and In Vitro–In Vivo Characterization of Natamycin-Loaded PEGylated Nano-Lipid Carriers for Ocular Applications. *Journal of Pharmaceutical Sciences* **2018,** *107* (8), 2160-2171.

193. Gong, Q.; Huntsman, C.; Ma, D., Clathrin-independent internalization and recycling. *Journal of Cellular and Molecular Medicine* **2008,** *12* (1), 126-144.

194. Mathaes, R.; Mahler, H. C.; Roggo, Y.; Ovadia, R.; Lam, P.; Stauch, O.; Vogt, M.; Roehl, H.; Huwyler, J.; Mohl, S.; Streubel, A., Impact of Vial Capping on Residual Seal Force and Container Closure Integrity. *PDA J Pharm Sci Technol* **2016,** *70* (1), 12-29.

195. Morton, D. K.; Lordi, N. G., Residual seal force measurement of parenteral vials. I. Methodology. *J Parenter Sci Technol* **1988,** *42* (1), 23-9.

196. Victor, K. G.; Levac, L.; Timmins, M.; Veale, J., Method Development for Container Closure Integrity Evaluation via Headspace Gas Ingress by Using Frequency Modulation Spectroscopy. *PDA J Pharm Sci Technol* **2017,** *71* (6), 429-453.

197. Nieto, A.; Roehl, H.; Brown, H.; Nikoloff, J.; Adler, M.; Mahler, H. C., Evaluation of Container Closure System Integrity for Frozen Storage Drug Products. *PDA J Pharm Sci Technol* **2016,** *70* (2), 120-33.

198. Hao, J.; Wang, F.; Wang, X.; Zhang, D.; Bi, Y.; Gao, Y.; Zhao, X.; Zhang, Q., Development and optimization of baicalin-loaded solid lipid nanoparticles prepared by coacervation method using central composite design. *Eur J Pharm Sci* **2012,** *47* (2), 497-505.

VITA

Pranjal Sameer Taskar

Education

Ph.D., Pharmaceutics and Drug Delivery — *Joined August 2014*

University of Mississippi, University

Bachelor of Pharmacy — *April 2013*

Institute of Chemical Technology, Mumbai, India

Work Experience

Plough Center for Sterile Drug Delivery Solutions, UTHSC

Research Scientist

BioMarin Pharmaceutical Inc. — *May 2017-December 2017*

Intern-Formulations Associate

Unilever Ltd. — *May 2012-July 2012*

Intern

Certifications

- Hands-on course in tablet technology, University of Mississippi, March 2015
- Comprehensive Pharmaceutical Aseptic Course, University of Tennessee Health Science Center, August 2018
- Aseptic manufacturing technique BSL 2, BioMarin Pharmaceutical Inc. May 2017
- Assistant Laboratory Animal Technician (ALAT) 19: Rats (2009), ALAT 23: Rabbits (2009) & Laboratory Animal Allergy on AALAS learning library

Publications

- **Taskar P**, Tatke A, Majumdar S. Advances in the use of prodrugs for drug delivery to the eye. Expert Opin Drug Deliv. 2016;14(1):49-63.
- Adelli GR, Bhagav P, **Taskar P**, Hingorani T, Pettaway S, Gul W, ElSohly MA, Repka MA, Majumdar S. Development of a Delta9-Tetrahydrocannabinol Amino Acid-Dicarboxylate Prodrug With Improved Ocular Bioavailability. Invest Ophthalmol Vis Sci. 2017;58(4):2167-79.
- Patil A, Lakhani P, **Taskar P**, Majumdar S. "Formulation Development, Optimization, and In vitro – In vivo Characterization of Natamycin Loaded PEGylated Nano-

lipid Carriers for Ocular Applications" April 2018, *Journal of Pharmaceutical Sciences* 10.1016/j.xphs.2018.04.014

- Lakhani P, Patil A, **Taskar P**, Majumdar S. "Curcumin-loaded Nanostructured Lipid Carriers for Ocular Drug Delivery: Design Optimization and Characterization" Journal of Drug Delivery Science and Technology, Volume 47, 2018, Pages 159-166, ISSN 1773-2247

Achievements

- Inducted in Rho Chi Pharmacy's Academic Honor Society
- Associate editor, Journal of Advanced Drug Delivery Research, MedCrave publications
- Multiple publications in international peer-reviewed journals
- Over 10 posters in national and international conferences, 3 intra-school podium presentations/ talks
- Participated in three-minute thesis competitions